Characterization of a 6 MV photon beam in terms of primary and scattered dose components

Christoph Jan Trauernicht

trrchr001

Thesis presented in fulfillment of the requirements for the degree of Master of Medical Sciences at the University of Cape Town.

Supervisors: Jaime Nieto-Camero; iThemba LABS

Prof. ER Hering; University of Cape Town

October 2009

DECLARATION

I, Christoph Jan Trauernicht, hereby declare that the work on which this thesis is based is my original work (except where acknowledgements indicate otherwise) and that neither the whole work nor any part of it has been, is being, or is to be submitted for another degree in this or any other university.

I empower the university to reproduce for the purpose of research either the whole or any portion of the contents in any manner whatsoever.

Signature: ……

Date: ……

ABSTRACT

The purpose of this work was to partition the 6 MV photon beam of a Philips SL75-5 linear accelerator into primary and scattered dose components in water.

The two quantities that are necessary to define the primary beam component are a reference dose D_R and a primary linear attenuation coefficient μ_0. D_R describes the magnitude of the primary dose as a fraction of the total dose in a reference field at a reference depth, while μ_0 describes how the primary dose changes with depth in a medium. The scattered component is the difference between the primary and total dose.

μ_0 for the beam in water was determined in four different ways, namely through the extrapolation of measured TMRs to zero field size, through linear attenuation measurements, through the fit of a convolution model to CAPDD data and through a method involving a central axis attenuator. The primary dose component was determined in two ways, namely by the extrapolation of the phantom scatter correction factor to zero field size and also by the central axis attenuator method.

μ_0 varied from 0.0445 cm^{-1} to 0.0469 cm^{-1} with an average of 0.0455 ± 0.0012 cm^{-1}.

D_R for a 10 cm x 10 cm field at the depth of maximum dose was found to vary between 0.933 Gy/ 100 MU and 0.935 Gy/ 100 MU, with an average of 0.934 Gy/ 100 MU.

These values agree very well with values published in the literature. It has thus been shown that the 6 MV photon beam is separable into primary and scattered dose components.

ACKNOWLEDGEMENTS

I would like to thank my supervisors for agreeing to supervise this work, especially Prof. Hering for regularly wanting to know how the thesis is coming along.

I would like to thank my colleagues from iThemba LABS, Evan for coming up with the idea and encouraging me to start writing as early as possible, Julyan for his helping hand and Mark for good conversation and partial derivatives.
Thanks also to my colleagues at Groote Schuur Hospital, Gerrie and Tobie for their encouragement and interest and Jan for an open ear and constructive criticism.

A big thank you goes to the people in the workshops (Basil and Marius, as well as Robin and Charlie) for manufacturing phantoms and build-up caps.

I would like to thank my wife Sonja for her love and understanding and Max for being a really great motivator!
And finally a thank you to my Creator, for giving me the ability to do this work.

CONTENTS

LIST OF FIGURES

LIST OF TABLES

CHAPTER 1 INTRODUCTION

1.1 Introduction

X-rays were discovered by WK Röntgen in 1895 and radioactivity by Becquerel the following year. While experimenting with cathode rays, Röntgen noted that fluorescent crystals some distance from the tube glowed when the cathode tube was activated with a high voltage (Stanton & Stinson, 1996). This radiation could penetrate opaque substances, produce fluorescence, blacken a photographic plate and ionize a gas. He named the new radiation X-rays. The understanding of the nature of X-rays was greatly enhanced when they were classified as one form of electromagnetic radiation (Khan, 2003).

X-rays have a several basic properties:

- they are unaffected by gravity
- they are unaffected by electric or magnetic fields
- they travel in straight lines
- they are exponentially attenuated in matter
- they cannot be focused

X-rays are produced by the interaction of electrons with matter. There are two broad classes of these electron interactions – **collision interactions** with subsequent characteristic radiation production and **radiative interactions**, which produce bremsstrahlung radiation. (Klevenhagen, 1985 and Stanton & Stinson, 1996)

The fundamental difference is that the collisional losses involve the outer atomic electrons while the radiative losses involve the atomic nucleus (Klevenhagen, 1985).

1.1.1 Collision Interactions

In collision interactions electrons interact with electrons in the target and transfer energy and momentum like balls on a pool table. These collisions can either be elastic, i.e. energy and momentum are conserved, or inelastic, in which momentum is conserved but kinetic energy is not conserved. Different amounts of energy are exchanged in collisions. Excitation is the transfer of some of the incident particle's energy to electrons in the target material, promoting them to higher energy levels. Ionization occurs if enough energy is given to the electron to remove it from the atom. This can then result in the formation of characteristic X-rays or Auger electrons (Stanton & Stinson, 1996).

1.1.2 Radiative Interactions (Bremsstrahlung)

Sometimes an electron interacts with the positive charge (Coulomb field) of an atomic nucleus. This process is called bremsstrahlung, which is German for "braking radiation".

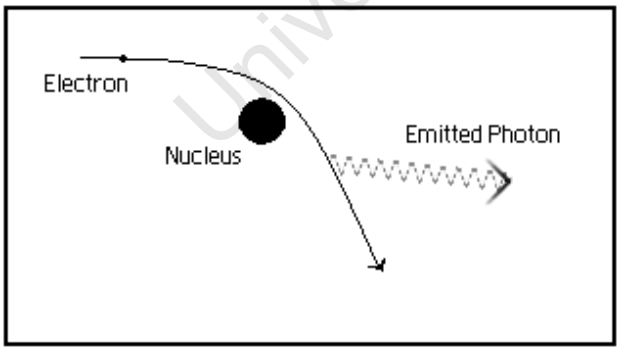

Figure 1.1: Illustration of the bremsstrahlung process

In this case the electric field of the nucleus exerts a force on the incoming electron and causes it to change its direction and velocity. This in turn corresponds to a loss in the kinetic energy of the electron, and by the law of conservation of energy this

energy shows up as an X-ray photon with energy equal to the energy loss of the electron (Stanton & Stinson, 1996).

In bremsstrahlung the maximum energy of the X-rays equals the kinetic energy of the incoming electrons. This occurs when all of the incoming electrons' kinetic energy is transformed into the resulting X-ray.

Bremsstrahlung production is governed by the Larmor relationship. It states that the power P emitted in the form of photons from an accelerated charged particle is proportional to the square of the particle charge q and the particle acceleration a:

$$P = \frac{q^2 \cdot a^2}{6 \cdot \pi \cdot \varepsilon_0 \cdot c^3} \tag{1.1}$$

where c refers to the speed of light in a vacuum and ε_0 is the permittivity of vacuum and is given by $\varepsilon_0 = 8.854 \cdot 10^{-12}\ C \cdot V^{-1} \cdot m^{-1}$.

The angular distribution of the emitted photons, i.e. the bremsstrahlung, is proportional to $\frac{\sin^2 \theta}{(1 - \frac{v}{c} \cdot \cos\theta)^5}$, where θ is the angle between the acceleration of the charged particle and a unit vector connecting the charge with the point of observation. At small velocities v of the charged particle the angular distribution goes as $\sin^2\theta$ and exhibits a maximum at θ = 90º (Podgorsak, 2005)

As the kinetic energy of the electrons increases, the direction of the X-ray emission becomes increasingly forward, i.e. in the direction that the electron would have travelled without the target present. This is the process by which X-rays for megavoltage therapy are produced in a linear accelerator (Khan, 2003).

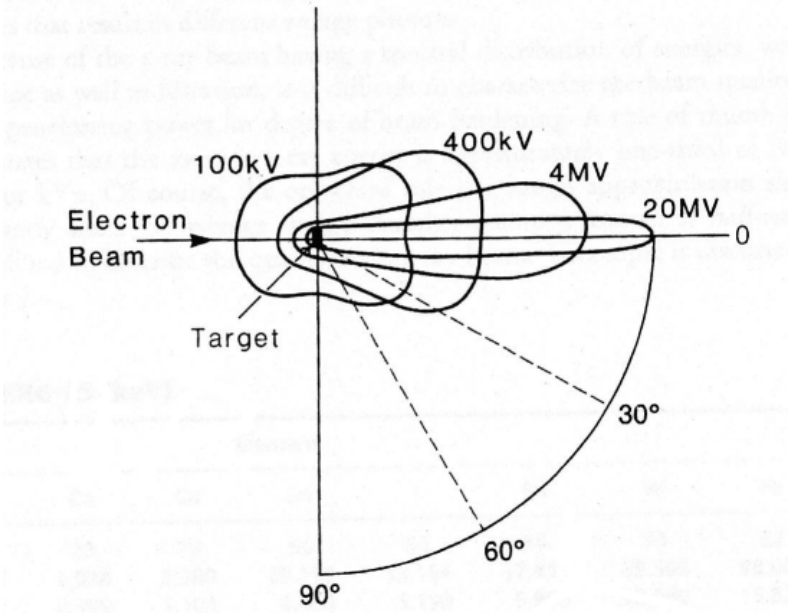

Figure 1.2: Schematic illustration of spatial distribution of X-rays around a thin target (From Khan: The Physics of Radiation Therapy, 2003, p.34)

For a more complete discussion on bremsstrahlung, see Koch *et al*, 1959.

For a discussion on energy and angular distributions of electron bremsstrahlung from thick targets see Isaev & Kovalev, 1985, Wayne Scott, 1967 or Nordell & Brahme, 1984.

As a rule of thumb, the polyenergetic beams produced by LINACs are often approximated by monoenergetic photons of energy equal to one third of the maximum spectral energy (Robinson & Scrimger, 1991).

1.2 Operating Principles of a Linear Accelerator

The linear accelerator (LINAC) was developed during the late 1940s and early 1950s by several different research groups (Stanton & Stinson, 1996).

It is a device which uses high-frequency radiowaves to accelerate charged particles through a linear tube. The high energy beam itself can be used for treating tumours, or it can be made to strike a tungsten target to produce X-rays (Khan, 2003).

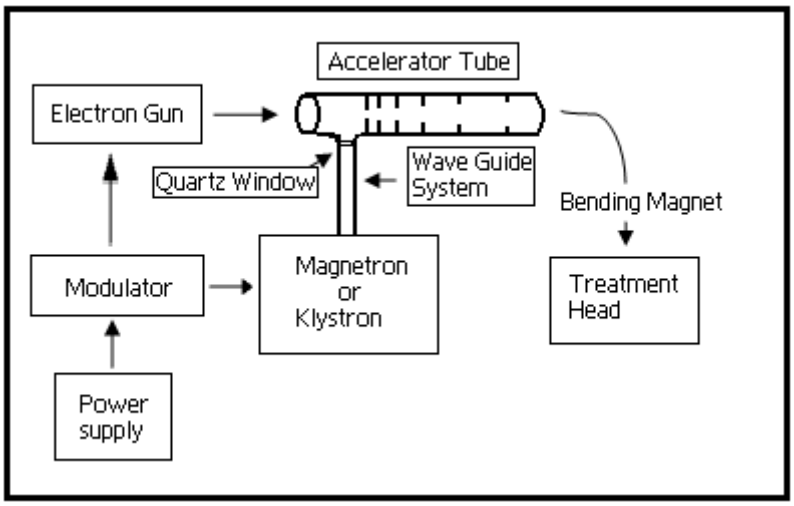

Figure 1.3: Block diagram of a linear accelerator

Figure 1.3 shows a block diagram of a linear accelerator. A power supply provides direct current to a modulator. High voltage pulses from the modulator are delivered to the magnetron or klystron and simultaneously to the electron gun. Magnetrons and klystrons are devices for producing microwaves (Khan, 2003). While magnetrons are cheaper than klystrons, they have a shorter life span and are not quite as high-powered as klystrons (Stanton & Stinson, 1996). Pulsed microwaves produced in the magnetron or klystron are injected into the accelerator tube via a waveguide system, which is filled with nitrogen gas under pressure (Hering, 1996). Electrons, which are produced by an electron gun, are pulsed in to the waveguide at the right moment as well (Khan, 2003). Electrons can only be accelerated in a vacuum and a quartz window separates the nitrogen under pressure from the vacuum in the corrugated waveguide (Hering, 1996).

The corrugated waveguide consists of a copper tube with its interior divided by copper discs or diaphragms of varying aperture and spacing, also called irises. As the electrons with an initial energy of ~50 keV are injected, they interact with the electromagnetic field of the microwaves (Khan, 2003). Although radiowaves travel at the speed of light, effectively they can be made to travel slower. In essence, the irises

provide resistance to the travel of the radiowaves. The closer together the irises or the tinier the center of the opening, the slower the wave will travel. (Stanton & Stinson, 1996)

The electrons gain kinetic energy similar to a surfer riding a wave (Khan, 2003). The electrons are then bent by a bending magnet. Bremsstrahlung X-rays are produced when the electrons hit a tungsten target. The target is water cooled and also thick enough to absorb most of the incident electrons (Khan, 2003). As a result of the bremsstrahlung type of interaction (see Chapter 1.1.2), the electron energy is converted into a spectrum of X-ray energies with maximum energy equal to the incident electron energy. The average photon energy of the beam is approximately one third of the maximum energy (Khan, 2003).

The treatment head of the linear accelerator consists of a shell of high-density shielding material like lead or tungsten. It contains the X-ray target, scattering foil, flattening filter, ion chamber, fixed and movable collimator and the lightfield system. The X-ray intensity of a linear accelerator is peaked in the forward direction, i.e. in the direction that the electrons were travelling before they hit the target. To make the beam intensity uniform across the field, a flattening filter is inserted in the beam. The treatment beam is first collimated by a fixed primary collimator located immediately beyond the X-ray target. The collimated beam then hits the flattening filter. The flattened X-ray beam then passes through the dose monitoring chambers, usually flat parallel-plate transmission chambers. The function of the ion chamber is to monitor dose rate, integrated dose and field symmetry. The ion chamber in the treatment head may also be sealed so that its response is not influenced by pressure or temperature variations.

After passing through the ion chambers, the beam is further collimated by a movable X-ray collimator. This collimator consists of two sets of lead or tungsten jaws which provide a rectangular opening to give the treatment field size. The field size definition is provided by the light localizing system in the treatment head. The light field should match the X-ray field exactly (Khan, 2003).

Linear accelerators are constructed so that the source of radiation can rotate about a horizontal axis. The collimator axis (coincident with the central axis of the beam) moves in a vertical plane. The point of intersection of the collimator axis and the axis of rotation of the gantry is known as the isocenter (Khan, 2003).

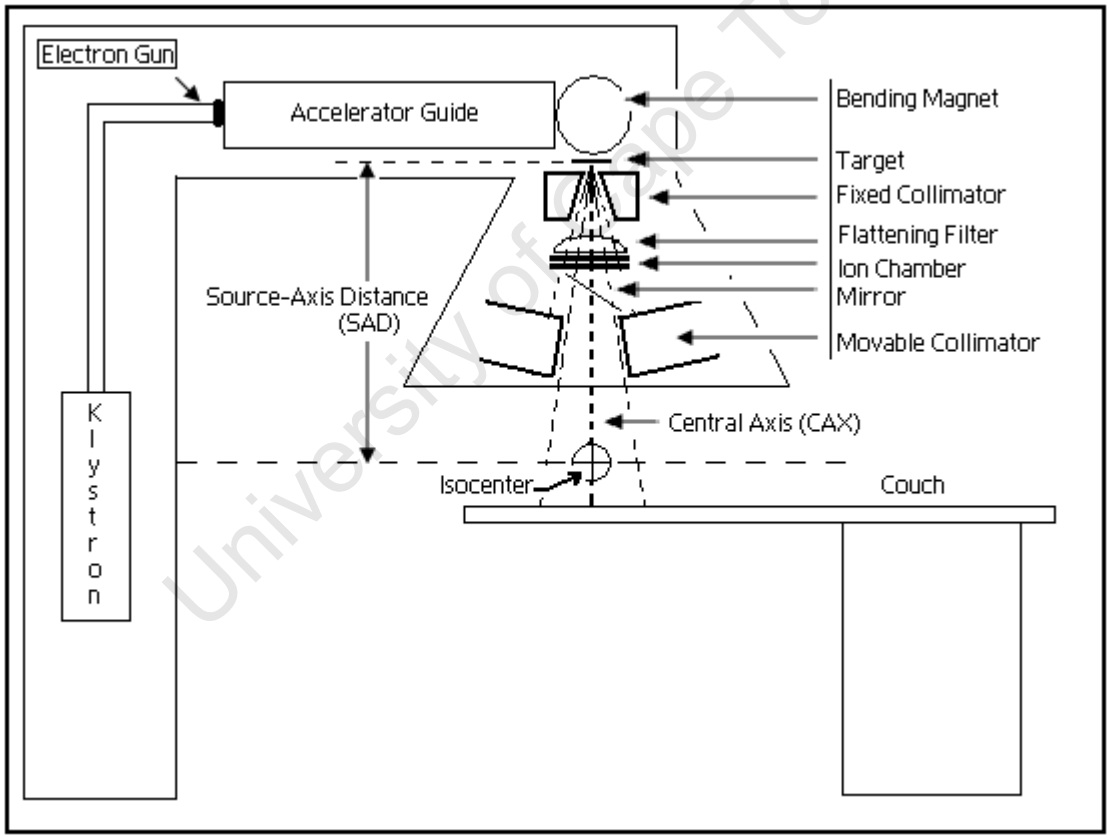

Figure 1.4: Diagram of a LINAC (not to scale)

1.3 Aim of Thesis

The delivered dose to a point in a medium can be expressed as the sum of two parts: the primary dose and the scattered dose (Meredith and Neary, 1944, Khan *et al.*, 1980, Day, 1983, Kijewski *et al*., 1986, Bjärngard *et al.*, 1988, Holt *et al.*, 1970). The primary dose (see Chapter 2.6) depends on the primary photon fluence, which in turn for a point source varies with distance by the inverse square law and exponential absorption. It is a common technique in radiotherapy treatment planning systems to simplify the calculations by splitting the radiation beam into these two components. The contributions of the two components are evaluated separately and then summed to give the dose at the point of interest (Khan, 2003).

Two quantities are required to define the primary dose component of a therapy beam, namely the primary linear attenuation co-efficient μ_0 and a reference dose D_R. μ_0 describes the depth dependence of the primary dose, while D_R is needed to establish the magnitude of the primary dose relative to the total dose at the reference depth and field size (Khan *et al*., 1980).

The aim of this thesis is to determine μ_0 for a 6 MV photon beam from a Philips SL75-5 linear accelerator using different methods. The reference dose D_R will be determined and hence the scattered component of the beam can be calculated.

The following four methods will be used to determine μ_0 in the photon beam:

- the extrapolation of measured Tissue-Maximum Ratios (TMRs) to zero field size (see definition in Chapter 2.8.4)
- linear attenuation measurements in water
- fitting a central axis kerma model, based on convolution techniques, to measured percentage depth dose data

- a method proposed by Nizin & Kase (1988) which comprises of dose measurements in phantom with and without a central axis attenuator

The methods are described in Chapter 3. The experimental details of the measurements are discussed in Chapter 4. The measured data is analyzed in Chapter 5. The value of μ_0 is obtained. Various scatter data and the value of the effective primary dose are obtained in Chapter 6. Chapter 7 gives a discussion of the results and the conclusions reached.

CHAPTER 2 THEORETICAL CONSIDERATIONS

2.1 Introduction

Photons are uncharged particles that interact mainly with the electrons in a medium. These charged particles then transfer their energy to the medium by excitation and ionization. The initial kinetic energy of the charged particles released by the photons per unit mass is known as the kerma (ICRU Report 60, 1998). The SI unit is the gray with 1 Gy = 1 J kg^{-1}. For a photon beam traversing a medium, kerma at a point is directly proportional to the photon energy fluence (Khan, 2003). Energy fluence is defined as the radiant energy incident per unit area and is measured in J m^{-2} (ICRU Report 60, 1998).

The energy of the electrons set in motion is not an exact measure of energy deposition in the volume of interest. Charged particles have finite ranges and can thus deposit their energy outside the volume. The absorbed dose is the quotient of the mean energy imparted by ionizing radiation per unit matter (ICRU Report 51, 1993), i.e. that part of the energy which is absorbed within a certain volume of the medium. A part of the absorbed dose may also be due to kerma that took place at a different location in the medium and is therefore not necessarily equal to the kerma in that volume (Khan, 2003). However, under conditions of charged particle equilibrium (see Chapter 2.4), kerma is approximately equal to absorbed dose (Attix, 1986). This is generally accepted and is also assumed to be true for this thesis for depths greater than or equal to the depth of maximum dose (d_{max}).

2.2 Photon Interactions

In radiation oncology ionizing radiation is used to damage and kill cells.

The overall process of attenuation (the combination of absorption and scatter) results from several different interactions of photons with atoms. The photons that do not interact are transmitted.

2.2.1 Coherent Scatter

Coherent scatter is sometimes called classical or Thomson scatter (Bushong, 2004). This mechanism is likely to occur only for very low-energy photons. In coherent scattering, incoming photons are absorbed by the atom's electrons. The electrons are not raised to higher orbits, but vibrate instead. They vibrate with the same frequency and phase as the incoming electromagnetic wave. The excess energy is immediately emitted in the form of photons. The new photons have the same energy and phase as the incoming photons, but are scattered in different directions.

In the high-energy ranges used in radiation therapy this interaction is of no importance (Stanton & Stinson, 1996).

2.2.2 Photoelectric Effect

In the photoelectric effect, an incoming high-energy photon interacts with a tightly bound inner orbit electron and transfers all its energy to the electron, which is ejected from the atom. The ejected electron is known as a photoelectron and the kinetic energy of the photoelectron is equal to the incident photon energy minus the binding energy of the orbital electron. The atom is left with a positive charge. Immediately an electron from an outer shell fills the hole, bringing the atom closer to its ground state. An L shell electron may fill the K shell, and then an M shell electron may fill the K

shell. Ultimately a free electron will neutralize the atom. When these electrons fall to lower orbits, photons are produced. The energy of each photon equals the energy difference between the electron shell levels through which the electrons fall. These energy differences are characteristic for each element and are thus known as characteristic radiation (Stanton & Stinson, 1996).

An electron cascade does not always result in the production of characteristic X-rays. A competing process, particularly for low Z elements, is Auger electron emission. The ejection of an Auger electron can be explained in a two-step process. In the first step, the energy needed to eject the Auger electron comes from the de-excitation of another electron from an outer to an inner orbit. The de-excitation energy is transferred to another electron in the atom. If the energy is greater than the binding energy of this electron, it will be ejected from the atom and is referred to as an Auger electron. Excess energy is transformed into kinetic energy of the Auger electron (Bushberg *et al.*, 2002 and Saw, 2002).

The probability of the photoelectric effect depends on both the energy of the incoming photon (E) and the atomic number (Z) of the material.

$$\text{Probability of photoelectric interaction} \approx \frac{Z^3}{E^3}$$

This means that the higher the atomic number of a material the more likely the interaction, but the higher the energy of the incoming photon the less likely the interaction (Stanton & Stinson, 1996).

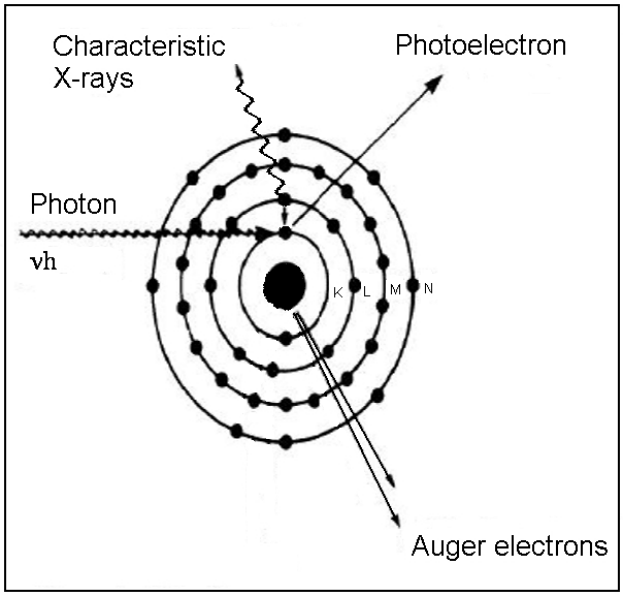

Figure 2.1: The Photoelectric Effect

2.2.3 Compton Scatter

In Compton scattering, a relatively high-energy photon interacts with a loosely bound electron in an atom's outer shell. Some of the energy of the incoming photon knocks the electron out of the atom, leaving behind a positively charged ion. The remaining energy emerges as a new photon with reduced energy and a change in direction.

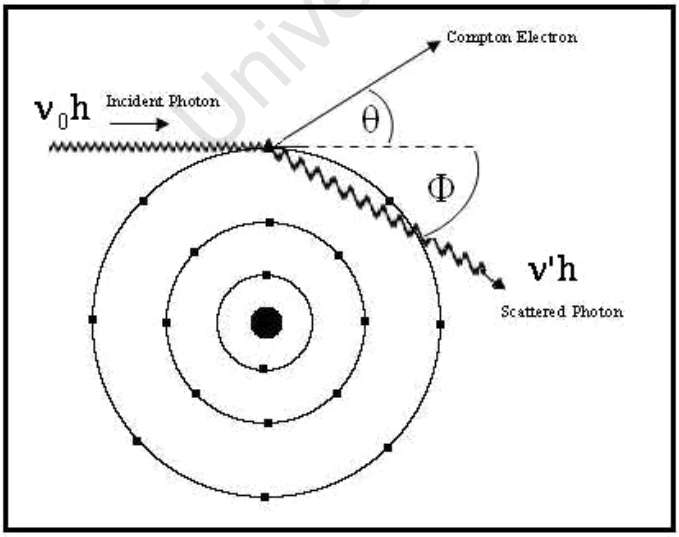

Figure 2.2: The Compton Effect

The Compton effect is the most probable interaction for the megavoltage energies in radiotherapy. This interaction probability is nearly independent of Z, but it is dependent on the electron density (electrons/kg) of the material. As it happens, electron densities show only a small variation over a wide range of atomic numbers Z. This means that for most materials electron density is proportional to mass density (kg/m^3) and therefore the Compton effect probability is largely dependent on mass density (Stanton & Stinson, 1996).

By applying the laws of conservation of energy and momentum, the following relationships can be derived (Marmier & Sheldon, 1969):

$$E = h\nu_0 \cdot \frac{\alpha \cdot (1 - \cos\Phi)}{1 + \alpha \cdot (1 - \cos\Phi)}; \qquad (2.1)$$

$$h\nu' = \frac{h\nu_0}{1 + \alpha \cdot (1 - \cos\Phi)}; \qquad (2.2)$$

$$\cot\theta = (1 + \alpha) \cdot \tan\frac{\Phi}{2} \qquad (2.3)$$

where $h\nu_0$, $h\nu'$ and E are the energies of the incident photon, scattered photon and electron respectively and θ and Φ are the angles as indicated on Figure 2.2.

$\alpha = h\nu_0/m_0c^2$ where m_0c^2 is the rest energy of the electron (0.511 MeV)

The laws of conservation of energy and momentum place limits on both scattering angle and energy transfer. The scattering angle of the ejected electron cannot exceed 90°, but the direction of the scattered photon can be at any angle, including 180°. The maximal energy of the scattered photon is limited to 511 keV at 90° scattering and to 255 keV for a backscatter event (Podgorsak, 2005).

2.2.4 Pair Production

Pair production can only occur when the energy of the X-ray exceeds 1.022 MeV and becomes more likely the higher the energy of the incoming photon is above this

threshold. Pair production only becomes important when using radiation energies above 10 MeV (Stanton & Stinson, 1996).

In pair production the incoming photon interacts with the electric field of the nucleus. The strength of the electric field is a function of Z. The photon's energy is transformed into an electron-positron pair, each with a rest mass energy equivalent of 0.511 MeV, thus the 1.022 MeV energy threshold. The incoming photon disappears totally and photon energy in excess of this threshold is imparted as kinetic energy (Figure 2.3: Initial Interaction).

The two new particles travel through matter depositing their energy through excitation and ionization. When the positron comes to rest, it combines with an electron near it. The two particles are annihilated and produce two photons of 0.511 MeV each which travel in opposite directions (Figure 2.3: Annihilation Interaction) (Stanton & Stinson, 1996; Bushberg *et al*, 2002).

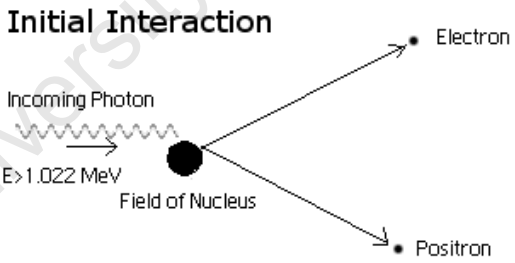

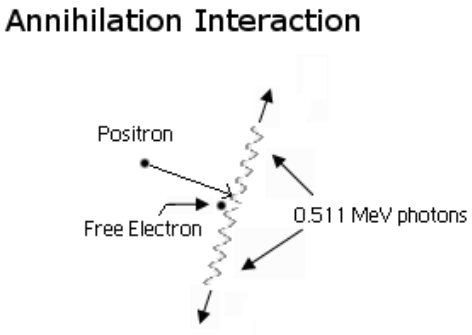

Figure 2.3: Initial interaction and annihilation interaction in pair production

Triplet production happens when pair production occurs in the field of an orbital electron instead of the electric field of the nucleus. An electron-positron pair and the orbital electron share the available energy. The energy threshold for this interaction is $4m_oc^2 = 2.044$ MeV (Podgorsak, 2005).

2.2.5 Photonuclear Interaction

Photonuclear interaction only starts to become important when the photon energy is above 15 MeV (Stanton & Stinson, 1996). In this interaction the incoming high-energy photon is absorbed by a nucleus, making the nucleus unstable. In order to regain stability, the nucleus emits a proton or a neutron. (γ, p) interactions are commonly neglected in dosimetric considerations (Attix, 1986). (γ, n) reactions have greater practical importance, because the neutron may interact with another nucleus, causing it to become radioactive. This interaction can cause accessories in accelerator heads to become radioactive, particularly beam-flattening filters and wedge filters. The photonuclear reaction has an energy threshold that depends on the element being irradiated (Stanton & Stinson, 1996).

The various processes of photon attenuation can now be considered by examining the effects of photon energy and atomic mass number of the absorber on their relative importance. Figure 2.4 shows the proportion of the various interactions. The lines in the figure indicate the values of the photon energy and Z where the probabilities of occurrence of two major processes are equal.

It can be clearly seen that at energies < 0.1 MeV in water ($Z_{eff}(H_2O) = 7.42$) (Jayachandran, 1971) the photoelectric effect is relatively important. Compton scatter

is the predominant interaction in water for energies used in radiotherapy, while pair production and photonuclear interactions increase at very high energies.

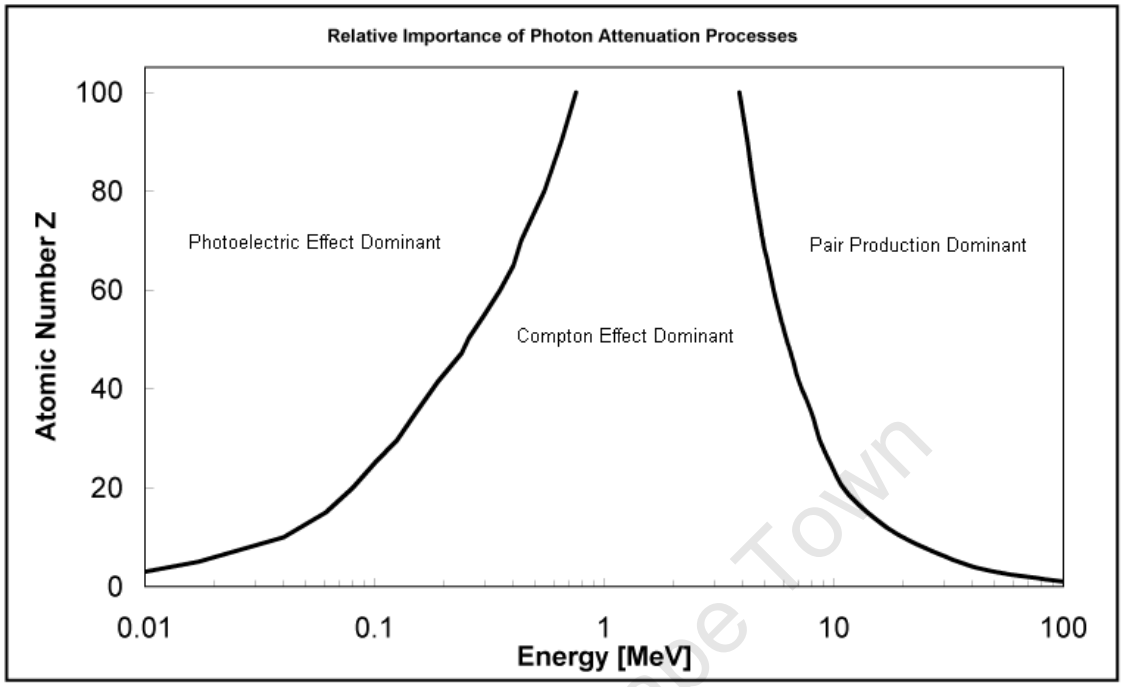

Figure 2.4: Relative Importance of Photon Attenuation Processes
(Data from XCOM: Photon Cross Sections Database: http://physics.nist.gov/cgi-bin/Xcom/xcom3_1 (Berger *et al*., 2009))

2.3 The Ionization Chamber

An ionization chamber is a device constructed to measure the number of ions in an irradiated medium. It consists of a gas-filled enclosure between two conducting electrodes, with a potential difference applied between the electrodes. The electrodes may be in the form of parallel plates or coaxial cylinders. One of the electrodes may be the chamber wall itself (Bushberg *et al*., 2002). If the chamber is not sealed, its response will be affected by temperature and pressure variations.

Figure 2.5 shows a diagram of a Farmer-type ionization chamber. One of the ionization chambers used for measurements in this thesis is the 0.6 cm^3 Nuclear Enterprises Farmer-type 2571 (NE 2571) ionization chamber.

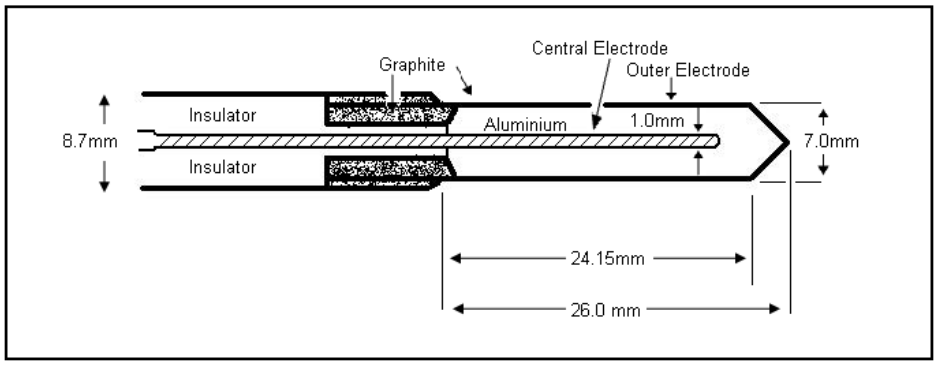

Figure 2.5: The Farmer Chamber

In 1955 Farmer designed a chamber which provided a stable and reliable secondary standard for X-rays and gamma rays in the therapeutic energy range (Farmer, 1955). The original design of the Farmer chamber was later modified (Aird & Farmer, 1972) to provide better energy response characteristics. According to the AAPM TG21 protocol (1983), for ^{60}Co rays about 20% of the dose to water at a depth of 5 cm and a field size of 10 x 10 cm^2 is due to scattered, energy-degraded photons. Therefore it is necessary for the ionization chamber with build-up cap to have a constant exposure-calibration factor down to photon energies of approximately 200 keV. The Farmer chamber complies in this regard.

The thimble wall of the Farmer chamber is made of pure graphite and the central electrode (the collector) is made of pure aluminium. The collecting volume of the Farmer chamber is 0.6 cm^3.

An electrometer is used to count the collected charge or give a current readout, while at the same time providing a potential difference (typically 250 V – 300 V) for efficient charge collection by the electrodes. The thimble is typically at ground potential. Most often the collector is operated with a positive voltage to collect negative charge although either polarity should result in the same amount of charge

being collected. The collected charge is proportional to the delivered dose (Khan, 2003).

The second kind of ionization chamber used for measurements is the "Mini Ionisation Chamber" designed by Schreuder *et al*. (1997). Figure 2.6 shows this chamber.

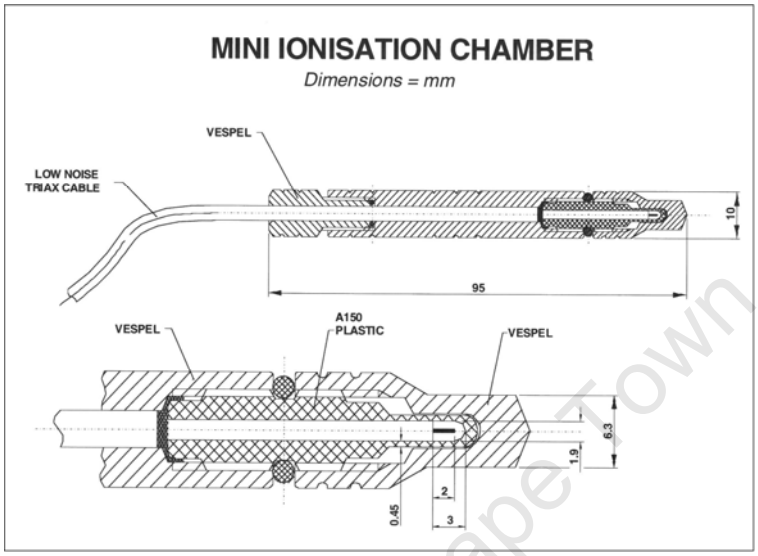

Figure 2.6: The Mini Ionization Chamber (picture used with permission)

The chamber has an active volume of 0.0067 cm^3 and was originally designed for dose distribution measurements in a clinical proton beam, but can also be used for photon dose distribution measurements. It is a waterproof chamber and can thus be used for measurements in water.

2.4 Charged Particle Equilibrium

According to Attix (1983) "Charged particle equilibrium (CPE) exists with respect to volume V if each charged particle of a given type and energy leaving V is replaced by an identical particle of the same energy entering".

The ICRU (1980) said "Charged particle equilibrium exists if the energies, number and direction of the charged particles are constant throughout the volume of interest", or in other words, CPE exists only at a point where the fluence of the charged particles in the immediate vicinity of that point is constant. That means that charged

particle equilibrium exists in a certain direction if the maximum distance of penetration of the released charged particles is less than or equal to the thickness of the medium covering the point of interest.

There are four basic causes for CPE failure in an indirectly ionizing radiation field (Attix, 1986):

- inhomogeneity of the atomic composition within a volume of interest
- inhomogeneity of density within a volume of interest
- non-uniformity of the radiation field
- presence of a non-homogeneous electric or magnetic field within the volume of interest

When a photon beam enters a uniform medium, CPE is established for the first time in the region where the maximum dose occurs. This depth of maximum dose thus corresponds approximately to the average range of the charged particles in the forward direction, i.e. the direction of the beam. For the 6 MV photon beam of the Philips SL 75-5 LINAC this depth is approximately 1.5 cm. According to the AAPM TG 21 protocol (1983), as well as the IAEA TRS 398 protocol (2000), absorbed dose measurements must take place under full charged particle equilibrium, i.e. forward and lateral charged particle equilibrium. The AAPM TG 21 report (1983) recommends that exposure-calibrated ionization chambers used in high-energy dosimetry should be regarded as Bragg-Gray cavities in dosimetry phantoms. Ideally all of the ionization of the gas in the cavity is due to electrons that arise in the phantom material, and the dose to phantom is related to the dose to gas by the ratio of their average stopping powers. The dose from interactions in the detector material should be negligible (Ma & Nahum, 1991). The IAEA TRS 398 protocol (2000)

insists that the primary standard ionization chamber should "fulfill as far as possible the requirements of a Bragg-Gray detector."

Ma & Nahum (1991) confirmed that the Bragg-Gray cavity theory can safely be applied to megavoltage photon radiation dosimetry.

Satisfying the condition of uniform charged particle fluence is strictly impossible for photon beams because of beam divergence and photon attenuation (AAPM Report 85, 2004).

"Transient charged particle equilibrium" is achievable along the central axis in a uniform absorber at depths greater than the maximum forward range of the released electrons, provided that the radius of the radiation field also exceeds the maximum lateral range of the released electrons (AAPM Report 85, 2004). Dose is being deposited by electrons originating upstream relative to the point of interest; therefore the dose is greater than the kerma in the region of transient electron equilibrium (Loevinger, 1981). Transient charged particle equilibrium exists at all points in a region where the dose is proportional to the kerma, with a proportionality constant greater than 1 (Attix, 1986).

2.5 Lateral Range of Charged Particles

For small fields the dose on the central axis is progressively reduced due to lateral electron disequilibrium, i.e. the lateral range (λ) of the secondary electrons starts to exceed the dimensions of the beam cross-section (Bjärngard, 1990 and Solberg *et al.*, 1995). In order to do narrow-beam measurements (see Chapter 2.7 for definition) it is important to know for what field dimensions lateral charged particle equilibrium is obtained or violated.

The formulas that describe Compton scatter (Equations 2.1, 2.2 and 2.3 in Chapter 2.2.3) can be solved for the energy of the scattered electron at a specific scattering angle. The electron range tables in Attix (1986) or Berger & Seltzer (1982) give the range of an electron at a specific energy in water. The lateral component of the range is shown in Figure 2.7.

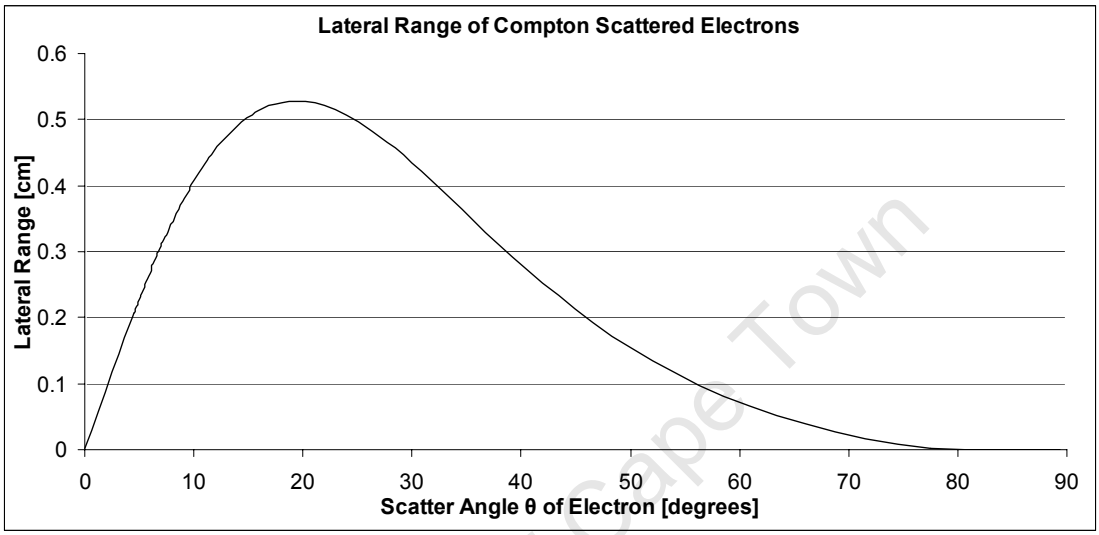

Figure 2.7: Lateral Range of Compton Scattered Electrons

It can be seen that the maximum lateral range of electrons liberated by 6 MV photons is about 0.53 cm in water.

2.6 Primary and Scattered Dose Components

When studying photon beams in absorbing medium, photons interacting within the medium for the first time are often treated separately from photons that have interacted more than once (Nizin, 1993). Primary dose is due to secondary electrons set in motion by primary photons only (Johns & Cunningham, 1983, Mohan & Chui, 1985, Bjärngard & Cunningham, 1986).

The scattered component is that part of the dose which is deposited by photons which have interacted at least once in the medium.

$$D_T(d,r) = D_p(d) + D_s(d,r) \qquad (2.4)$$

The total dose (D_T) is given by the sum of the primary (D_p) and scattered (D_s) components (AAPM Report 85, 2004), where r refers to the field radius and d to the depth in the phantom.

For high-energy X-ray beams, the scatter of photons is primarily single Compton-scattering events (Zhu & Bjärngard, 2003). Du Plessis (2009) presented a semi-qualitative argument to show that first scatter events are most dominant:

First scattered photons S_1 can be approximated by $S_1 = \mu \cdot P$, where P represents the primary photons. Approximately $\mu \cdot S_1$ of the first scattered photons will undergo second scatter. This amounts to $\mu^2 \cdot P$ of the primary photons that will undergo a second scatter interaction. The ratio of first to second scatter is then: $\frac{\mu \cdot P}{\mu^2 \cdot P} = \frac{1}{\mu}$.

For a 6 MV beam where $\mu \approx 0.04$ cm^{-1}, $\frac{1}{\mu} = 25$. Thus the first scatter photons outweigh the second scatter photons 25 to 1.

The photons which are incident upon the surface of the phantom are called primary photons. Some of those photons have traveled directly from the radiation source; others have been produced as a result of interactions within the treatment head, like scatter from the target, flattening filter and collimators (Luxton & Astrahan, 1988). Bjärngard & Cunningham (1986) write: "Photons that have been scattered in the head of the radiation-producing machine are traditionally included in the primary component. So far this has served as an acceptable approximation…"

If the head-scattered photons are included in the effective primary dose, then D_p becomes field size dependent. To remove the field size dependence, the effective primary dose must be divided by the collimator scatter correction factor (see Chapter 6.1.1).

Under full equilibrium conditions the primary beam has a radius equal to the lateral range of the released electrons. In very narrow beams and at shallow depths in the phantom the absorbed dose changes rapidly with beam radius r and the depth in the phantom d. This is attributed to a reduction in the photon fluence (AAPM Report 85, 2004), as well as the absence of lateral electronic equilibrium in radiation fields which are smaller than the maximum range of secondary electrons (Nizin, 1993). In such conditions, the primary dose can be used to model the total absorbed dose as a first approximation (Nizin, 1993).

Nizin and Chang (1991) show that under condition of lateral electronic disequilibrium the primary dose $D_p(r)$ for depths greater than the depth of maximum dose is a simple function of beam radius r: $D_p(r) = D_p(\lambda)\cdot(1-e^{-\gamma\cdot r})$, where $D_p(\lambda)$ is the primary dose in broad beams for which complete lateral electron equilibrium exists, λ is the threshold radius for electronic equilibrium/disequilibrium transition and γ (the lateral build-up coefficient for beam radii between 0 and λ) depends on photon energy and absorbing medium. They found a value for the lateral build-up coefficient of $\gamma = 2.572\ cm^{-1}$ for 6 MV photons using Monte-Carlo generated data from mono-energetic photons in beams of radii $0.006\ cm < r < 5.0\ cm$. Nizin (1999) later went on to develop a model for central-axis absorbed dose in therapeutic photon beams, including lateral electronic disequilibrium, using this expression for $D_p(r)$.

2.7 Narrow-Beam vs. Broad-Beam Geometry

Narrow-beam geometry refers to an experimental setup that is designed to exclude scattered photons from being measured by the detector. In broad-beam geometry the cross-section of the beam is wide enough that a significant fraction of the scattered photons remain in the beam. The scattered photons that remain in the beam will get measured by the detector and this results in an underestimation of the attenuation (Van Dyk, 1986, Bushberg *et al*., 2002).

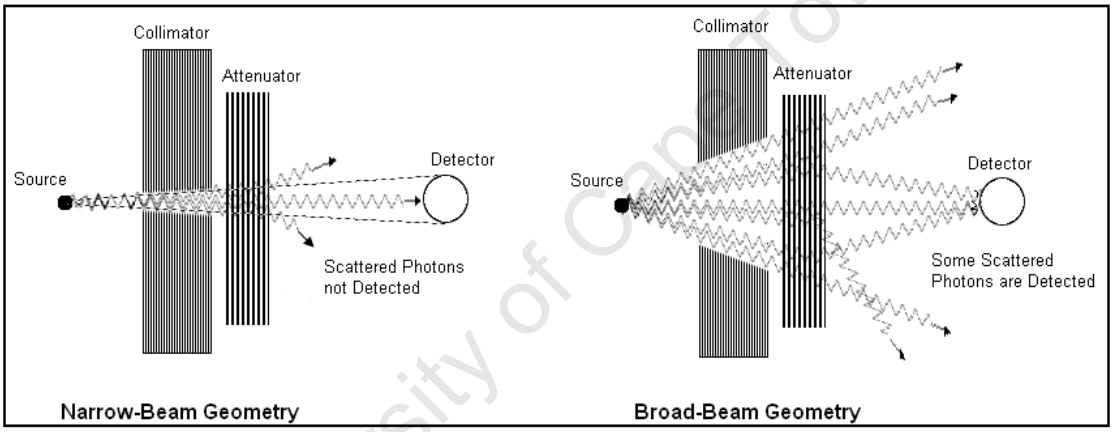

Figure 2.8: Narrow-Beam and Broad-Beam Geometry

2.8 Definitions

2.8.1 Source-Surface Distance (SSD) and Source-Axis Distance (SAD)

For the Philips SL75-5 LINAC the distance from the target of bremsstrahlung production to the isocenter of the treatment unit is 100 cm.

In **Fixed-SSD** setups the surface of the phantom lies at the isocenter of the treatment unit. Percentage Depth-Doses (see definition in Chapter 2.8.2) are measured using a setup like this. In this case the fieldsize is also defined on the surface of the phantom and the SSD = 100 cm.

In **isocentric** setups the SAD, i.e. the distance from the source to the axis of gantry rotation, is fixed at 100 cm. The isocenter does not have to lie on the surface of the phantom as in a fixed-SSD setup, but can be at any depth in the phantom. The fieldsize is defined at the isocenter. Tissue-Air Ratios (see Chapter 2.8.3), Tissue-Phantom Ratios and Tissue-Maximum Ratios (see Chapter 2.8.4) are measured in an isocentric setup

2.8.2 (Central Axis) Percentage Depth-Dose (PDD or CAXPDD)

For standard SSD techniques, the basic concept used to characterize central ray dose distributions in beam therapy is the percentage depth dose (PDD) (Van de Geijn & Fraass, 1984).

Dawson (1976) writes: “The accurate measurement of percentage depth doses for any radio-therapeutic device is essential for good treatment planning”.

The Percentage Depth-Dose (PDD) is defined as the quotient, expressed as a percentage, of the absorbed dose on the central axis at any depth d to the absorbed dose at depth of maximum dose d_{max} (Khan, 2003).

$$PDD = \frac{D_d}{D_{d_{max}}} \cdot 100 \qquad (2.5)$$

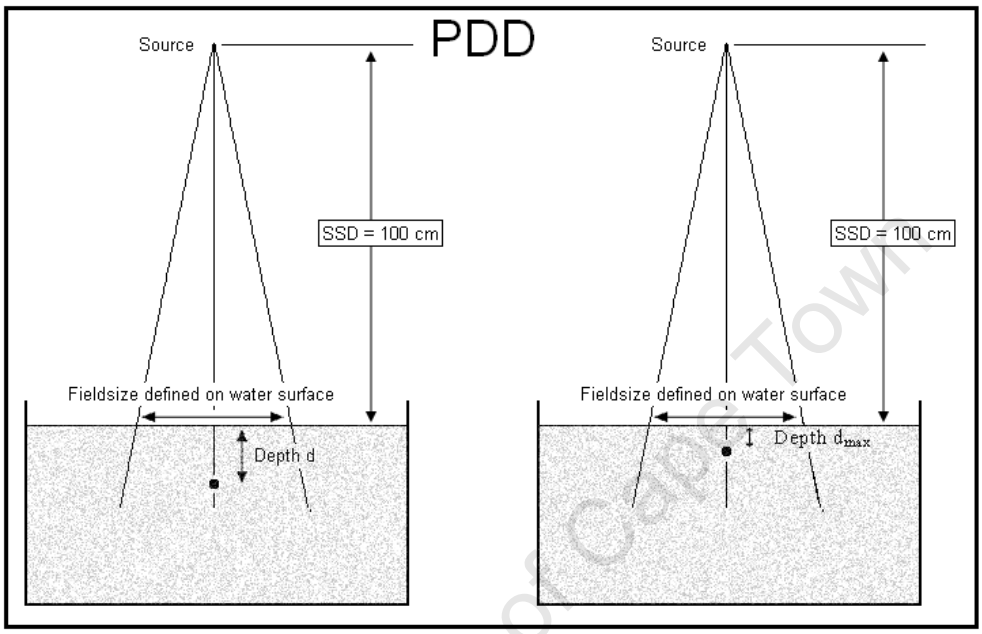

Figure 2.9: Definition of PDD

The percentage depth dose curves are affected by various factors (Hering, 1996):

- the energy of the radiation: higher energy beams have more penetrating power
- the field size: the PDD increases with field area (see Figure 2.10)
- the field shape: a round field with the same area as a square field will have a higher PDD than the square field, and a square field with the same area as a rectangular field will have a higher PDD than the rectangular field.
- the thickness of the underlying medium: backscattered components add dose to the point of interest
- the SSD: the PDD increases with an increase in SSD

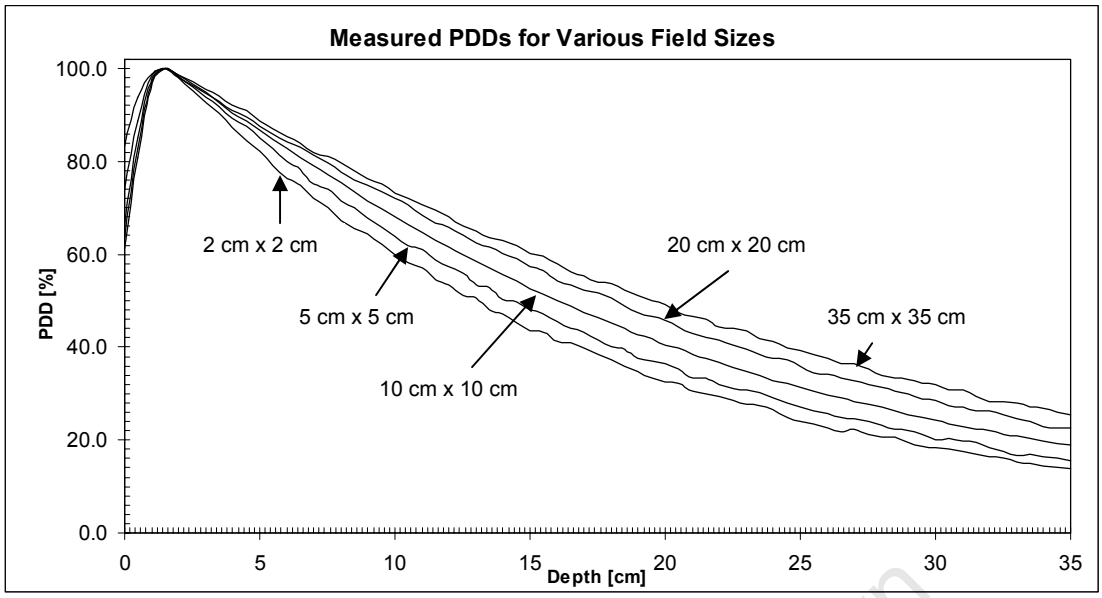

Figure 2.10: Measured PDDs (SL75-5 LINAC at iThemba LABS)

The dose at the surface of the phantom rises linearly with field size (Bjärngard *et al.*, 1994) and is also shown in Figure 2.11.

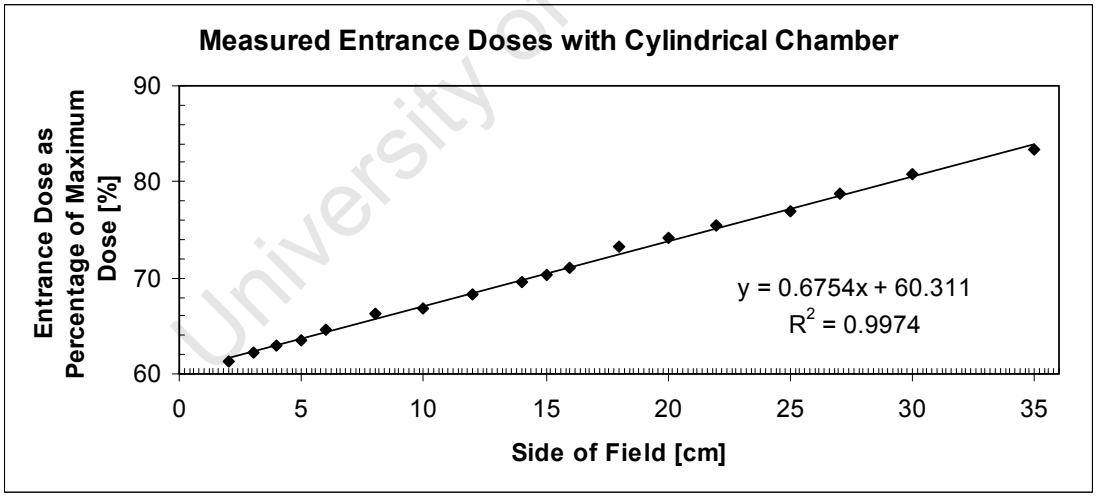

Figure 2.11: Measured Entrance Doses with a Cylindrical Chamber (SL75-5 LINAC at iThemba LABS)

However, the measured surface doses are much too high, because the PDDs were measured with a cylindrical ionization chamber. Unfortunately no waterproof parallel plate chamber was available.

Dose is only imparted when charged particles are released. Thus the dose at the surface of a phantom should be very low, because only very few electrons are present to add dose (Hering, 1996).

Velkley *et al.* (1975) showed that it is best to use extrapolation chambers to measure photon entrance and build-up doses in beams with maximum energy ranging from 1.2 to 25 MV. They measured entrance doses of 14% for a 4 MV beam at an SSD of 80 cm and 13% for a 8 MV beam at an SSD of 100 cm, both for 10 cm x 10 cm field sizes.

Nilsson & Montelius (1986) also recommend that extrapolation chambers should be used for dose measurements under non-equilibrium conditions.

Tannous *et al.* (1981) used a fixed volume parallel plate ionization chamber and corrected to zero-chamber volume to measure the skin-dose in a 6 MV beam. They found the skin dose to be 13% for a 10 cm x 10 cm field; TLD measurements yielded a skin dose of 20% in the same beam for the same field size.

Gerbi and Khan (1990) found that their fixed-separation plane-parallel ionization chamber over-responded at the phantom surface and found a surface dose that was more than 10% higher than that indicated by an extrapolation chamber. TLD chips used in the same 6 MV beam indicated a surface dose that was 12% too high, but TLD powder was within 3% of the extrapolation chamber's results.

Butson *et al.* (1999 and 2004) described a radiochromic film extrapolation method for the measurement of surface dose and found the surface dose in a 6 MV beam for a 10 cm x 10 cm field to be 15% ± 2%, for a 20 cm x 20 cm field to be 29% ± 3% and for a 30 cm x 30 cm field to be 38% ± 3%.

Bagne (1974) claimed that an increase in the dose in the build-up region that was observed for decreasing SAD in a 45 MV beam was due to low energy photons scattered by the collimator.

Biggs and Ling (1979) placed a sweeping magnet just below the treatment head of a linear accelerator and showed that the dose in the build-up region is continually reduced as the magnetic field is increased, until a point is reached where no further reduction is observed. Their results showed that electrons are the primary cause of dose increase in the build-up region.

Ling *et al.* (1982) used an electromagnet to separate out contaminant electrons and photons in a 10 MV beam and came to the conclusion that the increase in surface and build-up dose can be primarily attributed to scattered electrons originating in the treatment head of the LINAC.

Petti *et al.* (1983) found a decrease in build-up dose when electrons were eliminated from the beam. They arrived at this conclusion using Monte Carlo techniques and comparing their results with measured data.

LaRiviere (1983) did measurements of surface dose in air and in helium in a 6 MV beam and found that for a 10 cm x 10 cm beam the surface dose is 13.4% of the dose at maximum depth in air and only 10.9% in helium. He came to the conclusion that the surface dose increase due to air generated electrons is at least 2.5% for a 10 cm x 10 cm field and more for larger field sizes.

Attix (1983) also found a "marked reduction in beam contamination in every case" when exchanging air for helium in a Co-60 beam.

Jursinic *et al*. (1996) used a light-weight electromagnet with a field strength up to 0.1500 T to sweep electrons out of a 10 cm x 10 cm field and found that secondary contamination electrons (i.e. electrons caused by interactions of the primary X-rays

before entering the patient or phantom) produced 18% of the surface dose in a 6 MV photon beam. They found the total surface dose to be 16.7% of the dose at d_{max}, of which 13.7% is the portion of the total surface dose due to X-rays and 3.0% the portion of the total surface dose due to electrons. The application of the magnetic field also caused a decrease in the absolute dose at the depth of maximum dose.

Purdy (1986) measured the surface dose in a 6 MV beam using a fixed volume parallel-plate ionization chamber at an SSD of 100 cm. He found the surface dose measurements ranged from about 8% of the maximum dose for a 5 cm x 5 cm field to 36% for a 40 cm x 40 cm field.

After the dose enters the phantom there is an initial dose build-up up to a maximum at a depth of about 1.5 cm for the 6 MV beam of the Philips SL75-5 LINAC. This build-up happens because the number of ejected electrons increases (and thus the dose increases), until an equilibrium is reached between produced and absorbed electrons (Hering, 1996). Also, the released charged particles have relatively long ranges (the range is about equal to d_{max}) and can deposit dose a distance away from where they were released (Podgorsak, 2005). The photon fluence decreases continuously with depth and at depths greater than that equilibrium depth so does the production of electrons. At that depth the attenuation of the photons as well as the inverse square law become more important than the added dose due to the electrons and the depth dose curve starts to decrease exponentially.

Almond (1970) found that the depth of maximum dose is field size dependent in a 25 MV linear accelerator.

Van Dyk (1977) found a shift in d_{max} with field size and changing SSD for a 10 MV beam.

Padikal & Deye (1978) claimed that in a 10 MV beam the shift in d_{max} with field size is due to a relative enhancement in the soft X-ray component as the collimator jaws are opened.

Arcovito *et al.* (1985) found that for a given beam energy d_{max} increases with field size for narrow beams, reaches a maximum and then decreases with increasing field size. Sixel & Podgorsak (1994) found similar results for 6 MV, 10 MV and 18 MV X-ray beams. They say that for small fields (1 cm x 1 cm to about 5 cm x 5 cm) the increase in d_{max} is attributed to variations in dose deposition by electrons originating in the phantom, while for large fields the decrease in d_{max} with increasing field size has been attributed to scattered electrons generated in the machine head (Sixel & Podgorsak, 1993, Biggs & Ling, 1979).

Abdulla *et al*. (2002) found that d_{max} in a 6 MV beam increases for a 10 cm x 10 cm field compared to a 5 x 5 cm^2 field using Ge-doped optical fibre.

Thomadsen *et al.* (1993) says that while TMRs for Co-60 treatment units have been shown to be independent of the SAD, high-energy photon beams demonstrate variations in their TMR as a function of SAD. He concluded that for a 24 MV X-ray beam the variations in the peak depth and the shallow-depth values of the TPR observed with changes in the SDD originate solely from secondary electron contamination in the photon beam.

However, Sixel and Podgorsak (1994) also say that while the energy dependence of d_{max} is of major clinical importance, the field size dependence is relatively unimportant and generally ignored in standard radiotherapy. It is therefore not taken into account in this thesis, either.

2.8.3 Tissue-Air Ratio (TAR)

Tissue-air ratio was first introduced by Johns *et al*. in 1953 (Johns *et al*., 1953) and was originally called the "tumor-air ratio". This quantity was intended for rotation therapy calculations, where the radiation source moves in a circle around the axis of rotation. Although the source-surface distance (SSD) may vary depending on the shape of the surface contour, the source-axis distance (SAD) remains constant. Since the percentage depth dose depends on the SSD, a correction factor would have to be applied for each SSD. The TAR was introduced to remove the SSD dependence. Tissue-air ratio is defined as the ratio of the dose at a given point in the phantom to the dose in free space at the same point.

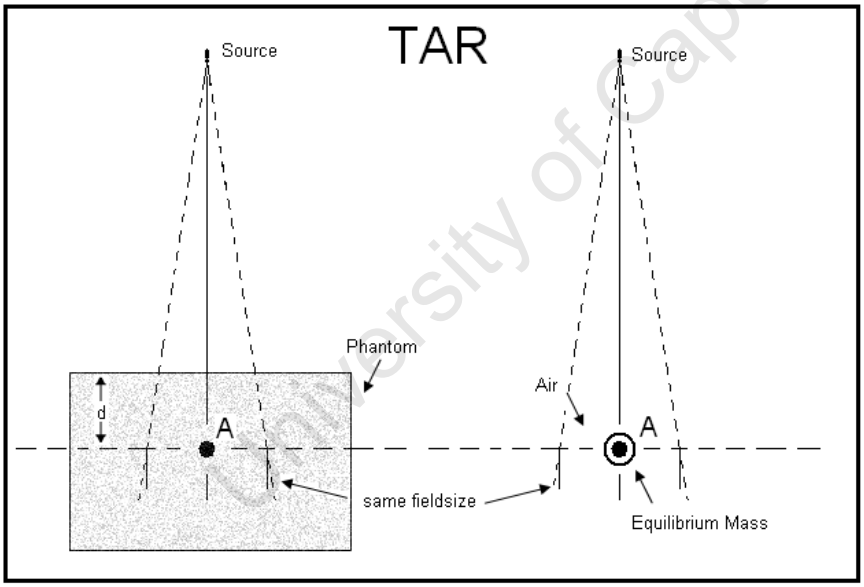

Figure 2.12: TAR

$$\mathrm{TAR}\,(d,S) = \frac{\text{Total dose at A}}{\text{Dose at A due to primary radiation only}} \qquad (2.6)$$

For a given beam quality, the TAR depends on the depth d and the field size at that depth. The absorbed dose due to primary radiation only can be measured with an ion chamber freely suspended in air, but with a build-up cap just big enough to provide charged particle equilibrium at the point of measurement.

2.8.4 Tissue-Maximum Ratio (TMR) and Tissue-Phantom Ratio (TPR)

For isocentric treatment techniques the basic concept to characterize the central-axis dose distribution is the TAR, or for beams above a few MV the TMR or TPR (Van de Geijn & Fraass, 1984).

The Tissue-Maximum Ratio (TMR) was first introduced by Holt *et al*. (1970) and revised by Khan *et al*. (1980) to retain the properties of the TAR, but instead of doing all the measurements in air, they are done in a phantom.

The TMR is defined as the ratio between the absorbed dose in a phantom at a certain depth d and field size S_d at that depth, and the absorbed dose at the same point but at a fixed depth d_{max} in the phantom, where d_{max} is the depth of the maximum dose (Khan *et al*., 1980). According to Figure 2.13, the TMR is expressed as (Burns, 1983):

$$TMR\,(d, S_d) = \frac{\text{Total dose at A}}{\text{Total dose at B}} \tag{2.7}$$

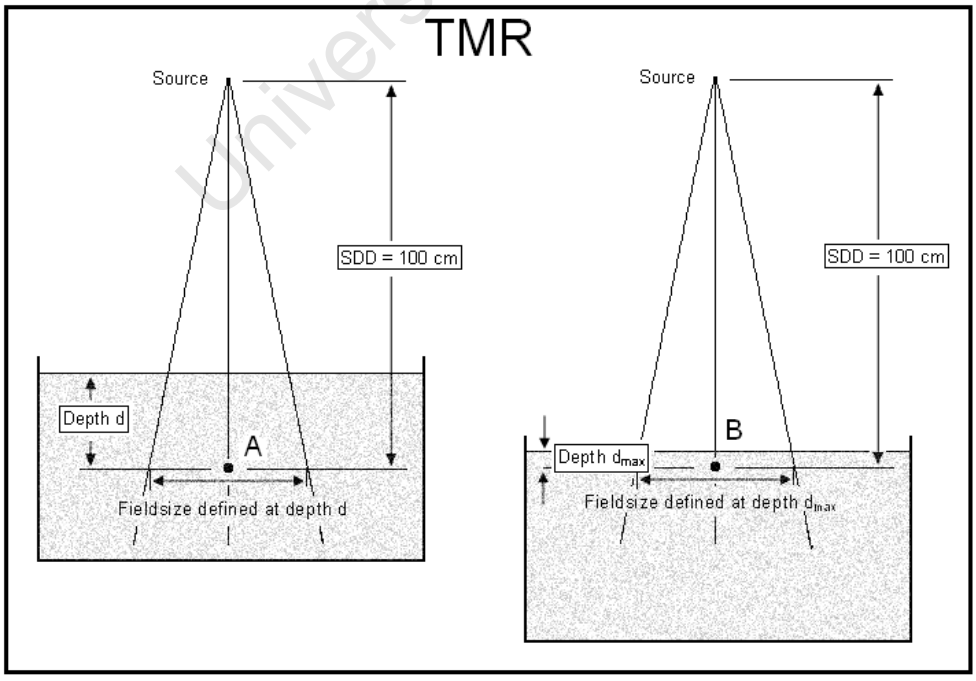

Figure 2.13: TMR

If the reference depth d_{ref} is not d_{max} but a different depth, then the ratio of the doses at depth d and at depth d_{ref} is known as the tissue-phantom ratio (TPR). The TPR was originally defined by Karzmark *et al*. (1965). Thus, the TMR is a special case of the TPR.

TAR, TMR and TPR can be determined from actual measurements, or tables can be derived from PDD data (Purdy, 1977, Paul *et al*., 1983, van de Geijn & Fraass, 1984, Bjärngard *et al*., 1996, Burns, 1983, Burns, 1996).

However, the main factor to take into account when converting from percentage depth doses to tissue-phantom ratios accounts for the different source-detector distances in each setup and is based on the inverse-square law (Bjärngard *et al*., 1996). By using only this factor one can get an accuracy of about 1.0 % for high-energy X-ray beams, provided the normalization depth is at the depth of maximum dose or deeper (Paul *et al*., 1983, Lovelock *et al.*, 1994).

The conversion as given by Khan *et al*. (1980), using their notation, is:

$$TMR(d,r_d) = \frac{PDD(d,r,f)}{100} \cdot \left(\frac{f+d}{f+d_{max}} \right)^2 \cdot \left(\frac{S_p(r_{d_{max}})}{S_p(r_d)} \right) \qquad (2.8)$$

where $TMR(d,r_d)$ is the tissue-maximum ratio at depth d and field size r_d at that point, PDD(d,r,f) is the percentage depth dose at depth d, with field size r defined on the surface of the phantom at an SSD = f,

$\left(\frac{f+d}{f+d_{max}} \right)^2$ is an inverse square correction factor,

$S_p(r_{d_{max}})$ is the phantom scatter correction factor (see Chapter 6.1.3) for the field size at $f + d_{max}$,

and $S_p(r_d)$ is the phantom scatter correction factor for the field size at f + d.

Various reference points have been described in literature:

Bagne (1979) proposed the normalization point to be "the depth of transient charged particle equilibrium". This point is determined by plotting the normalized percentage depth doses at an infinite SSD on semi-logarithmic paper and "the extrapolation of the straight portion of the curve at 100% dose corresponds to the depth of transient charged particle equilibrium". This point lies a little deeper than the depth of maximum dose, but has never caught on as reference point.

Karzmark *et al*. (1965) suggested a reference depth of 5 cm for phantom measurements.

Khan *et al*. (1980) proposed a reference depth equal to the maximum depth of maximum dose, since d_{max} is field size dependent.

Day (1983) proposed the depth of maximum dose in a 10 cm x 10 cm field to be the normalization depth. Sätherberg *et al*. (1996) confirmed that the depth most commonly used for normalization is the depth of dose maximum.

Ten Haken (1995) suggests "that there are much better places to normalize doses than at the depth of maximum dose". He suggests using a TPR setup with a normalization depth of 10 cm for photon beams up to 25 MV.

Sjögren *et al*. (1997) proposed a reference depth of 10 cm for all megavoltage beam qualities up to 50 MV. The quality index is given by: QI = TPR_{10}^{20} in a 10 cm x 10 cm beam.

The NCS Report 12 (1998) uses a reference depth of 10 cm, regardless of photon beam quality. Van Gasteren *et al*. (1990) used a reference depth of 5 cm for beams with a quality index up to 0.75, and a depth of 10 cm for beams with a quality index larger than 0.75. The IAEA TRS 398 protocol (2000) recommends a measurement

depth for the determination of absorbed dose of either 5 cm or 10 cm in water for beams of quality index QI < 0.7, and a reference depth of 10 cm for beams of QI ≥ 0.7.

2.8.5 Peak Scatter Factor (PSF), Scatter-Air Ratio (SAR) and Scatter-Maximum Ratio (SMR)

The peak scatter factor (PSF), sometimes also known as the backscatter factor (BSF), is simply the tissue-air ratio at the depth of maximum dose on the central axis of the beam. It can be defined as the ratio of the dose on the central axis at the depth of maximum dose and the dose at the same point in free space, i.e. the primary dose in the same field. (Khan, 2003)

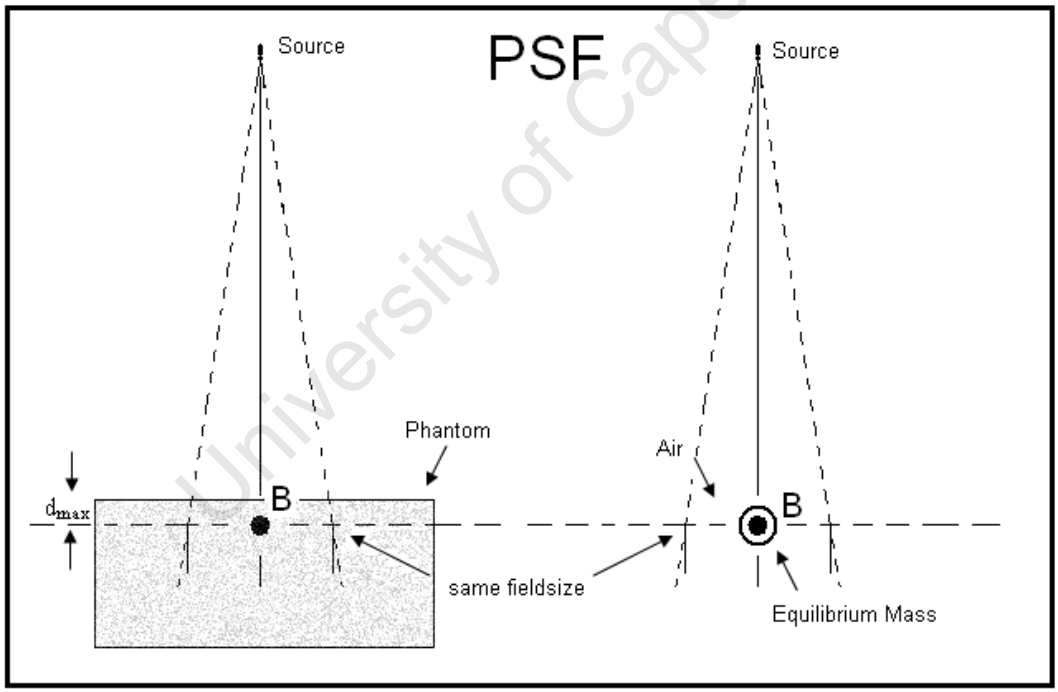

Figure 2.14: Peak Scatter Factor

$$\text{PSF (S)} = \frac{\text{Total dose at B}}{\text{Dose at B from primary radiation only}} \qquad (2.9)$$

The PSF obtained in this work are shown in Appendix C.

Scatter-air ratios are used for the purpose of calculating scattered dose in a medium. The SAR can be defined as the ratio of the scattered dose at a given point in a phantom to the dose in free space at the same point. The SAR is independent of the SSD, but depends on beam energy, depth and field size (Cunningham, 1972).
The scattered dose at a point in the medium is equal to the total dose minus the primary dose at that point, thus:

$$SAR(d,S) = TAR(d,S) - TAR(d,0) \tag{2.10}$$

where TAR(d,0) represents the primary component of the beam. (Cunningham, 1972 and Khan, 2003)

The scatter-maximum ratio is also a quantity designed for the calculation of scattered dose in a medium. Holt (1972) defined the scatter-maximum ratio as the difference of TMR for a given field and the TMR for the 0 cm x 0 cm field for the same depth. When the SMR is defined like this, then its value is zero at the depth of maximum dose for all field sizes and does not represent true scattered dose.

$$SMR(d,S) = TMR(d,S) - TMR(d,0) \tag{2.11}$$

Khan *et al*. (1980) revisited the SMR and defined it as the ratio of the scattered dose at a given point in the phantom to the effective primary dose at the same point at the reference depth of maximum dose.
Khan *et al*. redefined the SMR as:

$$SMR(d,S) = TMR(d,S)\cdot\frac{S_p(S)}{S_p(0)} - TMR(d,0) \tag{2.12}$$

where $S_p(S)$ and $S_p(0)$ are the phantom scatter correction factors (see Chapter 6.1.3) at field size S and field size 0.

If it is assumed that the dose in air has no scatter contribution from the build-up cap, then the SMR as Khan *et al*. (1980) defined it is identical to the SAR.

2.8.6 Scatter-Primary Ratio

The scatter primary ratio is defined as the ratio between the scattered and primary dose components and can be expressed as:

$$SPR\ (d,S) = \frac{D_s(d,S)}{D_p(d)} \tag{2.13}$$

The scatter-primary ratio is looked at in more detail in Chapter 6.3.

2.9 Energy of the Linear Accelerator

Various factors determine the penetrating properties of an X-ray beam (Zefkili *et* al., 1994 and Jordan, 1996)

- the energy/spectrum of the accelerated electrons
- the atomic composition and thickness of the target
- possible added filtration (e.g. beam flattening filter)
- the design of the beam defining/collimating system (e.g. some systems may have less electron contamination than others)

The quality of a radiation beam refers to its energy spectral distribution. It is quite useful to be able to characterize a photon beam by its nominal MV (Jordan, 1996). However, it became clear that nominal MV was no longer a sufficient specification of radiation beam quality (Greene and Williams, 1983).

Coffey *et al*. (1980) described the beam quality of a 6 MV photon beam from a Varian Clinac 6-100 in terms of half value layers (HVL) in lead, saying that the first HVL = 12.0 mm and the second HVL = 13.0 mm. However, the attenuation of photons is not strongly dependent on photon energy in the 2 - 43 MV energy range, so

the use of HVL is not an adequate index of radiation quality (Greene and Williams, 1983).

Greene and Williams (1983) selected d_{80}, the depth to a dose level of 80% in a 10 cm x 10 cm field as the index of radiation quality. Other depths which have been used to characterize a beam in terms of a single point are d_{50}, the depth to a dose level of 50%, the percentage dose at a depth of 10 cm (D_{10}) (AAPM TG51, 1999) and even the depth of dose maximum (d_{max}) (Jordan, 1996).

Brahme & Svensson (1979) were the first to quantitate beam quality using the ratio of absorbed dose at depths of 10 cm and 20 cm with constant SSD, ($\frac{PDD_{10}}{PDD_{20}}$). They also suggested the possible use of $\frac{PDD_5}{PDD_{10}}$ for beam energies below 10 MV.

A number of dosimetry protocols use the ratio of the dose at 20 cm to the dose at 10 cm deep in water for a 10 cm x 10 cm field at a constant source-detector distance, ($\frac{TPR_{20}}{TPR_{10}}$). These include the "Code of practice for high-energy photon therapy dosimetry based on the NPL absorbed dose calibration service" (NPL, 1990), the TG21 protocol (1983), as well as the IAEA TRS398 protocol (2000).

Followil *et al*. (1998) found that the $\frac{TPR_{20}}{TPR_{10}}$ and the $\frac{PDD_{20}}{PDD_{10}}$ are closely related by the following formula:

$$\frac{TPR_{20}}{TPR_{10}} = 1.2661 \cdot \frac{PDD_{20}}{PDD_{10}} - 0.0595 \qquad (2.14)$$

They used data from 685 photon beams ranging from 4-25MV. All the differences were within 2%.

For advantages and disadvantages of the various beam quality specifiers the reader is referred to Kosunen and Rogers (1993), Jordan (1996) and the IAEA TRS398

protocol (2000). The depth of the 80% dose level has not been generally adopted, while the $\frac{TPR_{20}}{TPR_{10}}$ has been widely used (Jordan, 1996). The percentage dose at 10 cm deep seems to be preferred by manufacturers (Jordan, 1996).

Brahme and Svensson (1979) propose that the effective attenuation coefficient ("practical attenuation coefficient") of the beam can be approximated by:

$$\mu\ [cm^{-1}] = 0.1 \cdot \ln\left(\frac{PDD_{10}}{PDD_{20}}\right) \text{ in a 10 cm x 10 cm field.} \quad (2.15)$$

Using the data from the 6 MV beam in this work, the obtained values for μ are (see Appendix B for PDD data):

$\mu = 0.0520\ cm^{-1}$ using equation 2.15

$\mu = 0.0516\ cm^{-1}$ fitting an exponential curve to the 10 cm x 10 cm PDD data.

Brahme and Andreo (1986) found that the mean attenuation coefficient, $\bar{\mu}$, of the photon spectrum can be described by: $\bar{\mu}\ [cm^{-1}] = 0.1 \cdot \ln\left(\frac{TPR_{10}}{TPR_{20}}\right)$. (2.16)

$\bar{\mu}$ for the beam in a 10 cm x 10 cm field has been used as a quality descriptor (Andreo & Brahme, 1986). As the field sizes become smaller $\bar{\mu}$ approximates the narrow beam attenuation coefficient. Using the values of $\frac{TPR_{10}}{TPR_{20}}$ $(= \frac{TMR_{10}}{TMR_{20}})$ from this work gives (see Appendix C: TMR data):

$\bar{\mu} = 0.0378\ cm^{-1}$ for a 10 cm x 10 cm field

$\bar{\mu} = 0.0439\ cm^{-1}$ for a 4 cm x 4 cm field

$\bar{\mu} = 0.0449\ cm^{-1}$ for a 3 cm x 3 cm field

$\bar{\mu} = 0.0464\ cm^{-1}$ for a 2 cm x 2 cm field

For small field sizes the obtained $\bar{\mu}$ approximates the value of the primary linear attenuation coefficient obtained in this work.

Greene & Williams (1983) give d_{80} for a typical 6 MV beam as d_{80} = 6.8 cm, while Jordan (1996) gives d_{80} for a typical 6 MV beam as d_{80} = 6.7 cm and D_{10} = 67.5%.

Various $\frac{TPR_{20}}{TPR_{10}}$ for 6 MV beams in literature are:

Castellanos & Rosenwald (1998): $\frac{TPR_{20}}{TPR_{10}} = 0.683$

Zefkili *et al.* (1994): $\frac{TPR_{20}}{TPR_{10}} = 0.668,\ \frac{TPR_{20}}{TPR_{10}} = 0.683,\ \frac{TPR_{20}}{TPR_{10}} = 0.666$

Jursinic & Mackie (1996): $\frac{TPR_{20}}{TPR_{10}} = 0.678$

Li *et al*. (1995): $\frac{TPR_{20}}{TPR_{10}} = 0.680$

Sätherberg *et al*. (1996): $\frac{TPR_{20}}{TPR_{10}} = 0.689$

Lind (2008): $\frac{TPR_{20}}{TPR_{10}} = 0.681$

The NCS Report 12 (1998) lists 8 different LINACS from 5 different manufacturers with a nominal accelerating potential of 6 MV with a range of $\frac{TPR_{20}}{TPR_{10}}$ from 0.650 to 0.687. In this work d_{80} = 6.7 cm, D_{10} = 68.0% and $\frac{TPR_{20}}{TPR_{10}} = 0.685$.

CHAPTER 3 METHODS OF DETERMINING THE PRIMARY LINEAR ATTENUATION COEFFICIENT

3.1 Extrapolation of Measured Tissue-Maximum Ratios

The separation of the dose into a primary and a scattered component can be formulated as (Cunningham, 1972):

$$TAR(d,S) = TAR(d,0) + SAR(d,S) \quad (3.1)$$

where TAR (d,0) denoted the zero-area TAR at depth d and represents the primary component. SAR (d,S) is the scatter-air ratio at depth d and field size S and is considered to be the scattered component. The primary component of the dose is therefore defined as the dose on the central axis of a zero-area beam.

However, the use of TARs for beams of higher energy than Co-60 has been questioned (Holt *et al*., 1970, Karzmark *et al*., 1965). When the size of the build-up cap required for in-air measurements to obtain charged particle equilibrium "exceeds a few millimeters" (Holt *et al*., 1970), the size of the build-up cap starts to affect the measurements by contributing scatter from the build-up material itself.

It also becomes very difficult to measure the TAR for small field sizes, because it becomes impossible to include the build-up material in the radiation field (Holt *et al*., 1970).

Since the TAR is practically independent on SSD (Khan, 2003), it is possible to do measurements at an extended SSD to include the whole build-up, or to use different build-up cap materials like aluminium, brass, lead or steel to reduce the size of the cap required to achieve charged particle equilibrium (Weber *et al.*, 1997, Luxton and Astrahan, 1988, Kase and Svensson, 1986 and Georg *et al*., 2004).

Another problem is that some or other means of extrapolation is needed to obtain TAR(d,0). Nizin and Mooij (1998) used a quadratic polynomial to extrapolate tissue-air ratios of a ^{60}Co beam with radii < 6 cm to zero-field size.

Holt *et al*. (1970) introduced the tissue-maximum ratio (TMR) and the concept was revisited by Khan *et al*. (1980). Henry (1974) pointed out that if the tissue-phantom ratio was used instead of the tissue-air ratio in dose calculations, then the problem of measuring scattered photons from the "small sample of phantom material used in the 'free-air' measurement" would be avoided.

The TMR is related to the TAR by the PSF. Points A and B in Figures 2.12, 2.13 and 2.14 are the same geometrical point. Thus, a combination of equations 2.6, 2.7 and 2.9 results in:

$$\text{TAR}(d, S) = \frac{\text{Total dose at A}}{\text{Total dose at B}} \cdot \frac{\text{Total dose at B}}{\text{Dose at B from primary radiation only}} \qquad (3.2)$$

or

$$\text{TAR}(d,S) = \text{TMR}(d,S) \cdot \text{PSF}(S) \quad \text{(Burns, 1983 \& 1996)} \qquad (3.3)$$

From this it can be seen that the TMR (d,0) is proportional to the TAR (d,0) and can therefore also be used to determine the primary dose in a radiation beam.

The primary dose at depth d can be expressed as (Khan *et al.*, 1980):

$$D_p(d) = D_R \cdot \text{TMR}(d,0) \qquad (3.4)$$

where D_R is a reference dose which is needed to establish the magnitude of the primary dose relative to the total dose at the reference depth and field size, and TMR(d,0) is the zero area TMR at depth d.

For megavoltage beams, the primary attenuation can be approximately represented by:

$$TMR(d,0) = e^{-\mu_0 \cdot (d - d_{max})} \quad \text{(Paul } \textit{et al.}\text{, 1983, Khan, 2003)} \qquad (3.5)$$

Using TMRs solves the problem encountered with the size of the build-up cap in the TAR measurements. However, an extrapolation to zero field size is still necessary to obtain TMR (d,0). Nizin (1990) writes: "The accuracy of extrapolation depends on the type of function used to approximate an absorbed dose when the field radius r is the only variable, D(r). This essentially means that such a function must closely fit the scatter dose component." Unfortunately the scatter dose component is non-linear and thus accurate determination of the primary dose is fairly problematic.

Godden (1983) writes: "Making the appropriate assumption that log(TAR) varies linearly with depth, an effective linear attenuation coefficient was determined for each small field size using a least-square fit technique. These values were then used to extrapolate to zero area … for the effective linear-attenuation coefficient for zero-area field size."

Since the TMR is related to the TAR by the PSF,

$$TAR(d,S) = TMR(d,S) \cdot PSF(S) \quad \text{(Burns, 1983 \& 1996)} \qquad (3.3)$$

and the PSF(S) is not depth dependent, it should be possible to take a similar approach with the TMRs. Unfortunately, Godden (1983) does not specify what type of extrapolation he used, therefore cubic, fourth order and fifth order polynomials were used to extrapolate the linear attenuation coefficient to zero field size in this work. This was done in Chapter 5.1.

Bjärngard and Petti (1988) introduced a geometrical parameter $z = \frac{r \cdot d}{r + d}$ and showed that for small r and d, where r is the radius of the equivalent circle for the square field S and for $\frac{r}{d}$ = constant, the Scatter Primary Ratio (SPR) is proportional to z for different photon beams and can be expressed as:

$$SPR\ (r,d) = \frac{D_s(r,d)}{D_p(d)} = K \cdot \mu \cdot z \qquad (3.6)$$

where K is a constant and μ is the linear attenuation coefficient for the primary photons. The Scatter Primary Ratio cannot be used to determine μ directly, since the SPR is not directly measurable.

Nizin (1991) modified this Bjärngard-Petti approximation (r/d = constant) for the SPR. He proposed that any set of absorbed doses, measured at a fixed SDD in a relatively small field at depth d, can be expressed as a linear function in z. According to Nizin's modification the dose can be expressed as:

$$D_t\ (z,d) = D_p\ (d) \cdot (1 + K'\mu z) = D_p\ (d) + N(d) \cdot z \qquad (3.7)$$

where K'(d) is a modified proportionality constant and $N(d) = D_p\ (d)\ K'(d)\ \mu$ is constant at a fixed depth and for small field radii r.

He found that for the range of nominal photon energies from Co-60 to 18 MV in water, absorbed dose is linearly proportional to z in fields where lateral electronic equilibrium holds, but with a radius of less than 9 cm within the depth interval $2d_{max} < d \leq 30$ cm. Bjärngard (1994) confirms that the accuracy of this method is limited at small depths.

Nizin *et al*. (1993) confirmed the linearity of his method for a ^{60}Co, 6 MV and 15 MV photon beam with Monte Carlo calculations and found a maximum discrepancy of

~1.5% in primary dose when comparing the two methods, which "is comparable to the calculational accuracy of the Monte Carlo method".

The non-linearity for larger radii can be attributed to the fact that in this model only first-order scatter is accounted for and the attenuation of scattered photons is ignored. As the field size or depth increases the simple proportionality of the SPR to z is no longer sufficiently accurate, but can be written as $SPR = a \cdot z + b \cdot z^2$, where $z = \frac{r \cdot d}{r + d}$ and the coefficients a and b are approximately proportional to μ and μ^3, respectively (Bjärngard & Petti, 1988).

The measurements of TAR and TMR are done at a fixed SDD and are thus independent of the SSD. Therefore, Equation 3.7 can be applied directly to TARs and to TMRs.

Nizin *et al*. (1996) applied Equation 3.7 to TARs to get:

$$TAR(d,z) = TAR(d,0) + N'(d) \cdot z \tag{3.8}$$

In a similar fashion, the TMR at depth d in a field with equivalent radius r can be expressed as:

$$TMR\ (d,z) = TMR\ (d,0) + M(d) \cdot z \tag{3.9}$$

where $M(d) = TMR\ (d,0) \cdot K'(d) \cdot \mu$

This equation is a linear function in z which can be fitted to TMR(d,z) at different depths to yield TMR(d,0) at the corresponding depths.

$TMR\ (d,0) = \frac{D_p(d)}{D_R}$ and as such can be considered as relative $D_p(d)$ values. Fitting an exponential function to the TMR (d,0) data yields μ_0, the linear attenuation coefficient of the primary photons in water.

3.2 Attenuation Measurements

Fluence of radiation (Φ = number of particles per unit area (ICRU report 60, 1998)) decreases as it passes through an absorbing medium in such a way that the change in fluence $\Delta\Phi$ as the radiation passes through a small thickness of absorber Δx is proportional to the thickness of the medium and the incident fluence (Johns & Cunningham, 1983). This can be expressed as (Johns & Cunningham, 1983):

$$\Delta\Phi = -\mu \cdot \Phi \cdot \Delta x \tag{3.10}$$

where μ is the proportionality constant, also known as the linear attenuation coefficient.

If the radiation is homogeneous then μ is constant and integration of the above equation yields:

$$\Phi = \Phi_0 \cdot e^{-\mu \cdot x} \tag{3.11}$$

where Φ_0 is the initial fluence of radiation, x is the thickness of absorber in cm and μ is the linear attenuation coefficient in units of cm^{-1}.

Attenuation measurements should be performed under narrow-beam conditions (see Chapter 2.7). The primary linear attenuation coefficient μ_0 is obtained when the area of the beam approaches zero.

If the shape of the fluence spectrum of a radiation beam does not change significantly when the beam passes through different thicknesses of an absorber, then the above equation can be applied to absorbed dose rather than to fluence measurements. This can be done because the absorbed dose at a point in a medium is proportional to the radiation fluence at that point. Relative absorbed doses are measured more easily and therefore the above assumption is assumed to be true for the 6 MV photon beam.

If μ is based on absorbed dose measurements, the results will depend on field size for a polyenergetic photon spectrum (Bjärngard *et al*., 1989).

It is difficult to obtain a sufficiently narrow beam and do absorbed dose measurements in such narrow beams, so μ was measured as a function of field size S and then extrapolated to obtain μ for a zero field size, as done in van Dyk (1977 & 1986) and Robinson *et al.*(1991).

Van Dyk (1986) suggested that a linear fit can be used on the broad-beam attenuation data as a function of side of square field for the extrapolation. Linear fits, used on data for ^{60}Co to 25 MV beams, "show agreement to 0.5 % on average and 4 % at worst". Robinson *et al.* (1991) applied a third-order polynomial fit to their measured data to obtain μ_0. Therefore a linear, quadratic and a third-order polynomial fit to the data will be used to determine μ_0 in the photon beam.

3.3 The Central Axis Kerma Model

3.3.1 The Central Axis Kerma Model

Pistorius developed a semi-empirical central-axis kerma model, based on convolution techniques, that describes the kerma along the central axis of a therapeutic photon beam. The following description of this model is basically an extraction from the work of Dr Pistorius (1991).

The model is for kerma rather than dose, i.e. charged particle transport is not considered and it is assumed that photons deposit their energy at the site of interaction. It is generally accepted that kerma is proportional to dose beyond the point of charged particle equilibrium and thus the model can be applied to dose distributions at depths greater than d_{max}.

Fitting this model, using a non-linear least squares fitting algorithm, to the measured central axis percentage depth dose data (CAPDD) yields five field size and depth independent fitting parameters of which only one is a pure empirical parameter. The other four fitting parameters all have physical meaning. A major advantage of this model is that it enables the linear attenuation coefficient of the primary component to be obtained without field size extrapolation. This implies that μ_0 may be estimated from the measurement of a single field size although more accurate estimations are obtained if the weighted means of many measurements are taken.

The model writes the kerma as follows:

$$K(s,d) = N(S)\, e^{-\mu(S,d)\cdot d} \cdot G(SSD,d) \tag{3.12}$$

Where K(s,d) is the kerma at depth d in a field size S

N(S) is a normalization factor

μ is an effective attenuation coefficient dependent on both field size and depth

G (SSD,d) is an inverse square correction factor given by

$$G(SSD,d) = \left(\frac{SSD + d_{max}}{SSD + d} \right)^2 \tag{3.13}$$

where SSD is the source-surface distance and d_{max} is the nominal depth of maximum dose.

The main assumptions on which this model is based are:

(1) the photon fluence contains both primary and scattered components

(2) for an infinite SSD (SSD = ∞) the primary fluence is exponentially attenuated

(3) the scattered radiation may be subdivided into forward- and back-scattered components

(4) for a parallel beam under equilibrium conditions and with an effective attenuation coefficient which remains constant with depth, the backscattered component at any depth will be proportional to the fluence moving in the forward direction at that depth

(5) the contribution of the forward scattered fluence may be obtained by the convolution of the primary fluence with a function that describes the spread of the scattered photons, the so-called scatter kernel

(6) for a high energy beam where the scattering is predominantly in the forward direction, the spread function is separable and an exponential function may describe the spread of the forward scattered photons on the central axis

Pistorius confirmed assumption (6) by calculating the first order scattered radiation as a function of field size and depth. He showed that his approximation is best for small field sizes where lateral scattering is less significant.

The conversion of percentage depth dose to an infinite SSD is given by:

$$PDD(SSD = \infty) = PDD(SSD=SAD) * \left[\frac{SSD+ d}{SSD + d_{max}}\right]^2 \quad \text{(Van de Geijn \& Fraass, 1984)} \tag{3.14}$$

Summing the primary, forward- and back-scattered kerma gives the following equation for the total kerma:

$$K(S, d, SSD = \infty) = N_1(S)\, e^{-\mu(S)\cdot d} \cdot [1 - N_2(S) \cdot e^{-\Gamma(S)\cdot d}] \qquad (3.15)$$

With $N_1 = N_p \cdot BSF(S) \cdot \left(\frac{N_s(S) \cdot \eta(S)}{\Gamma(S)} + 1 \right)$

$$N_2 = \frac{N_s(S) \cdot \eta(S)}{N_s(S) \cdot \eta(S) + \Gamma(S)} = \frac{N_s(S)}{N_s(S) + 1 - \frac{\mu(S)}{\eta(S)}}$$

$$\Gamma(S) = \eta(S) - \mu(S)$$

where

N_p = primary kerma normalization

$N_s(S)$ = integral normalization of the scatter kernel

$BSF(S)$ = back-scatter factor

$\mu(S)$ = effective attenuation of primary component

$\eta(S)$ = effective attenuation of scattered component

Because a one-dimensional convolution has been carried out, these parameters are field size dependent. This Equation (3.15) must be written in the form of Equation 3.12 with μ some unknown function of S and d. The factor F (SSD,d) disappears if the kerma is expressed at SSD = ∞.

Pistorius showed with some mathematical manipulation that μ(S,d) may be expressed as:

$$\mu(S,d) = (\mu(\infty) + \Gamma) - d^{-1} \cdot [\ln(C(S) \cdot e^{\Gamma(S)d} - 1) + K'] \qquad (3.16)$$

where K' is a constant of integration and $C = 1/N_2$

This relationship must be defined for all $0 \leq d \leq \infty$. Thus K' = -ln(C(S)-1) and so the equation takes the form:

$$\mu(S,d) = (\mu(\infty) + \Gamma) - d^{-1} \cdot \ln[\{C(S) \cdot e^{\Gamma(S)d} - 1\}/\{C(S)-1\}] \quad (3.17)$$

For d = 0 the numerator and the denominator of the second term are both equal to zero. l'Hospital's rule can be used to establish that in the limit

$$\lim_{d \to 0} \mu(d) = \mu(\infty) - \frac{\Gamma}{C-1}$$

For $d \to \infty$ the $e^{\Gamma(S)d}$ term becomes very large and provided that $C \neq 1$ the limit is given by

$$\lim_{d \to \infty} \mu(d = \infty) = \mu(\infty) \equiv \mu_{\infty}$$

Pistorius goes on to say that if this were a one-dimensional problem the primary attenuation coefficient μ_0 would be equal to μ_∞. The lateral scattering however causes the beam to attenuate more slowly and $\mu_\infty \leq \mu_0$.

He goes on to describe that as the field size increases the effective attenuation co-efficient of the scattered photons decreases. For a non-diverging beam of infinite field size every photon scattered off the central axis will be replaced by a corresponding photon scattered from somewhere else in the medium. Thus the effective attenuation coefficient $\eta(S)$ will approach $\mu_0(S)$ in this limit. Pistorius suggests that μ_0 may be estimated by

$$\mu_0 \approx \frac{\mu_\infty(S)}{1 - N_2(S)} \quad (3.18) \qquad \text{and} \qquad \mu_0 \approx 2\,\eta(S)\,N_2(S) \quad (3.19)$$

It was found that that an additional empirical factor of $F \approx 1$ was required to relate the actual values of μ_0 and $N_2(S)$ (μ_{0act} and $N_2(S)_{act}$) to those estimated by the model (μ_{0est} and $N_2(S)_{est}$), so that the measured data could be represented more accurately by the model.

Thus

$$F = \frac{\mu_{0act}}{\mu_{0est}} \frac{N_2(S)_{est}}{N_2(S)_{act}} \quad \text{and} \quad \eta(S)_{act} = \frac{\mu_{0est}}{2 \cdot N_2(S)_{est}} \cdot F = \frac{\mu_{0act}}{2 \cdot N_2(S)_{act}}$$

and therefore

$$\mu_{0est} = \frac{2 \cdot N_2(S) \cdot \eta(S)}{F} \tag{3.20}$$

The relative scattering fraction $N_2(S)$ was found to be well approximated by

$$N_2(S) = N_\infty \cdot [1 - e^{-\lambda \cdot S}] \tag{3.21}$$

where N_∞ is the asymptotic limit for the scattering fraction for a field of infinite size and λ is an exponential growth function.

In summary, the convolution model can be expressed as:

$$K(S, d, SSD = \infty) = N(S) \cdot e^{-\mu(S,d) \cdot d} \tag{3.22}$$

where $\mu(S,d) = \mu_0 (1 - N_2(S)) + \Gamma(S) - d^{-1} \cdot \ln[\{C(S) \cdot e^{\Gamma(S)d} - 1\}/\{C(S)-1\}]$

$N_2(S) = N_\infty \cdot [1 - e^{-\lambda \cdot S}]$

$C(S) = 1/N_2(S)$

$$\mu_0 = \frac{2 \cdot N_2(S) \cdot \eta(S)}{F}$$

$\Gamma(S) = \eta(S) - \mu_\infty(S)$

$N(S)$ = field size dependent normalizing factor

and the PDDs are corrected for an infinite SSD.

The parameters that are obtained from a non-linear least squares fit of this model to the CAPDD (SSD = ∞) for $d \geq d_{max}$ are:

μ_0 = the primary attenuation coefficient

N_∞ = the relative scattering fraction

λ = the exponential scatter growth factor

N = primary kerma normalization factor

F = empirical scale factor

3.3.2 Equivalent Field Sizes

A further advantage of the kerma model is that it may be used to estimate to equivalent field sizes of fields with circular and rectangular dimensions.

The equivalent field is defined by Day (1983 & 1996) as the standard field which has the same central axis depth-dose characteristics as the given non-standard field. This method is based on the premise that with any given rectangular field it is possible to associate a pre-determined equivalent square or circle, regardless of the radiation quality, depth or SSD.

The equivalent field approach by Day is based on Clarkson's method of scatter integration (1941), as elaborated by Meredith and Neary (1944). They showed that the scatter dose in any field can be calculated from an integration involving the scatter-radius function. The scatter-radius function is given by:

$$S(r) = S_{\infty} \cdot (1 - e^{-\lambda r} - \mu \cdot \lambda \cdot r \cdot e^{-\lambda r}) \qquad (3.23)$$

Where $S(r)$ = central-axis scatter in the field of radius r

S_{∞} = central axis scatter in field of infinite radius

λ is a scale parameter of dimensions length^{-1}

μ is a dimensionless shape parameter lying between 0 and 1

The values chosen for the computation of equivalent squares in Day (1983) are:

$\lambda = 0.26$ cm^{-1} and $\mu = 0.5$

Tatcher and Bjärngard (1993) noted that equivalent squares tend to increase with depth d and therefore let λ in equation 3.23 be a linear function of depth:

$\lambda = 0.26 + a \cdot d$, where a is a constant of value a = -0.0043 cm^{-2}. The empirical scatter-radius function used to generate the equivalent square tables works fairly well up to

depths of 10 cm, but this slight modification resulted in better agreement with measured data.

Bjärngard & Siddon (1982) looked at the scatter function describing the scatter-to-primary ratio and, based on a linearization of the scatter contribution, proved that the radius of an equivalent circular field for a square field with side S is given by:

$$r = 2 \cdot S \cdot \ln(1+\sqrt{2})/\pi = 0.5611 \cdot S \tag{3.24}$$

In an analogous manner, the equivalent square S of a rectangular field of dimensions length L x width W is derived from:

$$S = \frac{2 \cdot LW}{L+W} \cdot \frac{1}{4 \cdot \ln(1+\sqrt{2})} \cdot \left[(1+\frac{L}{W}) \cdot \ln\frac{D+W}{L} + (1+\frac{W}{L}) \cdot \ln\frac{D+L}{W} \right] = \frac{2 \cdot LW}{L+W} \cdot Y \cdot \frac{L}{W} \tag{3.25}$$

where D is the length of the diagonal in the rectangle and Y·(L/W) is defined as the elongation factor which describes the error when using the area-to-perimeter ratio to find the equivalent square of a rectangular field.

The error in this formula is 0.8% if the (L/W) ratio is 1.5, 2.4% when (L/W)=2 and goes up to 12.5% when (L/W)=5.

Thus they conclude that this formula (3.25) can be used over a wide range of elongation ratios although the error increases with elongation ratio.

Equation 3.25 without the elongation correction factor is known as the "area-to-perimeter ratio" and was first used empirically by Sterling *et al*. (1964).

When the standard equivalent field tables were drawn up (Day, 1983), the scatter radius function was used with fixed parameters, so the depth and quality dependence were neglected.

The equivalent field size at a point within a field is defined by Pistorius (1991) as the size of the field of known geometry (square or circular) that has the same effective scatter kernel on the central axis as has the field in question. Pistorius showed that the total scatter contribution falls off exponentially away from the axis on which the scatter occurs. This allows a single energy dependent parameter λ to describe the overall effects of scatter as a function of radius r. The calculations are simpler for circular fields than for square fields, but most measurements are done in square fields. Pistorius developed a method to convert between circular and square fields. The relationship between a square field with side S and its equivalent circular field may be defined in terms of an equivalent radius $r_{eq}(S)$.

The scatter contribution of the square field N(S) is then given by:

$$N(S) = N_{\infty} \cdot [1 - e^{-\lambda \cdot r_{eq}(S)}] \tag{3.26}$$

where N_{∞} refers to the total scatter contribution on the central axis for an infinite field and λ refers to an exponential growth factor as mentioned in the previous section.

An equation for the relationship between S and r_{eq} was derived and takes the form:

$$\frac{S}{r_{eq}} = \frac{2 \cdot (1 + A \cdot (\lambda \cdot S)^{B})}{\frac{4}{\pi} \cdot \ln(1 + \sqrt{2}) + A \cdot (\lambda \cdot S)^{B}} \tag{3.27}$$

with A = 0.0252 ± 0.0004 and B = 1.042 ± 0.004 obtained by non-linear least squares regression (Pistorius, 1991). In this case a beam specific parameter λ, which is obtained from the central axis kerma model, is used to determine r_{eq}. The differences between the r_{eq} obtained using this model or the one's from the standard BJR Supplement 17/25 are small. The BJR equivalent radius is consistently smaller than the equivalent radius obtained using this method, the differences become larger with increasing field size. The largest difference occurs for a 35 cm x 35 cm field, where the difference in r_{eq} between the two methods is 1.4%.

3.4 The Central Axis Attenuator Method

Nizin & Kase (1988) introduced an approach for deriving the primary component of dose from measurements in a megavoltage gamma or X-ray beam. The method was successfully applied in a ^{60}Co beam (Nizin & Kase, 1990). The advantage of his method is that no non-linear extrapolation to zero field size is required. The method is based on the difference in spatial origin of primary and scattered photons. A small attenuator of thickness h is positioned between the source and the detector (Figure 4.8). The idea behind this is that the primary photon fluence will be modified, while the perturbation of the scatter component remains small. This is then also one of the requirements for the attenuator: the attenuator must alter the primary radiation significantly, but at the same time the phantom generated scatter must be negligible. The second requirement is that the radius of the attenuator is greater than $\overline{\lambda}$, where $\overline{\lambda}$ is the effective lateral electron mean free path in the phantom material.

The total dose D_T at a point of interest Q located on the central axis of a broad beam of photons at depth $d \geq d_{max}$ in a phantom can be described as the sum of primary (D_p) and scattered (D_s) components:

$$D_T = D_p + D_s \tag{2.4}$$

The total dose at the same point with the attenuator i in the beam is given by:

$$D_T^i = D_p^i + D_s \tag{3.28}$$

The index i refers to the presence of the central axis absorber in the beam. If the attenuator meets the stated requirements, then the scattered component remains unchanged with or without the attenuator in the beam.

For a specified depth d in the phantom, the ratio of primary components D_p and D_p^i is independent of field size. Thus one can write:

$$D_p / D_p^i = \text{constant} = C_D \tag{3.29}$$

By combining these three equations one obtains:

$$D_p(d) = [1 - 1/ C_D(d)]^{-1} \cdot [D_T(d,S) - D_T^i(d,S)] \tag{3.30}$$

$C_D(d)$ compensates for a possible hardening of the beam in the attenuator. Unfortunately, $C_D(d)$ cannot be measured directly, because it is impossible to measure ionization resulting from primary radiation only. However, it is possible to measure $C_D(d)$ indirectly under narrow beam conditions.

3.4.1 Determination of $C_D(d)$

According to the Bragg-Gray cavity theory, the dose measured with an ionization chamber is proportional to the ionization created in the cavity of the chamber. The relationship between the ionization and the absorbed dose is given by:

$$D = \frac{I}{m} \cdot \frac{W}{e} \cdot {}_mS_p \tag{3.31}$$

where I is the ionization in the gas cavity, m is the mass of the gas in the cavity, W is the energy required to produce an ion pair in the gas cavity, e is the charge of an electron and ${}_mS_p$ is the mass collision stopping power ratio of the chamber wall material to the gas in the cavity.

If ${}_mS_p$ for the primary radiation does not change significantly when the central axis attenuator is in the beam, then $C_D(d)$ can be expressed in terms of ionization instead of dose to give:

$$C_D(d) = \frac{I_p(d)}{I_p^i(d)} \tag{3.32}$$

with I referring to ionization and the subscript i to the presence of the attenuator.

The primary ionization at depth d in a phantom can be expressed as:

$$\mathbf{I_p(d) = \sigma \cdot \Phi_0 \cdot e^{-\mu \cdot d} \cdot q} \tag{3.33}$$

where σ is the cross section for primary photon interactions in the phantom, Φ_0 is the fluence of primary photons at depth d, μ is the linear attenuation coefficient for the primary photons in the phantom and q is the charge of an electron.

When a small attenuator of thickness h is placed in the beam, the equivalent formula for $I_p^i(d)$ is:

$$\mathbf{I_p^i(d) = \sigma^i \cdot \Phi_0 \cdot e^{-\mu_h \cdot h} \cdot e^{-\mu^i \cdot d} \cdot q} \tag{3.34}$$

where μ^i and σ^i are defined as before, except that they correspond to the primary photon spectrum that was modified by the absorber and μ_h is the linear attenuation coefficient for the primary photons in the absorber. This then yields

$$C_D(d) = \frac{\sigma}{\sigma^i} \cdot e^{\mu_h \cdot h} \cdot e^{(\mu^i - \mu) \cdot d} \tag{3.35}$$

For a monoenergetic beam where $\mu = \mu^i$ and $\sigma = \sigma^i$ this reduces to

$$C_D(d) = e^{\mu_h \cdot h} \tag{3.36}$$

However, in a bremsstrahlung beam, the attenuator may cause sufficient change in the energy spectrum so that $\mu \neq \mu^i$ and $\sigma \neq \sigma^i$. Also, since beam hardening occurs with depth, both μ and μ^i will change slightly with depth and must be replaced with mean values $\bar{\mu}$ and $\bar{\mu}^i$.

So, if h is the thickness of the absorber, d is the phantom thickness and I denotes ionization, then in narrow beam conditions the following equations apply:

$$e^{-\mu_h \cdot h} = \frac{I(h)}{I(0)}, \tag{3.37}$$

$$e^{-\bar{\mu} \cdot d} = \frac{I(d)}{I(0)}, \tag{3.38}$$

$$e^{-\bar{\mu}^i \cdot d} = \frac{I(h+d)}{I(h)} \tag{3.39}$$

with I(0) being the ionization produced at the point of interest with only air as an attenuating medium.

The photon ionization cross section σ (and σ^i) is proportional to the linear attenuation coefficient μ (and μ^i) at a certain depth, thus σ (and σ^i) can be replaced by μ (and μ^i) in equation 3.35.

If I(d) is the ionization after a narrow beam has passed through a phantom material slab of thickness d and I(d+Δ) is the ionization after the beam has passed through a phantom material slab of thickness d+Δ, where Δ is a small increment in the thickness of the phantom material, then one can write:

$$\mu_d = \left[\ln \frac{I(d)}{I(d+\Delta)} \right] / \Delta \tag{3.40}$$

Similarly, if I(h+d) is the ionization after the beam has passed through a thickness d of phantom plus a thickness h of attenuator, and I(h+d+Δ) is the ionization after a thickness d+Δ of phantom plus a thickness h of attenuator, then:

$$\mu_d^i = \left[\ln \frac{I(h+d)}{I(h+d+\Delta)} \right] / \Delta \tag{3.41}$$

Substituting the expressions for μ_d and μ_d^i, as well as equations 3.37, 3.38 and 3.39 into equation 3.35 results in:

$$C_D(d) = \frac{\ln\left[\frac{I(d+\Delta)}{I(d)}\right]}{\ln\left[\frac{I(h+d+\Delta)}{I(h+d)}\right]} \cdot \frac{I(d)}{I(h+d)} \tag{3.42}$$

All the quantities in the above equation are measurable under narrow beam conditions. Thus, $C_D(d)$ values can be measured at various depths together with $D_t(d,S)$ and $D_t^i(d,S)$ and then used to calculate $D_p(d)$.

CHAPTER 4 MEASUREMENTS

4.1 Lateral range of charged particles

The lateral range of the charged particles in the 6 MV photon beam was measured in a 5 cm x 5 cm field with a Farmer type ionization chamber (Nuclear Enterprise, Type 2571) with an active volume of 0.6 cc. The chamber was co-axial with the central axis of the beam and build-up caps of varying diameter were successively mounted on the chamber. The build-up facing the beam was kept constant for all measurements. The measured ionization was recorded as a function of lateral build-up and is shown in Figure 4.1.

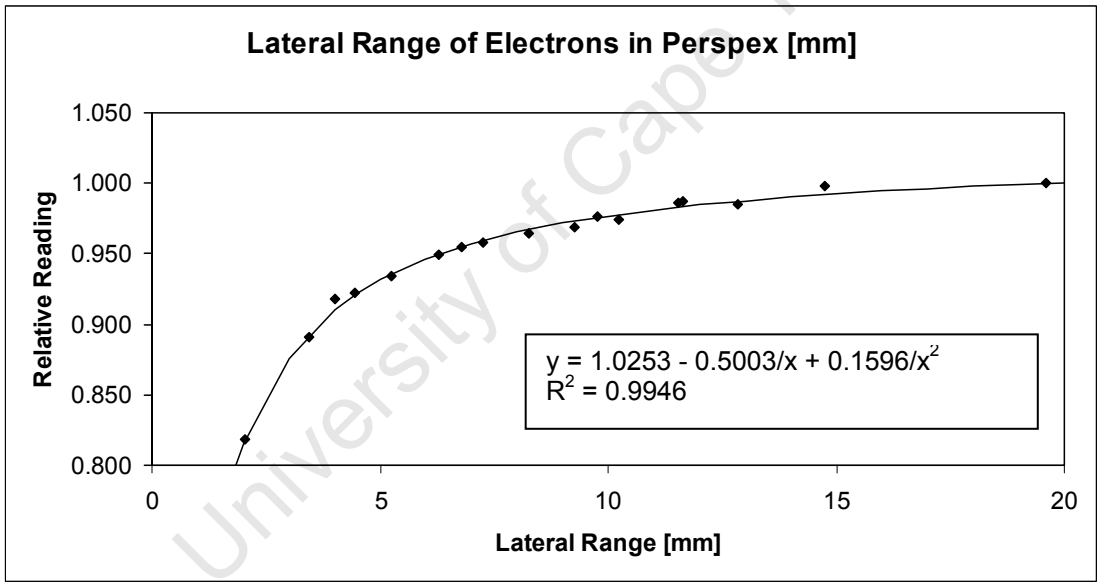

Figure 4.1: Lateral Range of Electrons in Perspex and an Inverse Quadratic Fit

Du Plessis (2009) recommended the use of an inverse quadratic function as a fit to the data points. The effective range of the lateral scattered electrons is then defined at the 93 % relative reading.

It can be seen that the chamber response shows a shoulder at about 5.2 mm Perspex build-up. This indicates that the effective lateral range of the liberated electrons is approximately 5.2 mm in Perspex. The steep decrease in dose from 5.2 mm lateral

Perspex build-up and smaller can be ascribed to the absence of lateral electronic equilibrium, while the increase in dose at a lateral build-up greater than 5.2 mm Perspex is due to more scattered photons in the build-up material.

According to Khan (2003), if the energy of the beam is in the region where the Compton effect is the only possible mode of interaction, then the attenuation is dependent on the electron density (Chapter 2.2.3) of the attenuating material. The electron density is given by the mass density times the number of electrons per gram of the material.

$$1\text{cm} \cdot \frac{(\rho_e)_{\text{perspex}}}{(\rho_e)_{\text{water}}} = 1\text{cm} \cdot \frac{1.18\text{g/cm}^3 \cdot 3.248 \cdot 10^{23}\text{electrons/g}}{1.00\text{g/cm}^3 \cdot 3.343 \cdot 10^{23}\text{electrons/g}} = 1.15\text{cm} \qquad (4.1)$$

(Data from Johns & Cunningham, 1983)

According to the TG 21 protocol (1983) scaling based upon electron concentration is applicable for energies from ^{60}Co to 25 MV, after which the cross section for pair production exceeds that for Compton interaction.

Therefore 1cm of Perspex is equivalent to 1.15cm of water and thus the lateral electron range in water is 5.2 mm* 1.15 = 6.0 mm.

Zefkili *et al*. (1994) used the following conversion between water and Perspex:

$$d_{\text{water}} = d_{\text{perspex}} \cdot \frac{\rho_{\text{perspex}}}{\rho_{\text{water}}} \cdot \frac{(Z/A)_{\text{perspex}}}{(Z/A)_{\text{water}}} \qquad (4.2)$$

where $(Z/A)_{\text{Perspex}} = 0.53937$ and $(Z/A)_{\text{water}} = 0.55508$

(Data from: http://physics.nist.gov/PhysRefData/XrayMassCoef/tab2.html)

Using the same density for water and Perspex as above we find 1cm Perspex = 1.15 cm water. This is an identical expression to 4.1 since: $\rho_{\text{electron}} = \rho_{\text{mass}} \cdot N_A \cdot \frac{Z}{A}$

Sometimes 10 mm of perspex is taken to be equivalent to 12 mm of water (NPL, 1990).

This figure of 6.0 mm is fairly good agreement to the calculated value of 5.3 mm using Compton kinematics in Chapter 2.4.

Bjärngard *et al.* (1989) say that for 6 MV X-rays a field of radius 1.5 cm is sufficient to satisfy lateral electron equilibrium. The same authors (Bjärngard *et al.*, 1990) revised that figure the following year and said that for radii < 1.0 cm the dose on the central axis of a 6 MV beam is progressively reduced due to electron disequilibrium.

Zefkili *et al.* (1994) showed that lateral electronic equilibrium is ensured in a 6 MV beam for a 2 cm x 2 cm beam dimension.

Haryanto *et al*. (2002) also confirm that output factor measurements for field sizes of less than 2 cm x 2 cm in a 6 MV beam start to vary for different detectors because of lateral electronic disequilibrium. Four different detectors (a pinpoint thimble chamber, an ionization chamber with sensitive volume = 0.125 cm^3, a diode detector and a diamond detector) measured equal output factors for a 2 cm x 2 cm field, but not for a 1 cm x 1 cm field. A larger detector will reduce the measured output factor for small fields, and the output factor measured with the diode detector, which is not water-equivalent, is larger than the output factor measured with the water-equivalent diamond detector for small fields. Monte Carlo calculations confirmed the diamond detector as the detector of choice for small field sizes.

Rice *et al*. (1987) estimated uncertainties for the central axis dose in a 6 MV beam due to lack of lateral electronic equilibrium of 2.5 % in a 12.5 mm diameter circular field and 1.5 % in a 15 mm field when using an ionization chamber with a diameter of 3.5 mm. These uncertainties were confirmed using Monte Carlo calculations.

4.2 Tissue-Maximum Ratios

The Tissue-Maximum Ratio is defined in Chapter 2.8.4.

TMRs were measured for the 6 MV photon beam in a Wellhöfer WP600 water phantom using the mini-ionization chamber described in Chapter 2.3. Unfortunately this particular tank did not have automated TMR capabilities, so the water level was adjusted manually.

The field sizes ranged from 2 cm x 2 cm to 35 cm x 35 cm. The field sizes could unfortunately only be set from inside the LINAC vault and not from the operator's console outside the vault. From the depth dose measurements the depth of maximum dose was found to be at a depth of 1.5 cm in water. This was used as the reference depth for these measurements.

4.3 Central Axis Percentage Depth Dose

The Central Axis Percentage Depth Dose (CAPDD or PDD) is defined in Chapter 2.8.2.

A Wellhöfer WP 600 water phantom with the "mini-ionization chamber" (see Chapter 2.3) was used to measure central axis percentage depth doses.

The Wellhöfer water tank was aligned with the central axis of the beam first by using the lightfield and crosshairs, and then by doing inplane and crossplane beam profile scans at different depths to check the alignment of the scanner's central axis with the radiation beam's central axis in both the inplane and crossplane directions.

The IAEA TRS 398 protocol states that if a cylindrical chamber is used to measure depth doses, the effective point of measurement must be taken into account. This requires that the complete depth ionization curve be shifted towards the surface by an

amount equal to $0.6 \cdot r_{cyl}$, where r_{cyl} is the cavity radius of the cylindrical ionization chamber. From the description of the mini-ionization chamber in section 2.3 it can be seen that the internal cavity diameter is 1.9 mm, this means that $0.6 \cdot r_{cyl} = 0.6$ mm. This value can be put into the Wellhöfer software to be used as an offset to correct for the effective point of measurement.

A second ionization chamber was used as a reference chamber and was placed in the beam between the phantom and the collimator. The reference chamber should be positioned in such a way that is doesn't disturb the dose on the central axis. Measuring the ratio of the field vs. reference chamber should correct for any possible drifts in photon fluence, since any changes cancel out in the ratio.

PDDs were measured up to a depth of 35 cm for field sizes ranging from 2 cm x 2 cm to 35 cm x 35 cm. The detector moved at a constant velocity along the central axis while continuously recording readings. The data was smoothed using the least-squares smoothing routine provided by the Wellhöfer software and discrete CAPDD values were extracted at 5mm intervals.

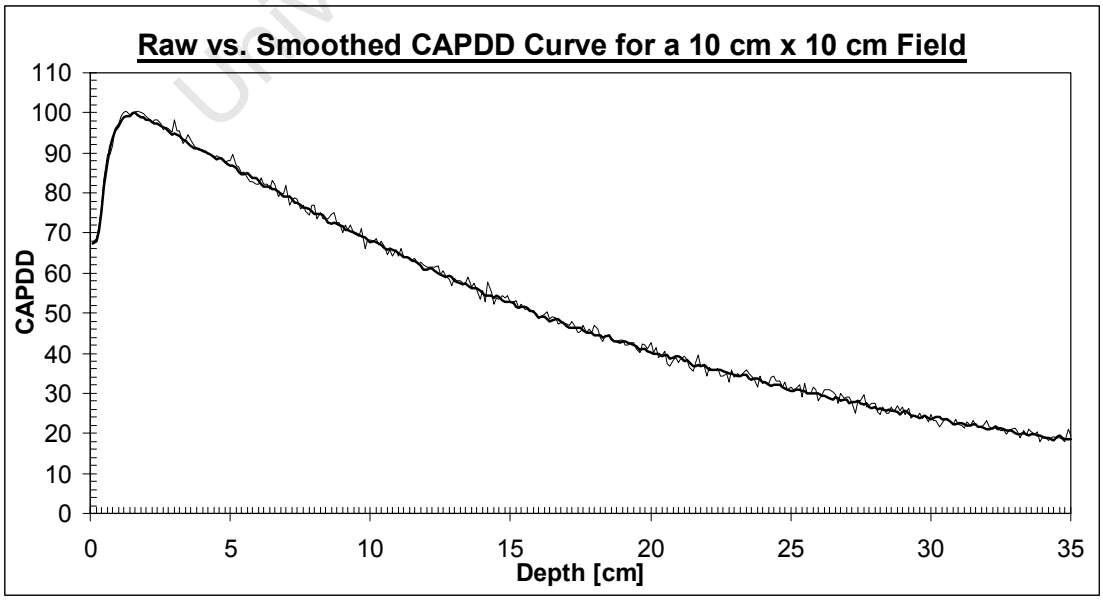

Figure 4.2: Raw vs. Smoothed PDD Data

To get an estimate of the electronic noise within a single scan, continuous inplane and crossplane scans were performed (see Figure 4.3 for an inplane scan). It was found that the noise adds an uncertainty of ±1.2% to the measured dose.

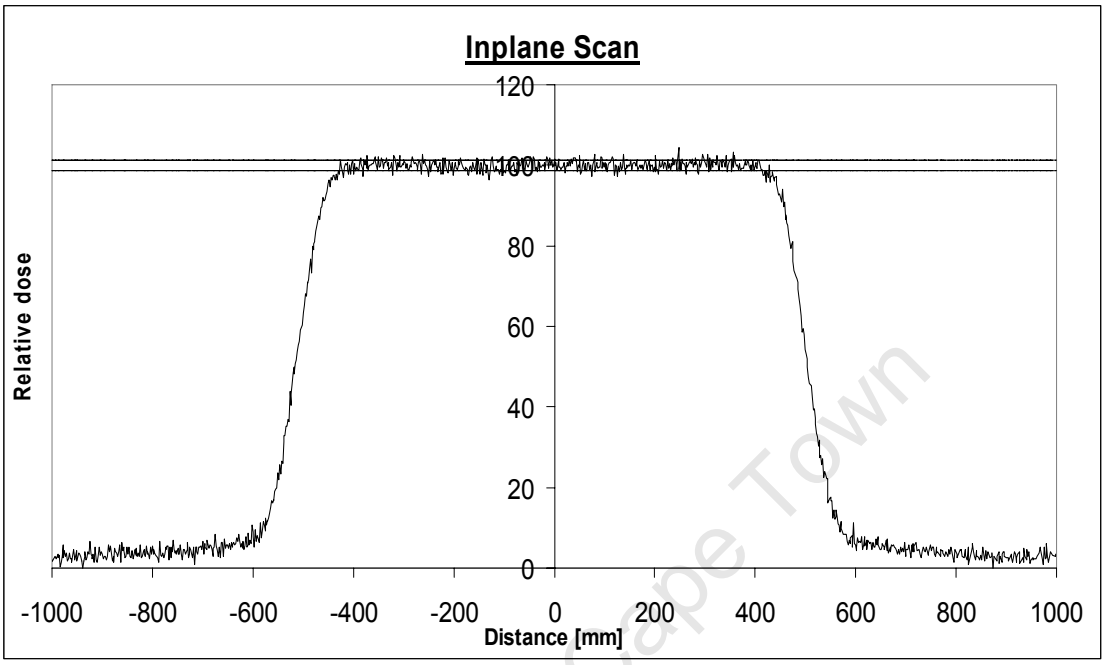

Figure 4.3: Inplane Scan at d = 1.5 cm

The beam symmetry is 0.2 % and the beam flatness is 1.1 % for both the inplane and crossplane directions. (For definitions of the beam symmetry and flatness, refer to the Wellhöfer WP600 manual (latest version: 2008))

To smooth the data, output factors were measured at d_{max} = 1.5 cm and at a depth of 5cm. The output factor OF(d,S) is defined as the ratio of the dose measured for a certain field size at a certain depth D(d,S) and the dose measured for a reference field at the same depth $D(d,S_{ref})$ (Williams & Thwaites, 1993)

$$OF(d,S) = \frac{D(d,S)}{D(d,S_{ref})} \tag{4.3}$$

Output factors are generally normalized to 1 at d_{max} for the reference field. The reference field size S_{ref} in this thesis is a 10 cm x 10 cm field.

The PDD at 5cm depth for any field size S can be obtained from (Schreuder, 1992):

$$\mathrm{PDD}(5\mathrm{cm},\mathrm{S}) = \mathrm{PDD}(5\mathrm{cm},\mathrm{S}_{\mathrm{ref}}) \cdot \frac{\mathrm{OF}(5\mathrm{cm},\mathrm{S})}{\mathrm{OF}(1.5\mathrm{cm},\mathrm{S})} \tag{4.4}$$

The depth dose for the reference field at 5cm depth can be measured accurately. Using the above equation, a set of depth doses at 5cm depth were constructed for all field sizes and the measured depth doses were smoothed through these values. Each curve was normalized to give 100% at d_{max}.

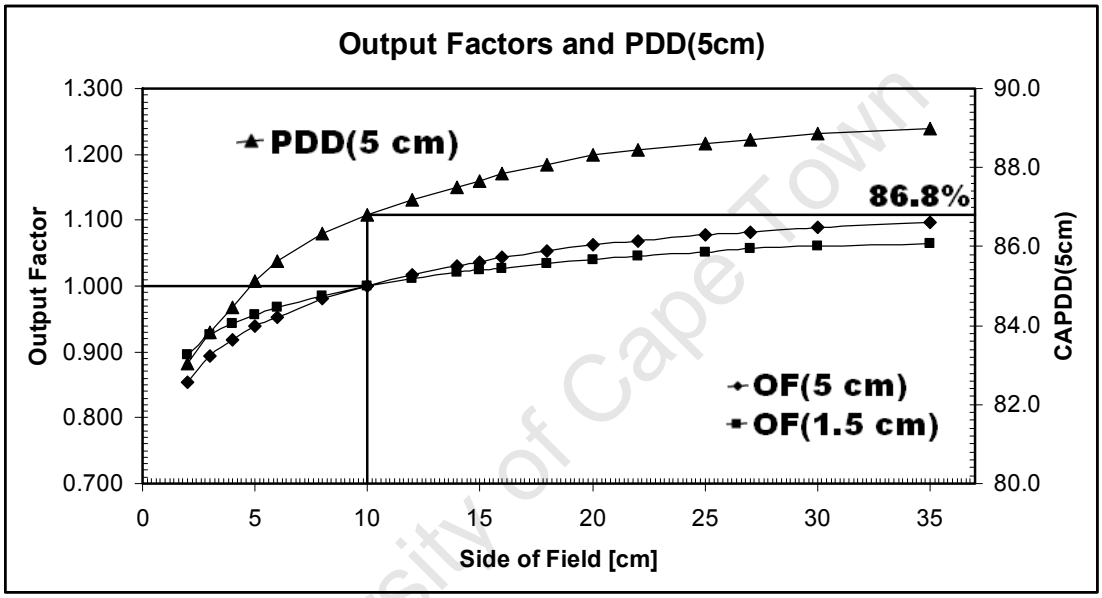

Figure 4.4: Output Factors and PDD(5cm)

4.4 Linear Attenuation Measurements

Attenuation measurements in the 6 MV photon beam were done for nine field sizes ranging from 2 cm x 2 cm to 20 cm x 20 cm with water depths ranging from 0 cm to 20 cm. The measurements were performed with the gantry at 180º and the beam passing through a water tank. The bottom surface of the water tank was at a distance of 100 cm from the source of radiation. The level of water in the tank was varied from 0 cm to 20 cm.

Bushberg *et al.* (2002) recommends a distance of at least 30 cm between the water surface and the detector to reduce the influence of scattered radiation on the reading. Measurements were done to confirm this. The ionization as a function of air gap was measured in a 5 cm x 5 cm field with a 5 cm thick wax block as attenuator in the beam, and repeated with a 2 cm lead attenuator. The wax/lead block was positioned at an SSD of 100cm, while the position of the 0.6cc Farmer ionization chamber with build-up was varied and the reading corrected for the inverse-square effect. Readings were normalized to 1 for the maximum reading in each case.

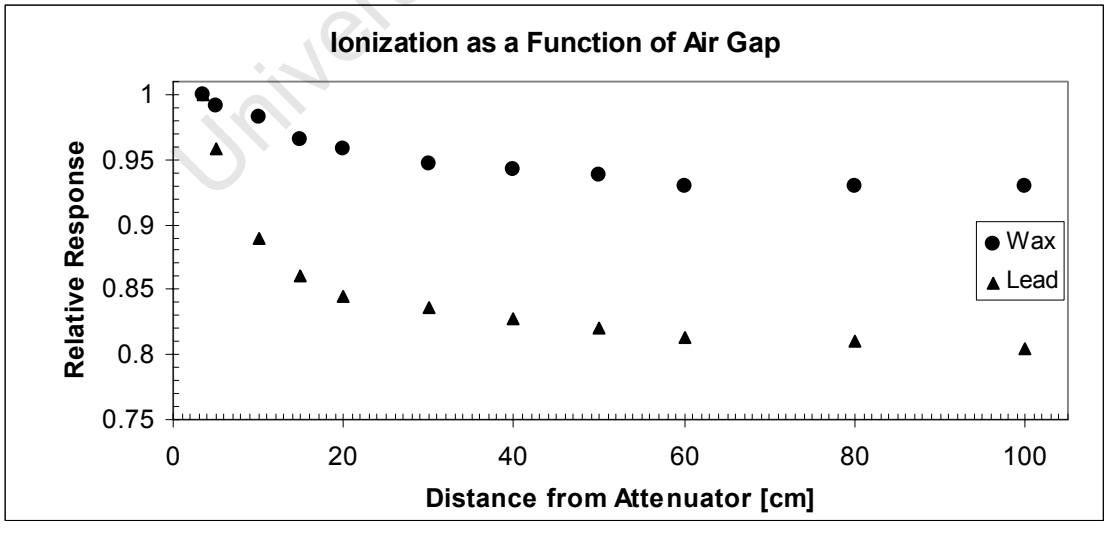

Figure 4.5: Ionization as a Function of Air Gap

It can be seen that the response drops off quite significantly as the air gap is increased from 0 cm to about 20 cm or so, after which the response flattens out.

Islam & van Dyk (1995) report a 14 % difference between transmission measured at 6.0 cm and 46 cm from the absorber (low melting point alloy) in a 6 MV beam. The transmission readings for this 6 MV beam at 5.0 cm and 50 cm from the lead absorber differ by 14.4%, in very good agreement with the value reported by Islam & van Dyk.

The ionization chamber, a NE 0.6cc Farmer 2571 thimble type ionization chamber, with build-up cap was positioned at an extended SSD of about 200cm, so that the 2 cm x 2 cm field covered the whole build-up cap. This means that at a water depth of 20 cm the chamber is 80 cm from the top of the water surface. The setup used is shown in Figure 4.6.

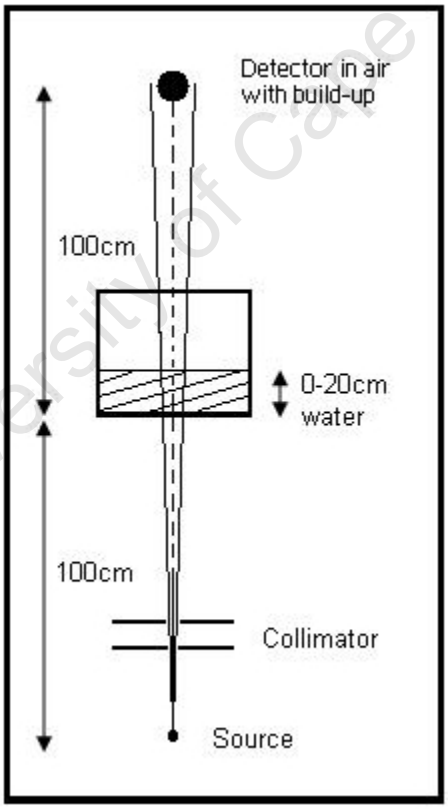

Figure 4.6: Attenuation Measurements

4.5 The Central-Axis Attenuator

Measurements of the dose with ($D_t^i(d)$) and without ($D_t(d)$) the central axis attenuator in the beam were measured at different depths in 5 cm x 5 cm, 10 cm x 10 cm and 20 cm x 20 cm fields using the mini-ionization chamber (see section 2.3). Two sets of measurements with two different central axis attenuators were made, the first set with a cylindrical lead attenuator of 1 cm radius and 1 cm height, the second set with a cylindrical lead attenuator of 1 cm radius and 2 cm height.

It is important to know how the height of the central axis attenuator above the water surface influences the reading of $D_t^i(d)$. Therefore the detector was positioned at depth d_{max} = 1.5 cm in a 10 cm x 10 cm field and the position of the lead attenuator between the collimator and the water surface was varied, while measurements were done at each attenuator position.

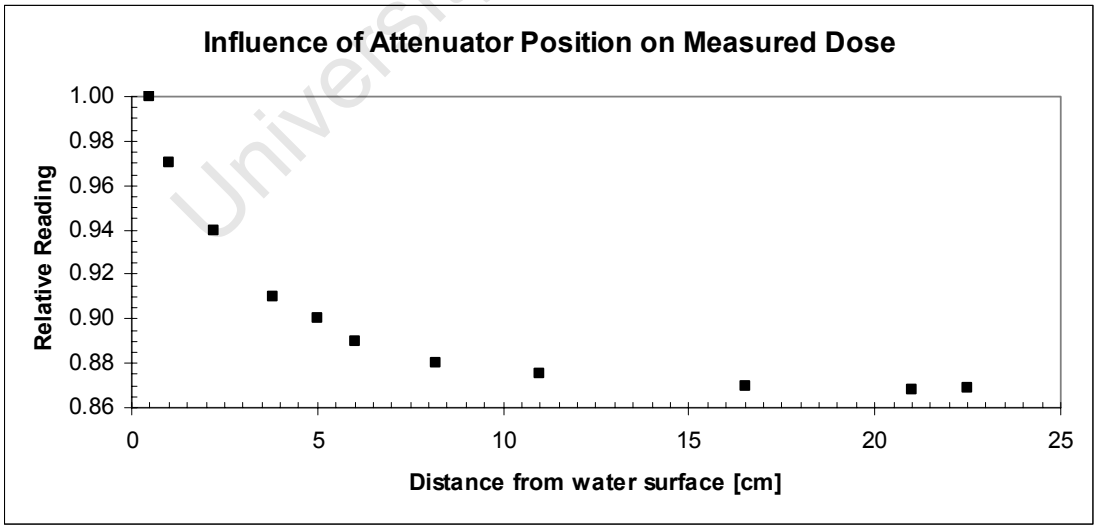

Figure 4.7: Influence of Attenuator Position on Measured Dose

It can be seen that $D_t^i(d_{max},\ 10cm\ x\ 10cm)$ becomes less dependent on the attenuator position as the distance between the attenuator and the water surface increases. Care was therefore taken to ensure that all measurements of $D_t^i(d)$ were made with the attenuator at about 30 cm above the water surface. Figure 4.8 shows the setup of measuring $D_t(d)$ and $D_t^i(d)$

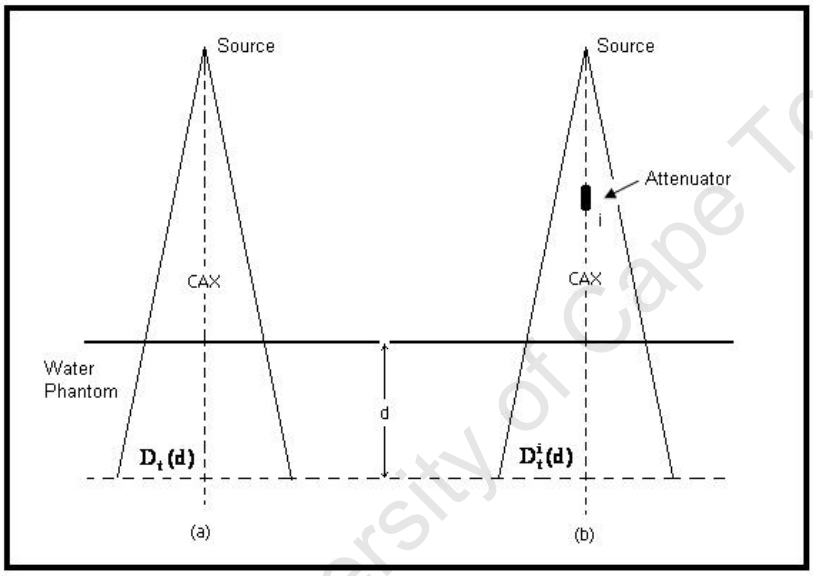

Figure 4.8: Measurement Setup

The experimental setup used to measure the $C_D(d)$ values is shown in Figure 4.9.

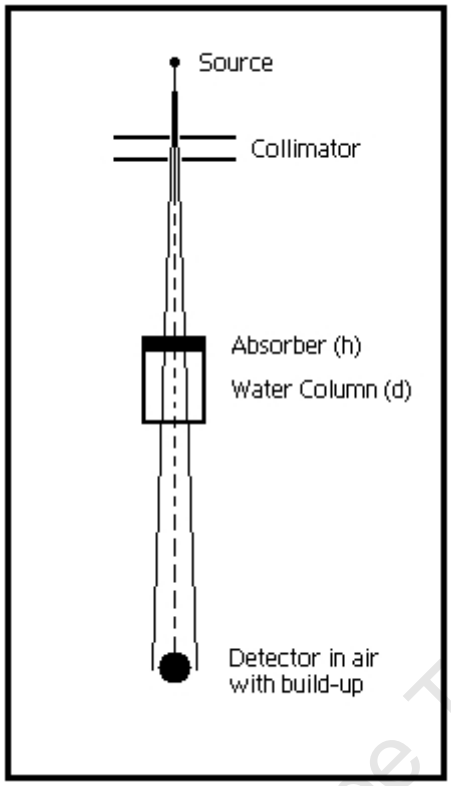

Figure 4.9: Measurement Setup

The setup is very similar to the one described in Chapter 4.4. Narrow beam measurements in a 2 cm x 2 cm beam with the detector (0.6cc Farmer type ionization chamber with build-up) at an extended SSD were done.

The absorber thickness h is identical to the thickness of the central axis attenuator used when measuring $D_t^i(d)$.

Ionization measurements with (I(d+h) and I(d+h+Δ)) and without (I(d) and I(d+Δ)) the additional attenuator in the beam were done at 2 cm intervals from 0 cm to 20 cm depth with Δ = 0.5 cm.

Additional measurements at d = d_{max} were done to determine the primary dose component at d_{max}.

CHAPTER 5 DATA ANALYSIS

5.1 Extrapolation of Measured Tissue-Maximum Ratios

The methods described in Chapter 3.1 were used to extrapolate the measured TMRs to zero field size at each depth. Some of the measured TMRs are shown in Figure 5.1.

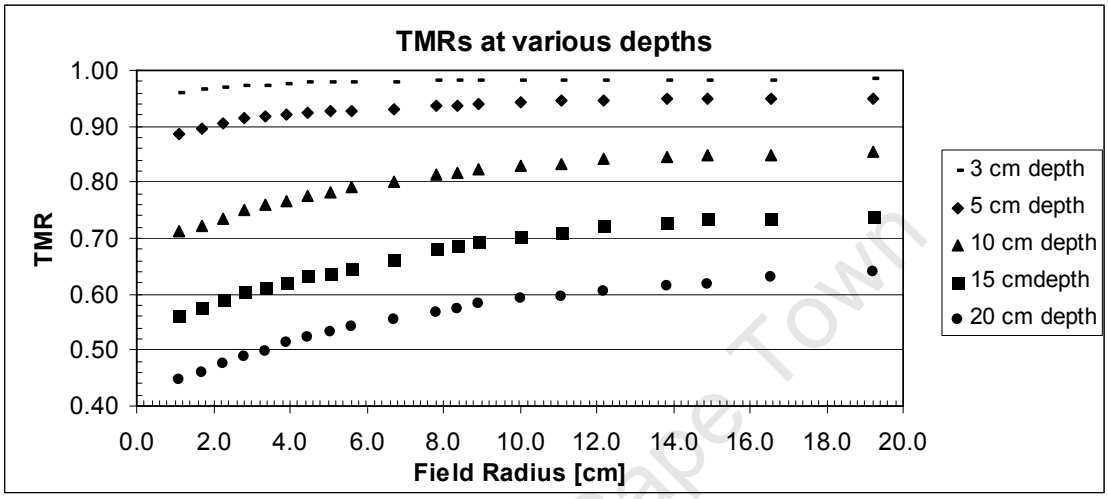

Figure 5.1: Measured TMRs

Using Godden's assumption (Godden, BJR Supp 17, 1983) that log (TMR) varies linearly with depth, an effective linear attenuation coefficient was determined for each field size (see Table 5.1) using the TMR data given in Appendix C.

Table 5.1: Determination of μ as a function of field size

Field Size [cm]	μ [cm^{-1}]	R^2 of fit		Field Size [cm]	μ [cm^{-1}]	R^2 of fit
2	0.043	0.9974		14	0.031	0.9879
3	0.042	0.9968		15	0.030	0.9880
4	0.040	0.9953		16	0.029	0.9862
5	0.039	0.9945		18	0.028	0.9869
6	0.038	0.9936		20	0.027	0.9861
7	0.036	0.9936		22	0.027	0.9854
8	0.035	0.9932		25	0.026	0.9867
9	0.034	0.9931		27	0.025	0.9855
10	0.033	0.9923		30	0.025	0.9871
12	0.032	0.9906		35	0.024	0.9866

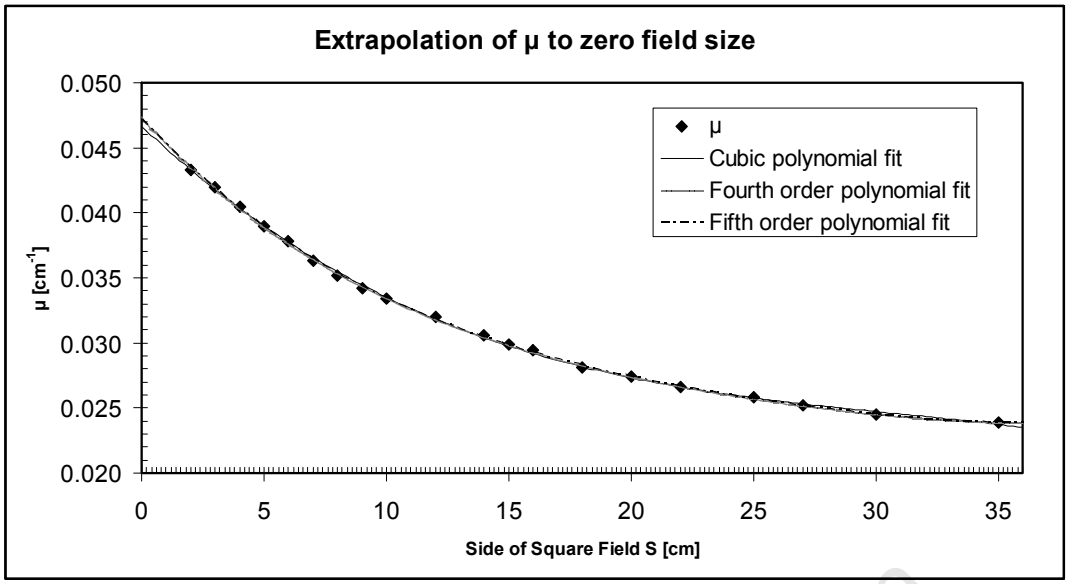

Figure 5.2: Extrapolation of μ to zero field size

A cubic, fourth order and fifth order polynomial fit was used to extrapolate μ as a function of field size to zero field size. The result of the fits is shown in Figure 5.2. It can be seen from Figure 5.2 that there is virtually no difference between the fourth and fifth order polynomial fits, and that the cubic polynomial fit gives a slightly lower value of μ(0) than the other two fits.

The fitting procedure yielded the following results:

Cubic polynomial:

$\mu(S) = (\mathbf{0.0467 \pm 0.0002}) - (0.0018 \pm 5E\text{-}5)*S + (5.15e\text{-}5 \pm 3E\text{-}6)*S^2$

$- (5.57e\text{-}7 \pm 5E\text{-}8)*S^3$

$R^2 = 0.9992$

Fourth order polynomial fit:

$\mu(S) = (\mathbf{0.0472 \pm 0.0002}) - (0.0020 \pm 8E\text{-}5)*S + (8.02e\text{-}5 \pm 9E\text{-}6)*S^2$

$- (1.77e\text{-}6 \pm 4E\text{-}7)*S^3 + (1.66e\text{-}8 \pm 5E\text{-}9)*S^4$

$R^2 = 0.9996$

Fifth order polynomial fit:

$\mu(S) = (\mathbf{0.0472 \pm 0.0004}) - (0.0020 \pm 0.0002)*S + (7.53e\text{-}5 \pm 2.9E\text{-}5)*S^2$

$- (1.42e\text{-}6 \pm 2.0E\text{-}6)*S^3 + (5.86e\text{-}9 \pm 6.08E\text{-}8)*S^4 + (1.19e\text{-}10 \pm 6.7E\text{-}10)*S^5$

$R^2 = 0.9996$

The fourth and fifth order polynomial fits give an identical $\mu(0)$ and an identical R^2 value of the respective fits. The standard error of $\mu(0)$ for the fourth order polynomial fit is smaller then the fifth order polynomial fit.

Therefore, for this method of extrapolation $\mu(0)$ was taken to be:

$$\mu(0) = 0.0472 \pm 0.0002 \text{ cm}^{-1}$$

The measured TMRs were also expressed as a function of $z = \frac{r \cdot d}{r + d}$, where r is the radius of the circular field which is equivalent to the square field with side S, and d is the depth in the phantom. This is shown in Figure 5.3 for various depths. A linear function was fitted to the data for depths $\geq 2 \cdot d_{max}$ and field radii < 9cm. It can be seen that TMR(d,z) is no longer linear for field sizes with radii > 9cm, as was also found by Nizin (1991). The intercept of the linear function at each depth yielded TMR(d,0).

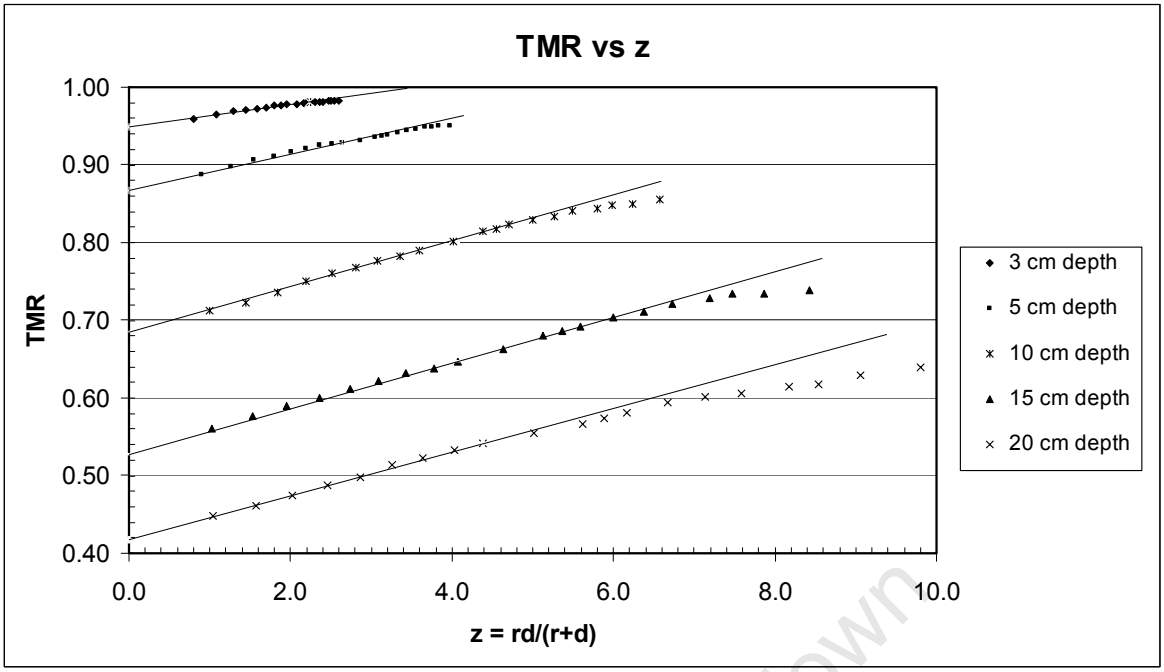

Figure 5.3: TMRs as a function of z

For megavoltage beams, the primary attenuation can be approximately represented by:

$$\text{TMR}(d,0) = e^{-\mu_0 \cdot (d - d_{max})} \quad \text{(Paul } et\ al.\text{, 1983, Khan, 2003)} \qquad (3.5)$$

Therefore an exponential function was fitted to the TMR(d,0) data to obtain μ_0.

It was found that $\mu_0 = 0.0466 \pm 0.0006\ \text{cm}^{-1}$. The error is obtained from the fitting procedure. This value is slightly less than the value obtained using Godden's method. Therefore the linear attenuation coefficient was taken to be the average of the two extrapolation methods: $\mu_0 = 0.0469 \pm 0.0006\ \text{cm}^{-1}$.

5.2 Attenuation Measurements

The attenuation of the 6 MV photon beam was measured in water for nine field sizes. Each measured set of attenuation data was fitted with a single exponential function up to a depth of 20 cm to determine the linear attenuation coefficient as a function of field size S. Table 5.2 shows the measured data together with the values for μ and their uncertainties. The uncertainties are obtained from the fitting procedure.

Depth [cm]	Side of Square Field [cm]								
	2	3	4	5	7	10	12	15	20
0	1.000	1.000	1.000	1.000	1.000	1.000	1.000	1.000	1.000
2	0.918	0.917	0.915	0.916	0.917	0.918	0.921	0.921	0.923
5	0.798	0.794	0.792	0.792	0.794	0.795	0.798	0.800	0.806
8	0.690	0.687	0.688	0.689	0.692	0.696	0.699	0.703	0.709
10	0.628	0.639	0.638	0.638	0.637	0.640	0.644	0.646	0.655
12	0.576	0.573	0.573	0.574	0.577	0.581	0.586	0.591	0.603
15	0.505	0.504	0.506	0.507	0.509	0.514	0.517	0.522	0.534
20	0.404	0.403	0.403	0.404	0.408	0.413	0.419	0.426	0.438
μ(S) [cm^{-1}]	0.046	0.046	0.046	0.046	0.045	0.045	0.044	0.043	0.042
Error	0.001	0.001	0.001	0.001	0.001	0.001	0.001	0.001	0.001

Table 5.2: Data used to obtain μ as a function of field size

A linear (van Dyk, 1986), quadratic and cubic polynomial (Robinson *et al.*, 1991) was fitted to the obtained values for μ(S) and extrapolated to zero-field size (Figure 5.4).

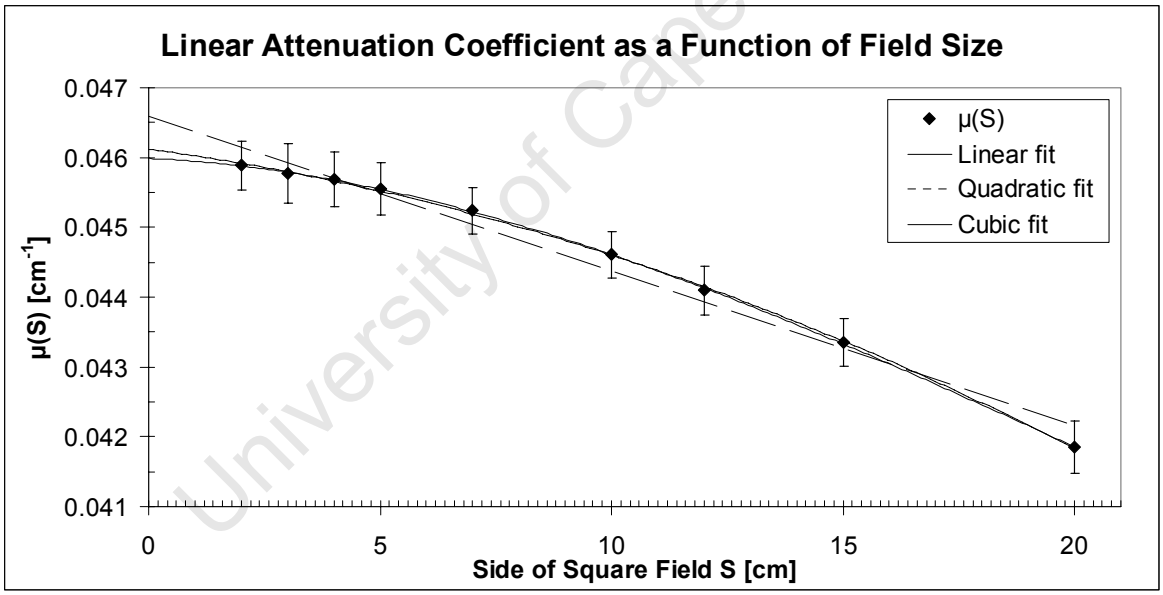

Figure 5.4: Extrapolation of μ to zero field size

The linear fit was given by:

$\mu(S) = (\underline{\mathbf{0.0466}} \pm 1E\text{-}04) - (2.215E\text{-}04 \pm 1.25E\text{-}05)*S$ with $R^2 = 0.9783$

The quadratic fit was given by:

$\mu(S) = (\underline{\mathbf{0.0461}} \pm 1E\text{-}04) - (8.91E\text{-}05 \pm 9.21E\text{-}6)*S - (6.27E\text{-}06 \pm 4.24E\text{-}07)*S^2$

with $R^2 = 0.9994$

The cubic fit was given by:

$\mu(S) = (\underline{\mathbf{0.0460}} \pm 1E\text{-}04) - (2.90E\text{-}05 \pm 1.67E\text{-}5)*S - (1.29E\text{-}05 \pm 1.76E\text{-}06)*S^2 + (2.00E\text{-}07 \pm 5.28E\text{-}08)*S^3$ with $R^2 = 0.9999$

As can be seen from Figure 5.4 and the R^2 values of the various fits, the best fit is obtained by fitting the cubic polynomial to the data of $\mu(S)$ vs. S and results in a primary linear attenuation coefficient of $\mu_0 = 0.0460 \pm 0.0001$ cm^{-1}.

5.2.1 Beam Hardening

Bjärngard & Shackford (1994) proposed to analyze measured attenuation factors in narrow beams in water in terms of an attenuation coefficient μ and a beam hardening coefficient η. The function they proposed takes the shape $T(x) = T_0 \cdot e^{-\mu x \cdot (1-\eta x)}$ (5.1), where x is the depth in the phantom.

Measured attenuation data for field sizes ≤ 4 cm x 4 cm was fitted to equation 5.1.

Results from the fit are:

2 cm x 2 cm field: $\mu = 0.0472$ cm^{-1} and $\eta = 0.0017$ cm^{-1}.

3 cm x 3 cm field: $\mu = 0.0467$ cm^{-1} and $\eta = 0.0012$ cm^{-1}.

4 cm x 4 cm field: $\mu = 0.0468$ cm^{-1} and $\eta = 0.0016$ cm^{-1}.

Average values: $\mu = 0.0469$ cm^{-1} and $\eta = 0.0015$ cm^{-1}.

The obtained values for μ are slightly different than the primary linear attenuation coefficient of $\mu_0 = 0.0460 \pm 0.0001$ cm^{-1}. This is because the standard definition of the attenuation coefficient is related to the change in transmission per unit thickness (i.e. $-(dT/dx)/T = \mu$). When the transmission factor T(x) behaves like Equation 5.1,

then $-(dT/dx)/T = \mu(1-2\eta x)$, which is not the same as the determined primary linear attenuation coefficient, except at $x = 0$.

Bjärngard & Shackford (1994) did measurements on a Philips SL75-5 LINAC at a nominal energy of 6 MV, they found $\mu = 0.0473\ cm^{-1}$ and $\eta = 0.0014\ cm^{-1}$, which is in close agreement to the obtained values in this work. They estimate the uncertainty in η to be about 20% and quote a reproducibility of ±1% for their attenuation coefficient μ, which was obtained from two attenuation measurements only.

Hossain *et al*. (2001) applied this model to a 6 MV beam as well, they found $\mu = 0.0469\ cm^{-1}$ and $\eta = 0.0015\ cm^{-1}$, which are exactly the same values as those obtained in this work. No uncertainties for these values were quoted in their work.

Yu *et al*. (1997) proposed a very similar formula to take into account any beam hardening with depth: $T(x) = T_0 \cdot e^{-\mu x/(1+\kappa \cdot x)}$ (5.2)

where κ is the hardening coefficient.

The same measured attenuation data for field sizes ≤ 4 cm x 4 cm was fitted to equation 5.2. Results from the fit are:

2 cm x 2 cm field: $\mu = 0.0472\ cm^{-1}$ and $\kappa = 0.0018\ cm^{-1}$.

3 cm x 3 cm field: $\mu = 0.0467\ cm^{-1}$ and $\kappa = 0.0012\ cm^{-1}$.

4 cm x 4 cm field: $\mu = 0.0469\ cm^{-1}$ and $\kappa = 0.0016\ cm^{-1}$.

Average values: $\mu = 0.0469\ cm^{-1}$ and $\kappa = 0.0015\ cm^{-1}$.

The results are almost identical to the results using Bjärngard & Shackford's method (Bjärngard & Shackford, 1994). As before, the obtained μ is not the primary linear attenuation coefficient except at $x = 0$.

The beam hardening coefficients η and κ were found to be quite small and it may be adequate to ignore them. The error in doing so can be estimated: If the beam hardening of 20 cm of water is ignored, the maximum error in transmission is about 3 %. However, this is not the case when empirical central-axis data is used in dose calculations.

Bjärngard & Vadash (1998) showed that the quality index (QI = TPR_{10}^{20}) of a beam can be worked out using the obtained μ and η from equation 5.1.

$$QI = e^{-10\cdot\mu\cdot(1-30\eta)} \cdot \frac{\left(1+\frac{200\cdot\mu}{37.3-171\cdot\mu}\right)}{\left(1+\frac{100\cdot\mu}{27.3-171\cdot\mu}\right)} \qquad (5.3)$$

Using the obtained values of $\mu = 0.0469\ cm^{-1}$ and $\eta = 0.0015\ cm^{-1}$, the resultant QI is: QI = 0.679.

Varying μ by 1% gives the QI a range from 0.676 to 0.681, while varying η by 20% gives the QI a range from 0.676 to 0.682.

The measured QI of this beam ($QI = \frac{TPR_{20}}{TPR_{10}}$ for a 10 cm x 10 cm field) is QI = 0.685.

The mini-ionization chamber has a standard deviation of 0.16 % for 10 consecutive measurements. According to Taylor (1982), when two quantities are divided the fractional uncertainty in the answer is the sum of the fractional uncertainties of the numerator and denominator. Therefore the measured QI ranges from 0.681 to 0.689 and the error bars of the two methods overlap.

The difference between the two methods of determining the QI of the 6 MV beam in this work is 0.9 %.

It should be noted that values quoted in the literature for the QI of a ^{60}Co beam are:

QI = 0.579 (Johns & Cunningham, 1983)

QI = 0.578 (Shortt *et al*., 1993)

QI = 0.570 (Nutbrown *et al.*, 2002)

QI = 0.572 (Godden, 1983)

QI = 0.572 (McKenzie, 1996)

The variation of the QI of a ^{60}Co beam is as large as 1.6 %. Therefore the two values of the QI obtained for the 6 MV beam in this work are in good agreement

5.3 The Central-Axis Kerma Model

The central-axis kerma model was fitted with the Marquardt-Levenberg non-linear least squares algorithm (Marquardt, 1963) to the measured PDD data for depths greater than d_{max} . The Sigmaplot Version 9.01 program was used for the fit, the format of the program is described in Appendix A.

Depth dose data for 18 field sizes ranging from 2 cm x 2 cm to 35 cm x 35 cm up to a depth of 35 cm were used in the fit, adding up to 1224 data points. The model was constrained to go through PDD(d_{max}) = 100%. The excellent fit of the model with the measured data is shown in Figure 5.5 for a number of field sizes.

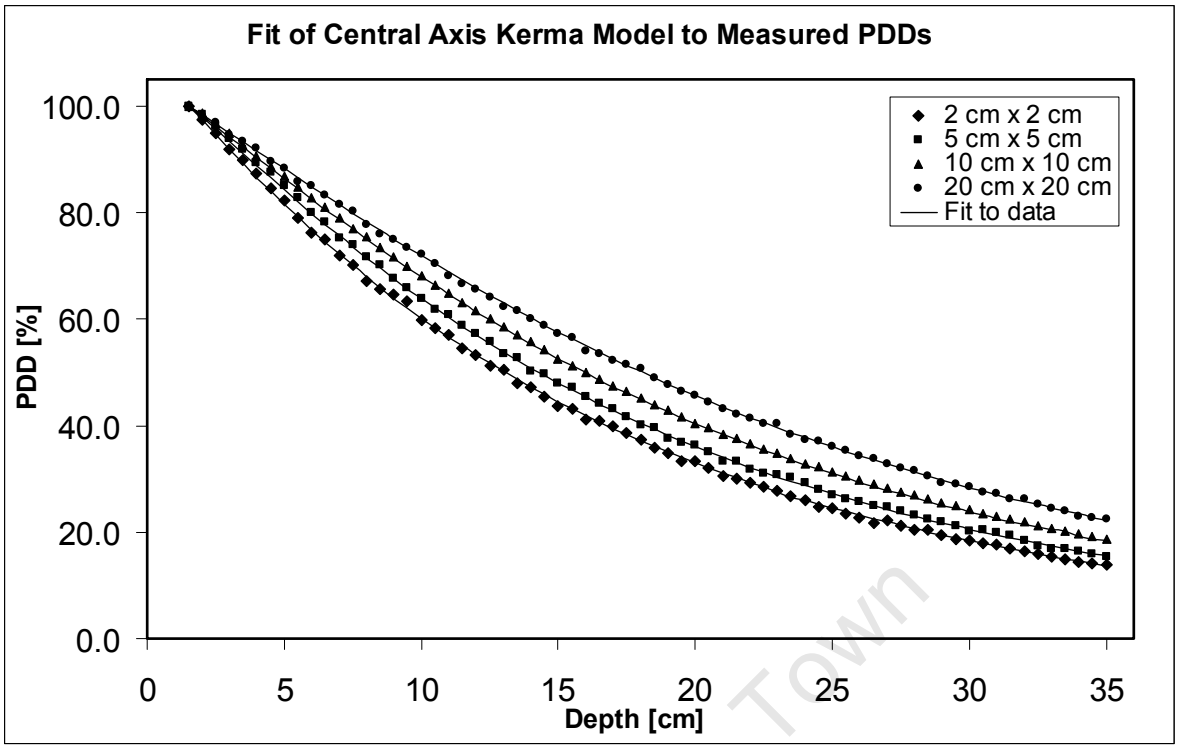

Figure 5.5: Fit of Central Axis Kerma Model to Measured PDDs

Schreuder (1992) did an error analysis on his central axis percentage depth dose data, the steps of which are followed here as well:

The percentage residuals of the fit are shown in Figure 5.6 with a bin width of 0.1%. The residuals are the difference between the observed and predicted values of the fit. The mean of the residuals is 0.0 with a standard deviation of 0.465. A Gaussian curve (solid line in Figure 5.6) for 1224 data points with a mean of 0.0 and a standard deviation of 0.465 is shown as well. It is quite clear that a Gaussian curve fits the data very nicely, showing that the errors are normally distributed around the mean.

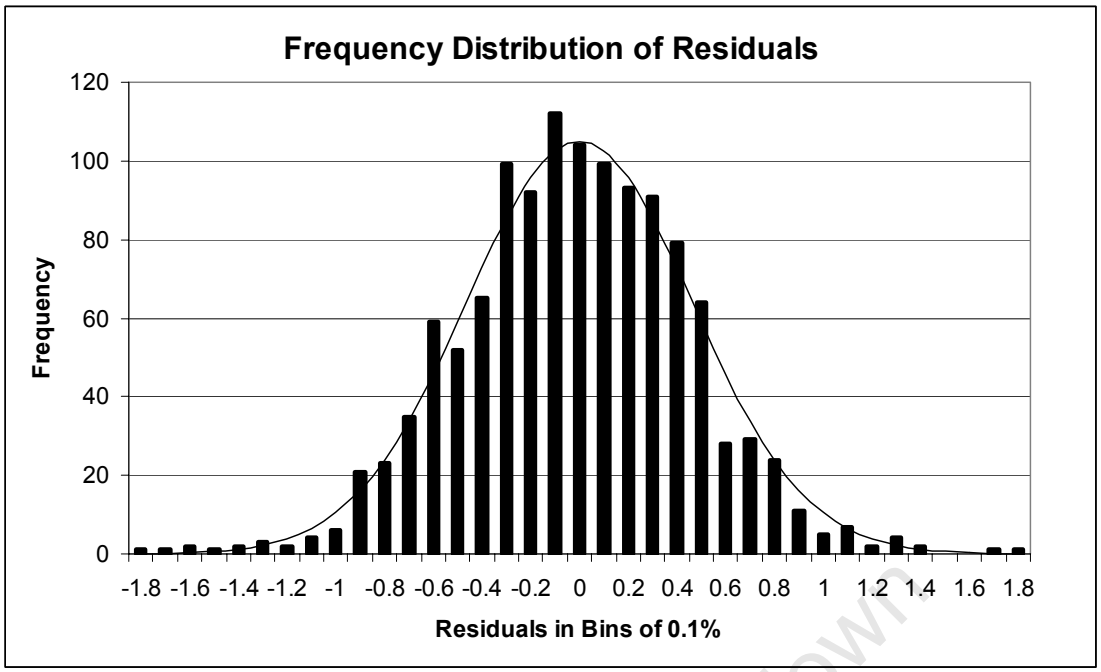

Figure 5.6: Frequency Distribution of Residuals

Even so, a test was done to determine whether there are any outliers in the data. Chauvenet's criterion (Taylor, 1982) was applied to the data. Chauvenet's criterion assumes that a measurement may be rejected if the probability of obtaining the deviation from the mean for that value is less than the inverse of twice the number of measurements, i.e. for N measurements the probability adjusts with 1/(2N).

A normal distribution is given by

$$f(x) = \frac{1}{\sqrt{2 \cdot \pi \cdot \sigma^2}} \cdot e^{-\frac{1}{2}\cdot\left(\frac{x-\bar{x}}{\sigma}\right)^2} \quad \text{with } -\infty \le x \le \infty \tag{5.4}$$

$\bar{x}$ is the mean and σ the standard deviation of the distribution. The integral of the normal distribution is called the normal error function. One can substitute

$z = \frac{x - \bar{x}}{\sigma}$ into this equation to get

$$\text{erf(t)} = \text{Probability(within } t\cdot\sigma) = \frac{1}{\sqrt{2 \cdot \pi}} \cdot \int_{-t}^{t} e^{\frac{-z^2}{2}} dz = 1\text{-}1/(2N) \tag{5.5}$$

This is the probability of a measurement within t standard deviations on either side of the mean. For 1224 data points the probability that a data point may be rejected or lies outside the interval $x \pm t\sigma$ using Chauvenet's criterion is 1/(2*1224) = 0.000408. Looking up the value for t in the normal error integral tables results in t = 3.60 (Taylor, 1982 or Underhill & Bradfield, 1994).

This is the same as saying that 1-0.000408 = 0.999592 = 99.9592 % of the area under the curve of the normal distribution is found between the mean ± 3.60 standard deviations. The standard deviation of this distribution is 0.465, thus any residual larger than 3.60*0.465 = 1.674 is regarded as an outlier. Only three data points in the data set of 1224 points are thus outliers.

The least squares fit was repeated with the three outliers removed from the data set. The influence of the excluded data was negligible. The values obtained in the fit with 1221 data points are:

Primary attenuation coefficient: $\mu_0 = 0.0445 \pm 0.0001$ cm^{-1}

Relative scattering fraction: $N_\infty = 0.307 \pm 0.002$

Exponential scatter growth factor: $\lambda = 0.0696 \pm 0.0008$ cm^{-1}

Empirical scale factor: $F = 1.21 \pm 0.01$

Pistorius (1991) did a fit of different 6 MV CAXPDD data with 524 data points, the following were his results:

Primary attenuation coefficient: $\mu_0 = 0.0451 \pm 0.0001$ cm^{-1}

Relative scattering fraction: $N_\infty = 0.269 \pm 0.002$

Exponential scatter growth factor: $\lambda = 0.0718 \pm 0.0009$ cm^{-1}

Empirical scale factor: $F = 1.04 \pm 0.01$

The results from this work and from Pistorius's fit are comparable. The primary attenuation coefficient is very similar for both data sets. The difference in the equivalent squares (equation 3.27) obtained using Pistorius's value of λ as opposed to the value of λ obtained in this work is negligible. The largest difference occurs for a 35 cm x 35 cm field, where the equivalent radius changes by 0.004 cm from 19.510 cm to 19.506 cm when changing λ from $\lambda = 0.0696$ cm^{-1} to $\lambda = 0.0718$ cm^{-1}. It seems that the 6 MV beam in this work has a slightly higher relative scattering fraction than the 6 MV beam that Pistorius used in his work.

5.4 The Central-Axis Attenuator

The central axis attenuator method was applied to the 6 MV photon beam of the SL75-5 LINAC. Two different attenuators were used in three different field sizes. The doses with ($D_t^i(d)$) and without ($D_t(d)$) the central axis attenuator in the beam were measured at different depths in 5 cm x 5 cm, 10 cm x 10 cm and 20 cm x 20 cm fields using the mini-ionization chamber.

Ionization measurements with (I(d+h) and I(d+h+Δ)) and without (I(d) and I(d+Δ)) the additional attenuator in the beam were done at 2 cm intervals from 0 cm to 20 cm depth with $\Delta = 0.5$ cm. Additional measurements at $d = d_{max}$ were done to determine the primary dose component at d_{max}. The values of $C_D(d)$ were determined according to equation 3.42.

Similar to Schreuder (1992) it was found that large uncertainties were introduced in the value of $C_D(d)$ and ultimately the primary dose component when using the measured ionization values directly for calculation. An exponential function was thus fitted to each I(d+h), I(d+h+Δ), I(d) and I(d+Δ) and the fitted data was then used in calculating $C_D(d)$.

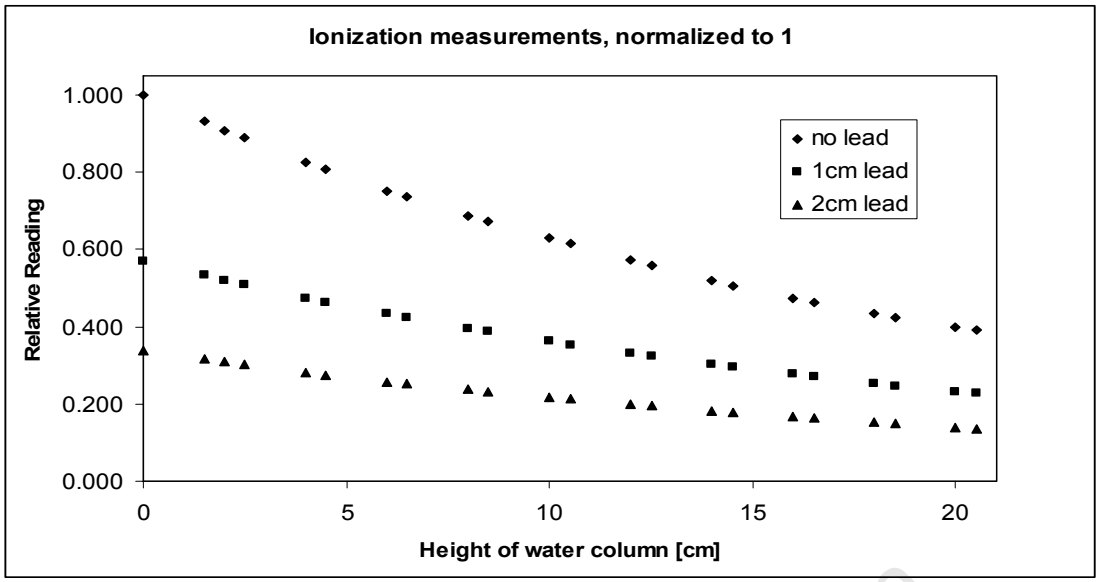

Figure 5.7: Ionization Measurements

Values for the primary dose component were calculated for the various field sizes and depths up to a depth of 20 cm.

Figure 5.8 shows the primary beam component as a fraction of the total dose for the three field sizes used at a depth of d_{max}. It can be seen that the scatter component at d_{max} increases with increasing field size.

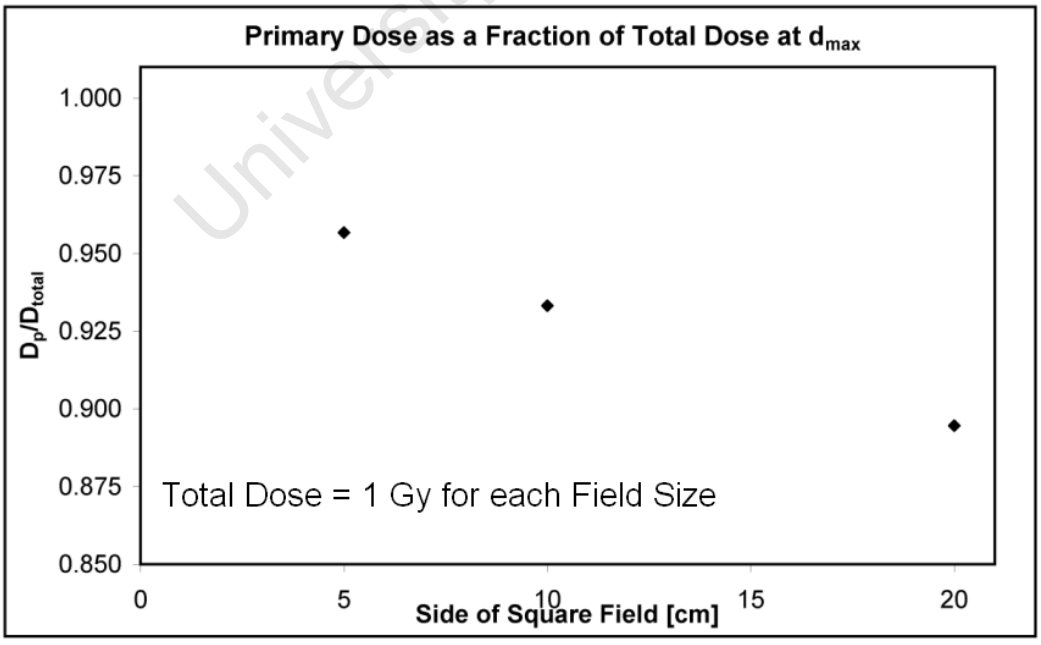

Figure 5.8: Primary Dose as a Fraction of the Total Dose at d_{max}

Figure 5.9 shows the total doses and effective primary doses, all normalized to 1 at the depth of maximum dose, for a 5 cm x 5 cm and a 20 cm x 20 cm field. It can quite clearly be seen that the scattered dose component increases with depth relative to the primary dose component. It can also be seen that the scattered dose component increases more rapidly for larger field sizes than for smaller field sizes. The effective primary dose with depth for the small and the large field size is identical when normalized to 1 for both field sizes.

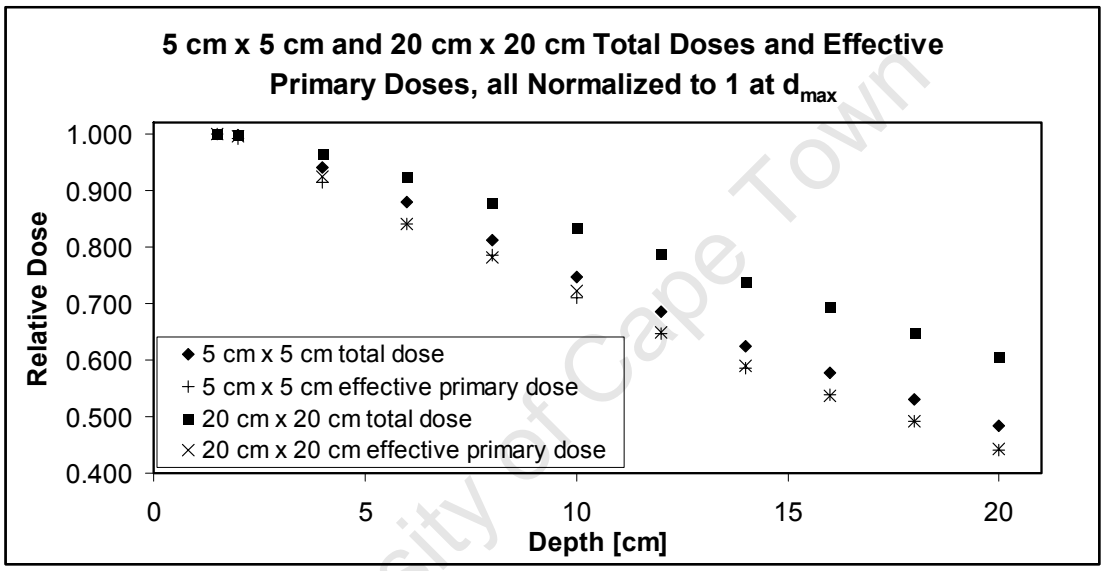

Figure 5.9: Total Doses and Effective Primary Doses

The values determined for the various dose components were normalized to 1 Gy for the total dose at the depth of maximum dose in a 10 cm x 10 cm field. Figures 5.10 and 5.11 show the results for a 10 cm x 10 cm field for the 1 cm thick lead attenuator and the 2 cm thick lead attenuator, respectively.

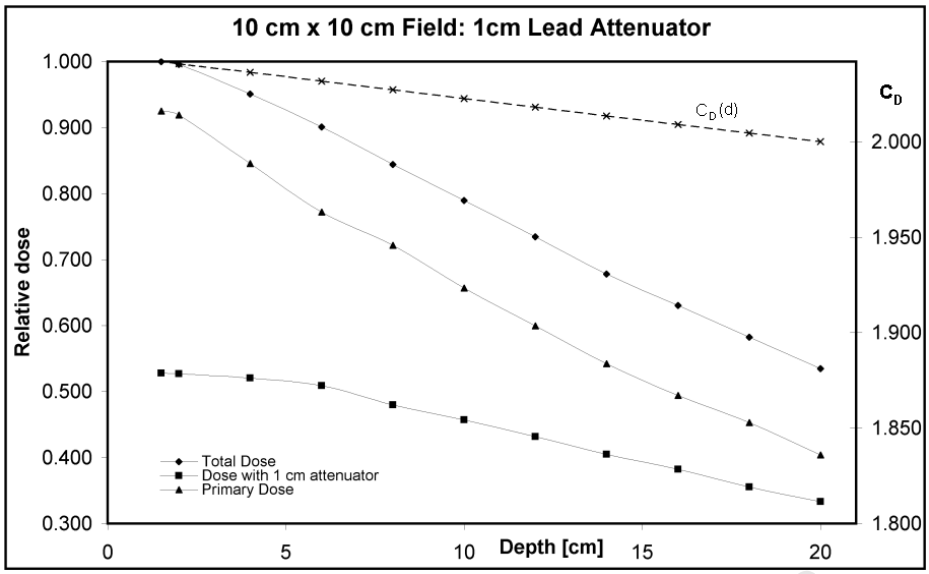

Figure 5.10: Results for the 10 cm x 10 cm field and 1 cm Attenuator

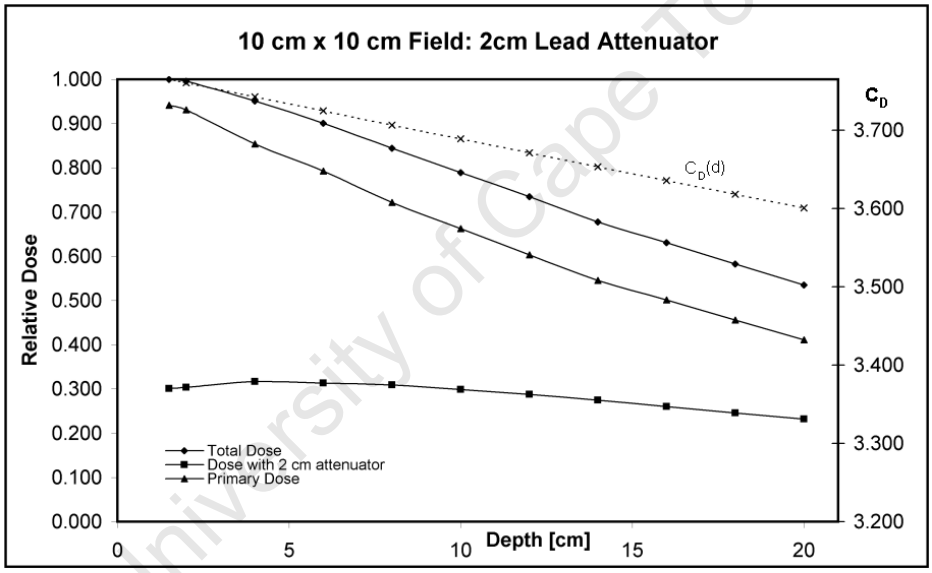

Figure 5.11: Results for the 10 cm x 10 cm field and 2 cm Attenuator

The primary dose component is attenuated exponentially (Khan *et al*. 1980), therefore an exponential function was fitted to the values of the primary dose at each field size, which yields the primary linear attenuation coefficient. The fitting procedure will also give an error estimation of μ_0.

Attenuator	Field Size [cm^2]	μ_0 [cm^{-1}]
1cm lead	5x5	0.0443 ± 0.0008
1cm lead	10x10	0.0447 ± 0.0007
1cm lead	20x20	0.0445 ± 0.0009
2cm lead	5x5	0.0443 ± 0.0007
2cm lead	10x10	0.0444 ± 0.0006
2cm lead	20x20	0.0446 ± 0.0007
	Average μ_0 [cm^{-1}]	**0.0445 ± 0.0007**

Table 5.3: Primary Linear Attenuation Coefficients

It can be seen from the results in Table 5.3 that the primary linear attenuation coefficient does not depend on the field size.

5.5 Average Primary Linear Attenuation Coefficient

Pistorius's central axis kerma model: $\mu_0 = 0.0445 \pm 0.0001$ cm^{-1}

Linear attenuation measurements: $\mu_0 = 0.0460 \pm 0.0001$ cm^{-1}.

CAX attenuator: $\mu_0 = 0.0445 \pm 0.0007$ cm^{-1}

TMR extrapolation: $\mu_0 = 0.0469 \pm 0.0006$ cm^{-1}

Average: $\mu_0 = 0.0455 \pm 0.0012$ cm^{-1}

The four different methods give fairly consistent results for μ_0. The error given for the average value of μ_0 is one standard deviation of the mean.

CHAPTER 6 SCATTER ANALYSIS

6.1 Various Scatter Factors

The dose to a point in a medium can be expressed as the sum of two parts: the primary dose and the scattered dose (Meredith and Neary, 1944, Khan *et al.*, 1980, Day, 1983, Kijewski *et al*., 1986, Bjärngard *et al.*, 1988, Holt *et al.*, 1970). The primary dose depends on the primary photon fluence, which in turn for a point source varies with distance by the inverse square law and exponential absorption. Strictly speaking the primary dose cannot be measured directly, because any measured dose will include some scatter from the collimator system. The effective primary dose is the dose due to the primary beam plus the photons scattered from the collimating system. The effective primary dose is thus a function of field size.

The scatter function (Meredith & Neary, Part I & II, 1944) was used at an early date to construct tables of scatter integrals to help in dose calculations. The use of scatter functions is based on the technique of summing sectors of circular beams (Clarkson, 1941). The Scatter-Air Ratio was introduced by Gupta & Cunningham in 1966. These ratios are linearly related to the early scatter function of Meredith & Neary (Thames, 1973) and simplified calculations significantly.

Various other factors have been introduced over the years (e.g., Normalized Peak Scatter Factor by Day, 1983, Tissue-Maximum Ratio by Holt *et al.*, 1970, revised TMR and SMR concepts by Khan *et al.*, 1980, revised equation relating TAR to PDD by Pfalzner, 1981).

It is useful to divide the scattered component ($S_{c,p}$) into two parts (Holt *et* al., 1970, Khan *et al.*, 1980): the collimator (S_c) and phantom (S_p) components. By increasing field dimensions scatter is added to the beam from the collimating system and the phantom. Systems for calculating monitor unit settings typically make use of empirical data such as percentage depth dose or tissue-maximum ratio, together with quantities that express the field size dependence of scatter radiation like the collimator scatter (S_c), phantom scatter (S_p) and total scatter ($S_{c,p}$) components (Tatcher & Bjärngard, 1992).

6.1.1 The Collimator Scatter Correction Factor

The **collimator scatter correction factor** (S_c) may be defined as the ratio of the effective primary dose for a given field size r to that of the reference field size r_0.

$$S_c = \frac{D_{air}(r)}{D_{air}(r_0)} \tag{6.1}$$

This factor is also known as the output factor in air, the head-scatter factor or the collimator-scatter factor (Zhu & Bjärngard, 2001). The factor describes the change of in-air output as a function of the collimator settings. It can be measured in air with an ion chamber with a build-up cap large enough to provide maximum dose build-up (Khan *et al.*, 1980). For high energy beams it becomes more difficult to measure S_c. The build-up cap must be fully included in the measurements and this becomes a problem for small field dimensions. Khan *et al.* (1980) showed that S_c is independent of distance from the source and can be measured at an extended SSD while the field size is still defined at the standard SAD. He also showed that build-up cap size is not critical in determining S_c, provided that the thickness of the cap is not less than what is required for maximum dose build-up. Khan *et al.* (1980) also proposed using build-

up caps of greater physical density (like aluminium) to reduce the size of the cap, which in turn will also allow smaller beams to be measured.

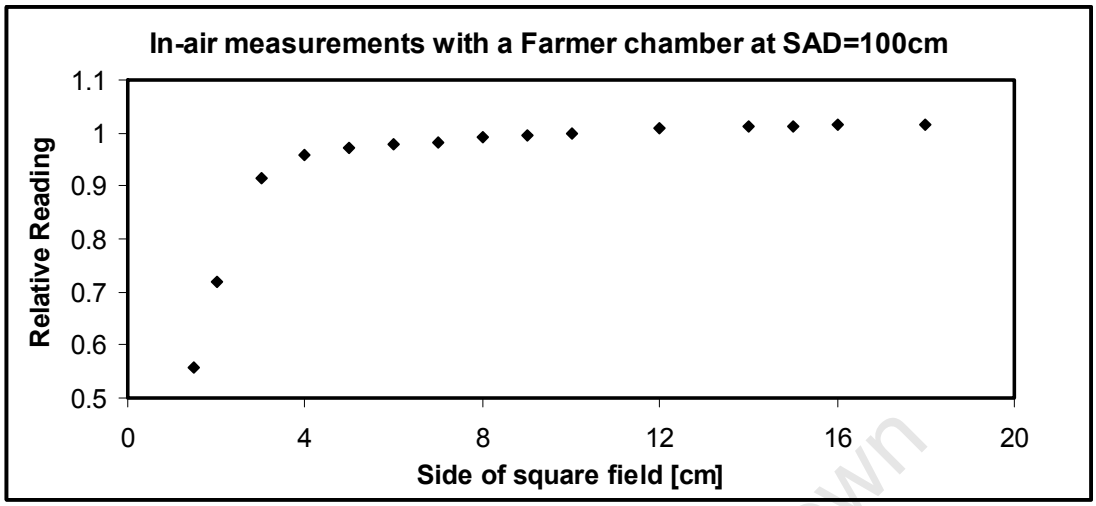

Figure 6.1: In-Air Measurements with a Farmer Chamber

Figure 6.1 shows in-air measurements done with a NE Farmer type 2571 chamber with Perspex build-up equal to d_{max} at SDD = 100 cm. There is a sudden drop in the readings at field sizes less than 4 cm x 4 cm, at this point the whole build-up is no longer included in the field.

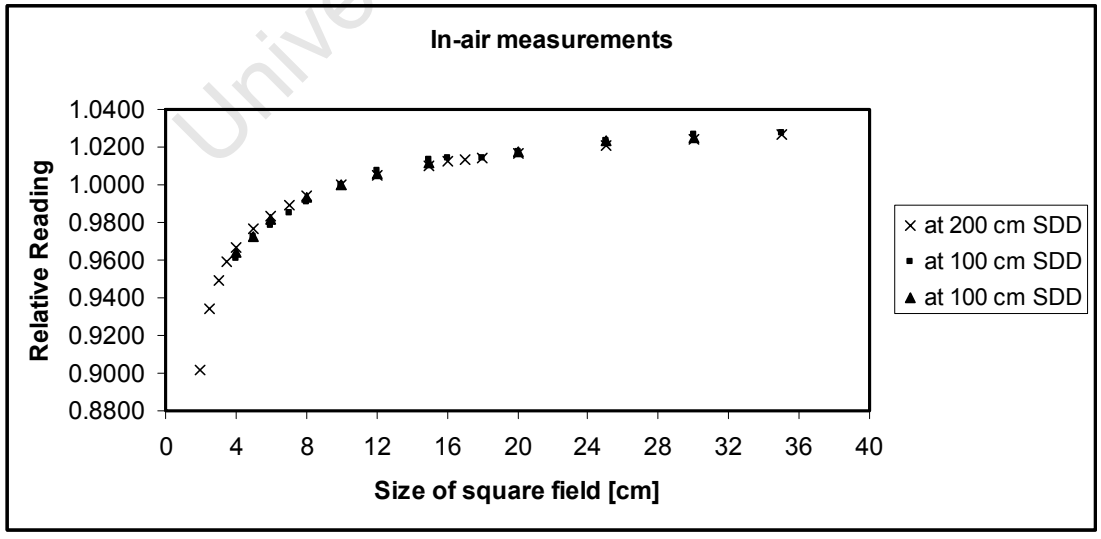

Figure 6.2: In-Air Measurements at Different SDDs

Figure 6.2 shows three sets of measurements of S_c done at two different SDDs. Two sets of data were measured at 100 cm SDD at different times. Using an extended SSD of 200 cm allowed for measurements down to field sizes of 2 cm x 2 cm. It can be seen that S_c does not depend on the distance to the source.

Van Gasteren *et al*. (1991) measured the collimator scatter component of megavoltage photon beams with a beam-coaxial narrow cylindrical phantom. They used a reference depth of 5 cm for photon beams with a quality index (QI) up to and including 0.75, and a depth of 10 cm for beams with QI larger than 0.75.

Lam & Ten Haken (1996) introduced a method of determining the collimator scatter factor from in-phantom measurements. They showed that by use of a series of field shaping blocks to define the field in the phantom, the collimator scatter factor can be determined from measurements in phantom when scattered radiation from the field shaping blocks is corrected for. The advantage of this method is that the smallest field size that can be measured is limited by the size of the detector since no build-up cap is necessary. The measurement is performed with full scatter.
Frye *et al*. (1995) showed that for a 6 MV beam there is no significant difference (0.5%) between head-scatter data measured with a build-up cap and head-scatter data measured with a cylindrical beam-coaxial miniphantom.

Venselaar *et al*. (1999) showed that the variation of the collimator scatter factor with field size is more prominent at d_{max} than at a depth of 10 cm for high-energy photon beams, because of the presence of contaminant electrons. For a 6 MV beam the

difference between collimator scatter factors measured at d_{max} and at 10 cm depth can be up to 2 % for very large field sizes.

Measurements are generally done for square fields. When this is not the case, the relevant phantom functions can be obtained by scatter integration or by a related procedure that replaces the actual field by an equivalent square.

When the length and the width of a rectangular radiation field are interchanged the collimator scatter factor can change by up to about 2 % (Tatcher & Bjärngard, 1992, Higgins *et al*., 1989).

Higgins *et al*. (1989) multiplied the collimator scatter factor for the equivalent square by an experimental correction factor depending on the collimator jaw selection and the elongation ratio (length L / width W) of the radiation field. Dawson (1978) proposed a method for correcting the output factor for elongation effects in which the equivalent square is bypassed and the output factor of the square field of side W is multiplied by a correction factor. Tatcher & Bjärngard (1992) proposed to use head-scatter data that was directly measured for rectangular fields. Vadash & Bjärngard (1993) proposed a simple formula to find the length c of the equivalent square of a rectangular field for collimator scatter factors: $c = (A+1)xy/(Ax+y)$. If A = 1 this formula reduces to the well-known "area-to-perimeter" relation of Sterling (1964). A was determined experimentally and was found to be 1.8 for the six X-ray beams studied.

In this work the collimator scatter factors were measured with a 0.6 cc NE 2571 Farmer chamber for 18 field sizes in air, with a Perspex build-up cap with a water-equivalent thickness of 1.5 cm = d_{max}. The scatter factors are show in Appendix C. In this work any elongation effects are ignored.

6.1.1.1 Parametrization of collimator scatter correction factors

Jager *et al*. (1997) compared several published methods of collimator scatter correction factor parametrization. The NCS Report 12 (1998) says that the required accuracy for any method, expressed as the maximum difference between a measured and calculated value of S_c, is 1 %. Jager *et al*. (1997) used measured values from field size ranging from 4 cm x 4 cm to 40 cm x 40 cm.

Jones (1978) presented an algorithm to determine the output of a 6 MV LINAC. It is given by:

$$S_c(x,x) = A \cdot x^B \tag{6.2}$$

where x is the side of a square field

Chen (1990) proposed a power polynomial to determine the beam output. Jager *et al*. (1997) used the same polynomial to investigate the collimator scatter factor only.

It is given by:

$$S_c(x,x) = (1 + \frac{a_1}{x} + \frac{a_2}{x^2} + \frac{a_3}{x^3} + ...)^{2\cdot(x-10)} \tag{6.3}$$

Only the first three parameters (a_1 to a_3) were used in the fit.

Szymczyk *et al*. (1991) proposed a cubic polynomial for the field size dependence of S_c in a Saturne II + accelerator:

$$S_c(x,x) = A + B\cdot x + C\cdot x^2 + D\cdot x^3 \tag{6.4}$$

Patomäki (1968) expressed the output as a first order function of the logarithm of the field size x in cm. Jager *et al*. (1997) expanded this expression to a polynomial of ln(x/10) given by:

$$S_c(x,x) = A + B\cdot \ln(\frac{x}{10}) + C\cdot \ln^2(\frac{x}{10}) + D\cdot \ln^3(\frac{x}{10}) \tag{6.5}$$

Bjärngard and Vadash (1995) described the output in air for the field size x in cm by:

$$S_c(x,x) = \frac{1 + A \cdot (x - 10)}{x - 10 + B} \tag{6.6}$$

It turns out that this formula does not work well at all. Zhu & Bjärngard (1994) used a formula that looks as follows:

$$S_c(x,x) = C \cdot \frac{1 + A \cdot x}{x + B} \tag{6.7}$$

This formula works very well, even if C = 1.

Yu *et al*. (1995) developed a head scatter factor parametrization for the Varian 600 and 2300 LINAC which looks like:

$$S_c(x,x) = A + B \cdot e^{C/x} \tag{6.8}$$

These 8 equations were fitted to the measured collimator scatter correction data.

The results of the various fits are given below.

Jones (1978): A = 0.9218 ± 0.0043; B = 0.0328 ± 0.0019

R^2 = 0.9495

Largest error: 1.69 % for 2.5 cm x 2.5 cm field

Chen (1990): a_1 = 0.0192 ± 0.0003; a_2 = -0.0504 ± 0.0026; a_3 = 0.0778 ± 0.0054

R^2 = 0.9995

Largest error: 0.14 % for 18 cm x 18 cm field

Szymczyk *et al*. (1991): A = 0.9165 ± 0.0056 B = 0.0136 ± 0.0015
C = -6.00E-4 ± 9.88E-5 D = 8.84E-6 ± 1.81E-6

R^2 = 0.9695

Largest error: 1.36 % for 2.5 cm x 2.5 cm field

Patomäki (1968): A = 1.0006 ± 0.0003 B = 0.0269 ± 0.0006
C = -0.0091 ± 0.0004 D = 0.0038 ± 0.0005

R^2 = 0.9991

Largest error: -0.18 % for 3.5 cm x 3.5 cm field

Bjärngard & Vadash (1995): A = 0.9950 ± 0.0062 B = 0.9807 ± 0.0176

$R^2 = 0.1255$

Largest error: 6.12 % for 2.5 cm x 2.5 cm field

Zhu & Bjärngard (1994): A = 0.9873 ± 0.2191 B = 1.3782 ± 0.2486
C = 1.0479 ± 0.2337

$R^2 = 0.9967$

Largest error: 0.32 % for 2.5 cm x 2.5 cm field

Zhu & Bjärngard (1994) with C = 1: A = 1.0344 ± 0.0007; B = 1.3273 ± 0.0049

$R^2 = 0.9967$

Largest error: 0.30 % for 2.5 cm x 2.5 cm field

Yu *et al*. (1995): A = 0.8637 ± 0.0186; B = 0.1701 ± 0.0177; C = -2.1038 ± 0.3394

$R^2 = 0.9963$

Largest error: 0.31 % for 2.5 cm x 2.5 cm field

The various fits for the collimator scatter correction factors are shown in Figure 6.3 for Jones, Chen, Patomäki, Szymczyk *et al*. and Yu *et al*., and in Figure 6.4 for Bjärngard & Vadash, Zhu & Bjärngard and Zhu & Bjärngard with C = 1.

It seems like the best fits to the data are given by Chen's expression and by Patomäki's expression. The NCS Report 12 (1998) prefers Patomäki's expression. It is quite obvious from Figure 6.4 that Bjärngard & Vadash's expression does not work well at all, but that the slightly modified expression by Zhu & Bjärngard works a lot better. The modified fit of Zhu & Bjärngard setting C = 1 is virtually the same as the fit when C is set as a variable, in which case C = 1.0479.

Jager *et al*. (1997) get similar results for Bjärngard & Vadash's formula.

Jones's, Szymczyk's and for Bjärngard & Vadash's expression should preferably not be used to calculate collimator scatter correction factors, because the maximum difference between a measured and calculated value of S_c is greater than 1 %.

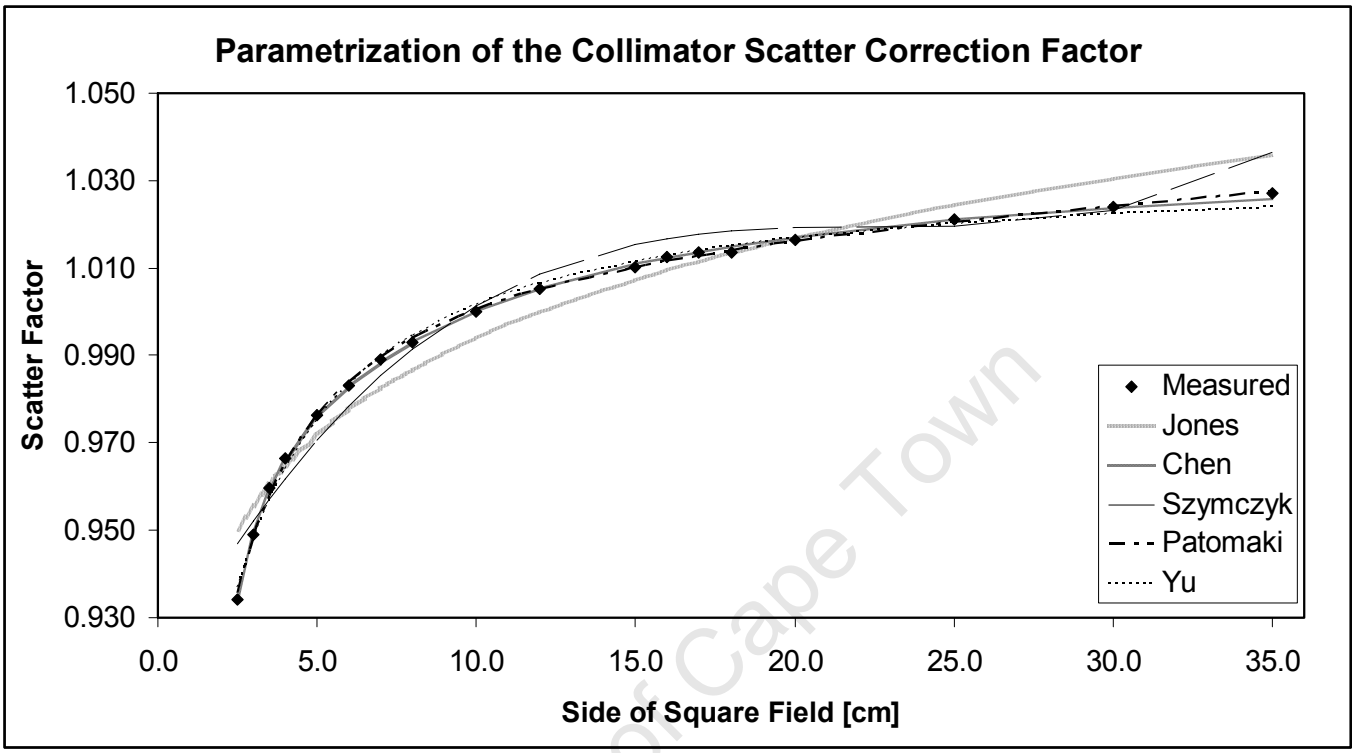

Figure 6.3: Parametrization of the Collimator Scatter Correction Factors

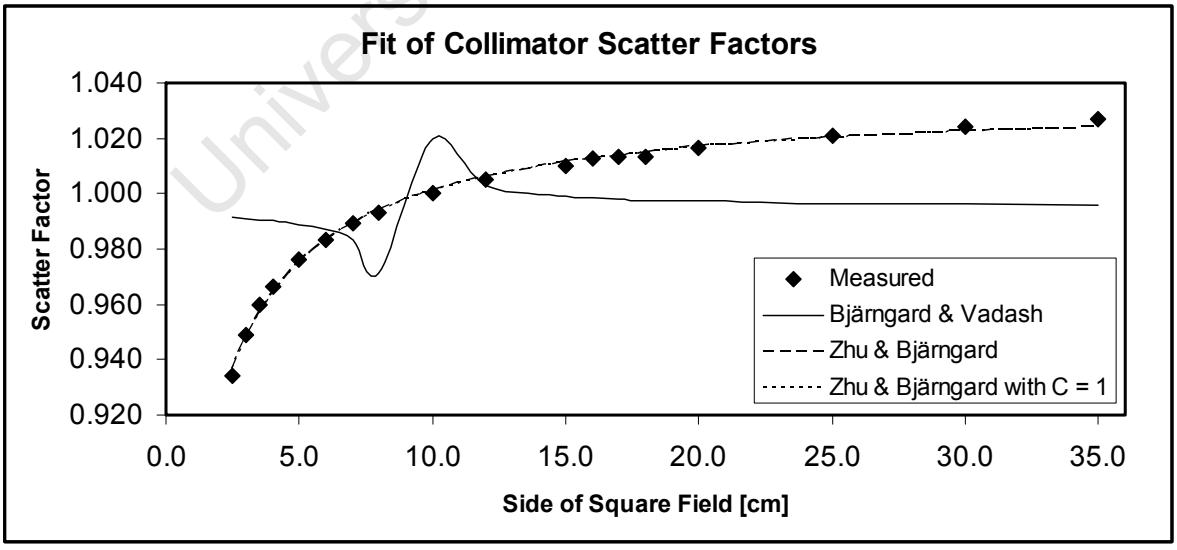

Figure 6.4: Fit of Collimator Scatter Factors

6.1.2 The Total Scatter Correction Factor

The **total scatter correction factor** $S_{c,p}$ is defined as the dose at a reference depth (in this work: d_{max}) in phantom for a given field size divided by the dose at the same point for the reference field size (10 cm x 10 cm). $S_{c,p}$ is measured at SDD = SAD (Khan *et al.*, 1980).

$$S_{c,p} = \frac{D(d_{max}, r)}{D(d_{max}, r_0)} \tag{6.9}$$

This is equivalent to the output factor defined in section 4.3, except that output factors are measured at SDD = SAD + d_{max}, not at SDD = SAD = 100 cm.

Measurements of $S_{c,p}$ are shown in Figure 6.5.

6.1.3 The Phantom Scatter Correction Factor

The **phantom scatter correction factor** S_p is defined as the dose for a given field in phantom at reference depth divided by the dose at the same point and depth for the reference field, with the same collimator opening (Khan *et al.*, 1980). S_p is thus related to the field size at the phantom while the collimator opening (and thus the effective primary dose) is kept the same. The direct measurement of S_p is very difficult and is not part of the standard dosimetry of a treatment unit (Storchi & van Gasteren, 1996), but can be calculated from:

$$S_p(r) = \frac{S_{c,p}(r)}{S_c(r)} \quad \text{(Khan } et\ al.\text{, 1980)} \tag{6.10}$$

where $S_{c,p}$ and S_c are the total and collimator scatter factors and are measurable as described. S_p is independent of SSD (van Gasteren *et al.*, 1991)

The definition of the normalized peak scatter factor (Day, 1983 & 1996) is identical to the definition of the phantom scatter correction factor.

Iwasaki (1996) formulated an expression for the phantom scatter correction factor as follows: $S_p(S,d_r) = \frac{TMR(d_r,0) + SMR(d_r,S)}{TMR(d_r,0) + SMR(d_r,10)}$ (6.11) where d_r = reference depth and the reference field is a 10 cm x 10 cm field. In this work the reference depth is d_{max} and this expression is simplified to:

$$S_p(S) = \frac{1 + SMR(d_{max},S)}{1.070} \qquad (6.12)$$

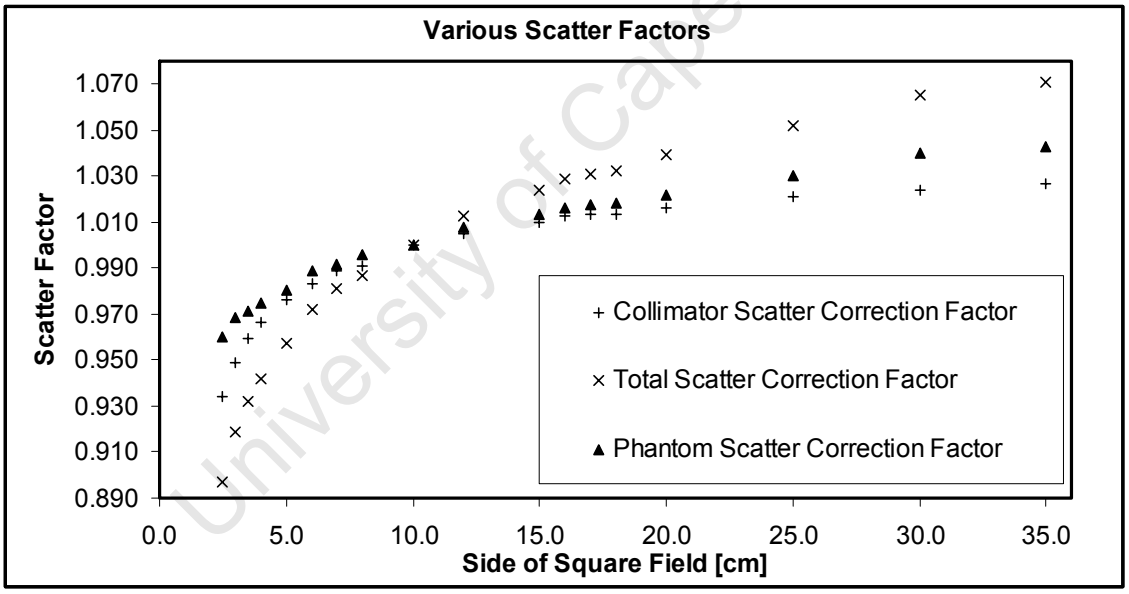

Figure 6.5: Various Scatter Factors

6.1.3.1 Parametrization of phantom scatter correction factors

Van Gasteren *et al*. (1998) showed that the phantom scatter correction factor can be described using a three-Gaussian fit. Their model assumes that the dose distribution due to a broad photon beam, in a plane perpendicular to its central axis at a certain depth in the phantom, can be considered as the summation of cross sections of pencil beams in this plane. In practice three Gaussians turn out to be sufficient for the model. The S_p is described as a function of the field radius r and the model is valid for beam qualities in the range from ^{60}Co to 25 MV. The model is described by:

$$S_p(r) = b_1 + a_1 \cdot \left\{ \frac{a_2}{b_2} \cdot (1 - e^{-b_2 \cdot r^2}) + \frac{a_3}{b_3} \cdot (1 - e^{-b_3 \cdot r^2}) \right\} \qquad (6.13)$$

The parameters a_1 to a_3 and b_1 to b_3 are found with a least-square method, again using Sigmaplot. The values were found to be:

$a_1 = 0.4371 \pm 0.0542$ $\qquad$ $b_1 = 0.9525 \pm 0.0025$

$a_2 = 0.0125 \pm 0.0022$ $\qquad$ $b_2 = 0.1397 \pm 0.0225$ cm^{-2}

$a_3 = 0.0009 \pm 0.0001$ $\qquad$ $b_3 = 0.0067 \pm 0.0009$ cm^{-2}

The R^2 value of this fit is: $R^2 = 0.9971$

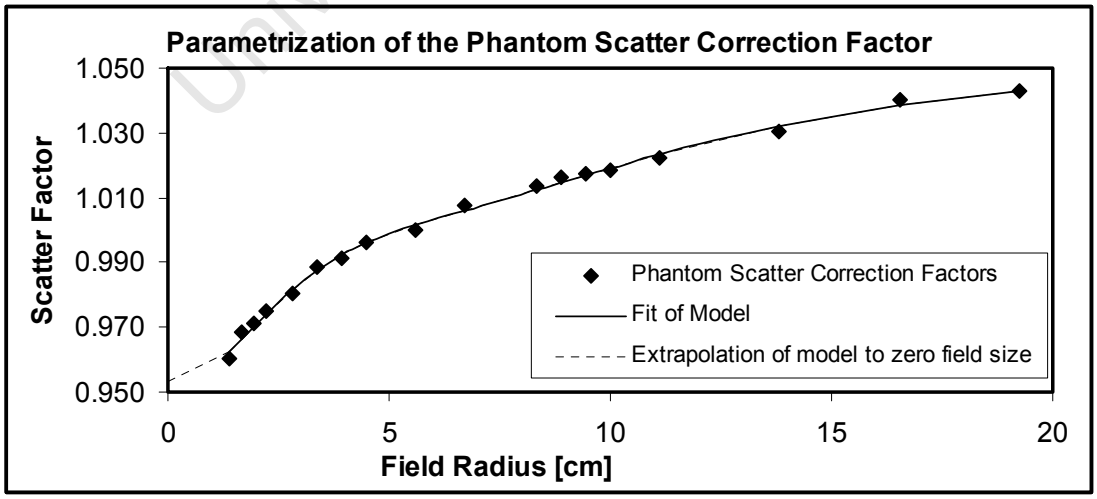

Figure 6.6: Parametrization of the Phantom Scatter Correction Factor using a Three-Gaussian Fit (Equation 6.13)

Van Gasteren *et al*. (1998) do not use this method to extrapolate to zero field size. For small fields as r approaches 0 the three-Gaussian fit approaches a parabola and will overestimate $S_p(0)$. (McDonough *et al*., 1999).

Sätherberg *et al*. (1996) fit an equation of the form below to measured S_p data:

$$S_p = a + b \cdot A + c \cdot A^2 + d \cdot A^{-1} \qquad (6.14)$$

where A refers to the field size and a, b, c and d are fitting parameters.

These fitting parameters are given by:

a = 0.9861 ± 0.0029; b = 0.0025 ± 0.0003
c = -2.297E-5 ± 5.537E-6; d = -0.0797 ± 0.076

$R^2 = 0.9979$

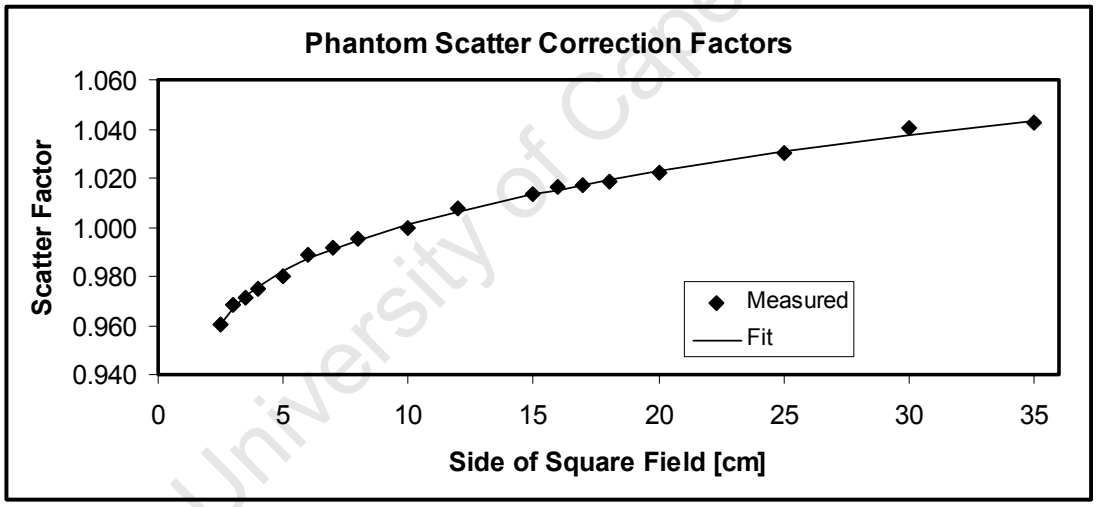

Figure 6.7: Parametrization of the Phantom Scatter Correction Factor using Equation 6.14

The model fits the data very well for field sizes ranging from 2.5 cm x 2.5 cm to 35 cm x 35 cm, but unfortunately no extrapolation to zero field size is possible because of the A^{-1} factor in the equation.

6.2 Determination of the Effective Primary Dose

6.2.1 Extrapolation of Measured Phantom Scatter

The effective primary dose was defined in the previous section. It includes the collimator scatter S_c and can thus be thought of as the dose at depth minus the phantom scatter.

The effective primary dose D_p at depth d is given by (Khan *et al.*, 1980):

$$D_p = D_R \cdot TMR\ (d,0) \tag{3.4}$$

where the reference dose D_R is the effective primary dose at maximum depth and TMR(d,0) is the tissue maximum ratio at the measurement depth extrapolated to zero field size and can be approximated by:

$$TMR\ (d,0) = e^{-\mu_0 \cdot (d - d_{max})} \quad \text{(Paul } \textit{et al.}\text{, 1983, Khan, 2003)} \tag{3.5}$$

where μ_0 is the primary beam linear attenuation coefficient.

The reference dose D_R is given by: (Khan *et al.*, 1980)

$$D_R = D_0(d_{max}, SSD_0 + d_{max}) \cdot \left(\frac{SSD_0 + d_{max}}{SSD + d}\right)^2 \cdot S_c(r_c) \cdot S_p(0) \tag{6.15}$$

where

D_0 is the calibration dose, i.e. the dose measured at $SDD_0 + d_{max}$ in the reference field,

$\left(\frac{SSD_0 + d_{max}}{SSD + d}\right)^2$ is an inverse square correction factor,

$S_c(r_c)$ is the collimator scatter correction factor for the reference field and

$S_p(0)$ is the zero field size phantom scatter correction factor

The reference conditions for the 6 MV beam of the Philips SL75-5 linear accelerator are a 10 cm x 10 cm field at an SSD_0 = 100 cm and a depth of maximum dose of d_{max} = 1.5 cm.

The LINAC has been calibrated to give a dose of 1Gy/100MU at the reference point. The inverse square correction factor in equation 6.15 is equal to 1 under the reference conditions, as is the collimator scatter factor (see also Figure 6.5).

This then leaves equation 6.15 as:

$$D_R = S_p(0) \tag{6.16}$$

TMR(d,0) at d = d_{max} = 1, thus equation 3.4 and equation 6.16 can be combined and written as

$$D_p = D_R = S_p(0) \tag{6.17}$$

Measured collimator and total scatter correction factors were used to determine the phantom scatter correction factors using equation 6.10 (see also Figure 6.5).

The phantom scatter correction values were extrapolated to zero field size using cubic, fourth- and fifth order polynomials fitted to the data.

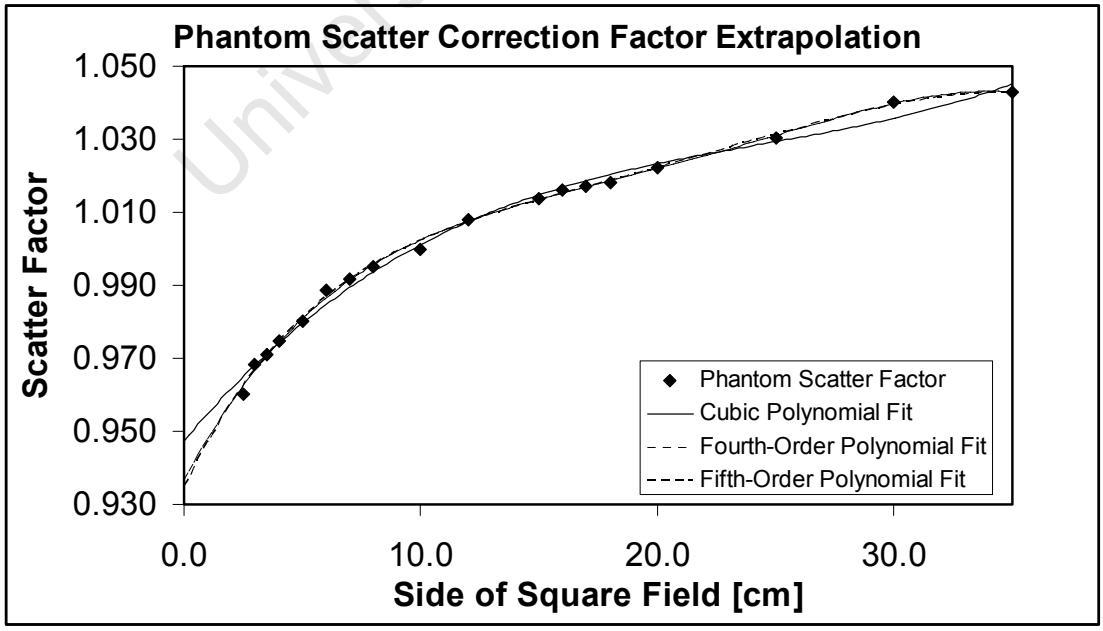

Figure 6.8: Phantom Scatter Correction Factor Extrapolation

It can be seen from the graph that there is very little difference between the fourth and fifth order polynomial, but also that the cubic polynomial does not fit the data quite as well as the other two.

The values obtained for $S_p(0)$ are:

Cubic polynomial: $S_p(0) = 0.947 \pm 0.003$ $(R^2 = 0.9921)$

Fourth order polynomial: $S_p(0) = 0.935 \pm 0.002$ $(R^2 = 0.9987)$

Fifth order polynomial: $S_p(0) = 0.934 \pm 0.003$ $(R^2 = 0.9987)$

with the error being the uncertainty of the intercept obtained from the fitting procedure.

Using the results of the fourth order polynomial one gets:

$$D_p\ (d_{max},\ 10\ cm \times 10\ cm) = 0.935\ Gy / 100\ MU$$

6.2.2 Measurement of D_p with Central Axis Attenuator Method

According to the central axis attenuator method (Chapter 3.4 and 4.5), the primary dose can be obtained by: $D_p(d) = [1 - 1/C_D(d)]^{-1} \cdot [D_T(d,S) - D_T^i(d,S)]$ (3.30)

This D_p is in fact the effective primary dose, as it includes the collimator scatter.

C_D can be obtained by a series of ionization measurements with and without an attenuator in the beam as described in Chapter 3.4.1.

D_T and D_T^i were measured accurately with a calibrated ionization chamber in a water phantom at d_{max} for two different central axis attenuators in a 10 x 10 cm^2 field.

The measured values are:

$D_T\ (d_{max},\ 10 \times 10\ cm^2) = 1.000\ Gy / 100\ MU$

$D_T^i\ (d_{max},\ 10 \times 10\ cm^2) = 0.528\ Gy / 100\ MU$ for 1 cm lead attenuator

$D_T^i\ (d_{max},\ 10 \times 10\ cm^2) = 0.309\ Gy / 100\ MU$ for 2 cm lead attenuator

C_D = 2.042 for 1 cm lead attenuator

C_D = 3.765 for 2 cm lead attenuator

The corresponding D_p (d_{max}, 10 cm x 10 cm) are:

D_p (d_{max}, 10 cm x 10 cm) = 0.925 Gy/100MU using 1 cm attenuator

D_p (d_{max}, 10 cm x 10 cm) = 0.941 Gy/100 MU using 2 cm attenuator

These two values differ by 1.7% even though great care was taken when doing the measurements. The results should be identical, because $C_D(d)$ takes into account beam hardening. Therefore an error analysis regarding the error in the primary dose was done.

6.2.3 Error in D_p (dmax)

Taylor (1982) writes the following: Suppose x,…,z are measured with uncertainties δx,…,δz and the measured values are used to compute the function q(x,…,z). If the uncertainties in x,..,z are independent and random, then the uncertainty in q is:

$$\delta q = \sqrt{\left(\frac{\partial q}{\partial x}\delta x\right)^2 + \ldots + \left(\frac{\partial q}{\partial z}\delta z\right)^2} \tag{6.18}$$

C_D is given by:

$$C_D(d) = \frac{\ln\left[\frac{I(d+\Delta)}{I(d)}\right]}{\ln\left[\frac{I(h+d+\Delta)}{I(h+d)}\right]} \cdot \frac{I(d)}{I(h+d)} \tag{3.42}$$

The four partial derivatives of C_D are given by:

$$\frac{\partial C_D(d)}{\partial [I(d)]} = \frac{\ln[I(d+\Delta)] - \ln[I(d)] - 1}{I(h+d)\cdot \ln\left(\frac{I(h+d+\Delta)}{I(h+d)}\right)} \tag{6.19}$$

$$\frac{\partial C_D(d)}{\partial [I(h+d)]} = I(d)\ln\left(\frac{I(d+\Delta)}{I(d)}\right)\left(\frac{1-\ln[I(h+d+\Delta)]+\ln[I(h+d)]}{[I(h+d)]^2\cdot(\ln[I(h+d+\Delta)]-\ln[I(h+d)])^2}\right) \tag{6.20}$$

$$\frac{\partial C_D(d)}{\partial [I(d+\Delta)]} = \frac{I(d)}{I(h+d)}\frac{1}{\ln\left(\frac{I(h+d+\Delta)}{I(h+d)}\right)}\frac{1}{I(d+\Delta)} \tag{6.21}$$

$$\frac{\partial C_D(d)}{\partial [I(h+d+\Delta)]} = \frac{I(d)}{I(h+d)}\ln\left(\frac{I(d+\Delta)}{I(d)}\right)\left(\frac{-\frac{1}{I(h+d+\Delta)}}{(\ln[I(h+d+\Delta)]-\ln[I(h+d)])^2}\right) \tag{6.22}$$

The measured ionization values are:

Depth	no attenuator	1cm Pb attenuator	2cm Pb attenuator
1.5 cm	0.8400	0.4852	0.2892
2.0 cm	0.8186	0.4747	0.2835

Table 5.4: Measured Ionization Values

A special phantom was constructed for these measurements. The phantom had an area of exactly 100 cm^2 (i.e. 10.0 cm x 10.0 cm), so that a syringe filled with 50 ml of water would increase the depth by 5 mm exactly.

The uncertainty in the ionization measurements was determined for the specific chamber used. The 0.6cc NE Farmer type 2571 chamber has an uncertainty in its reading of 0.05% (= standard deviation expressed as a percentage of the mean of 15 consecutive measurements).

Using the obtained ionization values, together with a fractional error of 0.05% for each measurement, the error in the ionization was obtained according to Equation 6.18.

This gives the following results

D_p (d_{max}, 10 cm x 10 cm) = 0.925 Gy/100MU ± 4.5% using the 1 cm attenuator

D_p (d_{max}, 10 cm x 10 cm) = 0.941 Gy/100 MU ± 4.8% using the 2 cm attenuator

Since the error bars in each result for D_p (d_{max}, 10 cm x 10 cm) overlap, the average of those two values was taken to be D_p (d_{max}, 10 cm x 10 cm).

Therefore: D_p (d_{max}, 10 cm x 10 cm) = 0.933 Gy/100MU

6.2.4 Average D_p (d_{max})

The values obtained for the effective primary dose under reference conditions are given below:

Extrapolation of $S_p(r)$:	D_p (d_{max}, 10 cm x 10 cm) = 0.935 Gy/ 100 MU
Central axis attenuator:	D_p (d_{max}, 10 cm x 10 cm) = 0.933 Gy/ 100 MU
Average:	D_p (d_{max}, 10 cm x 10 cm) = 0.934 Gy/ 100 MU

6.3 Scatter-Primary Ratio

The scatter primary ratio is defined as the ratio between the primary and scattered dose components and can be expressed as:

$$\text{SPR}\,(d,S) = \frac{D_s(d,S)}{D_p(d)} \tag{2.13}$$

But $D_t(d,S) = D_p(d) + D_s(d,S)$ (2.4) and therefore

$$\text{SPR}\,(d,S) = \frac{D_t(d,S)}{D_p(d)} - 1 \tag{6.23}$$

The SPR is also defined as: SPR(d,S) = SMR(d,S)/TMR(d,0) (Iwasaki, 1996) (6.24)

and can thus be written as: $\text{SPR}(d,S) = \frac{\text{TMR}(d,S)}{\text{TMR}(d,0)} - 1$ (6.25)

Thus the SPR is zero at zero field size. The TMR data, including the extrapolated zero field size TMRs, are shown in Appendix C. This data was used to construct a set of SPRs. Some of the data is shown in Figure 6.9.

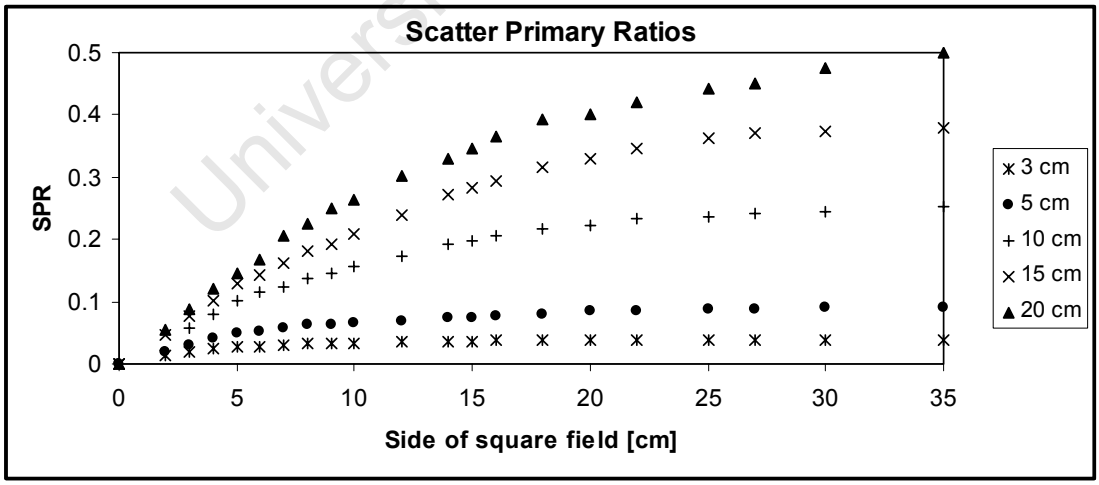

Figure 6.9: Scatter Primary Ratios

Bjärngard & Petti (1988) state that SPR = K·μ·z (see also section 3.1) with z = rd/(r+d). Thus the SPR is a linear function in z. If the SPRs are extrapolated to zero field size they should cross at zero. The SPR was therefore expressed as a

function of z. A linear extrapolation to zero field size was performed at various depths, but only a few are shown in Figure 6.10 to avoid cluttering

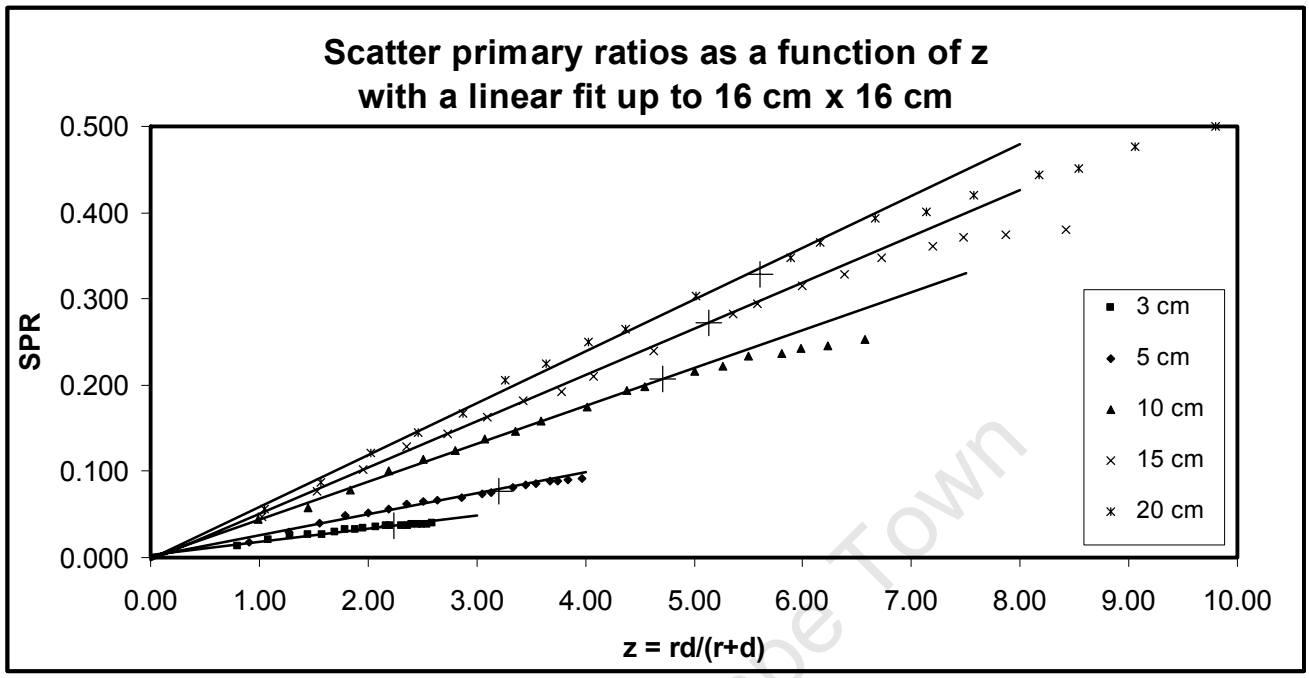

Figure 6.10: Scatter Primary Ratios as a Function of z

The + signs in Figure 6.10 represent the 16 cm x 16 cm field.

The average intercept of all the linear fits to field sizes up to 16 cm x 16 cm is $-7.5 \cdot 10^{-6}$. This then also confirms that the parametrization $z = rd/(r+d)$ is a valid concept for fields with a radius of less than 9 cm within the depth interval $2d_{max} < d \leq 30$ cm. As mentioned in Chapter 3.1, when the field size or depth increases, the simple proportionality of the SPR to z is no longer sufficiently accurate, but can be written as $SPR = a \cdot z + b \cdot z^2$. However, in this work this is not of relevance.

6.4 Peak Scatter Factor and Scatter-Maximum Ratio

Xiao & Bjärngard (1998) fitted backscatter factors for orthovoltage X-ray beams with the expression $BSF = 1 + m \cdot S/(S+n)$ (6.26), where S is the field size and m and n are adjustable parameters. Li (1999) confirmed that this expression describes the peak

scatter factors obtained with Monte Carlo calculations to within 0.4 % for energies from ^{60}Co to 24 MV. The PSF obtained in this work are shown in Appendix C.

The obtained values for m and n in this work are:

m = 0.1396 ± 0.0022 and n = 9.4606 ± 0.3733.

R^2 = 0.9967 and the maximum error of the fitted vs. measured values is 0.3 %.

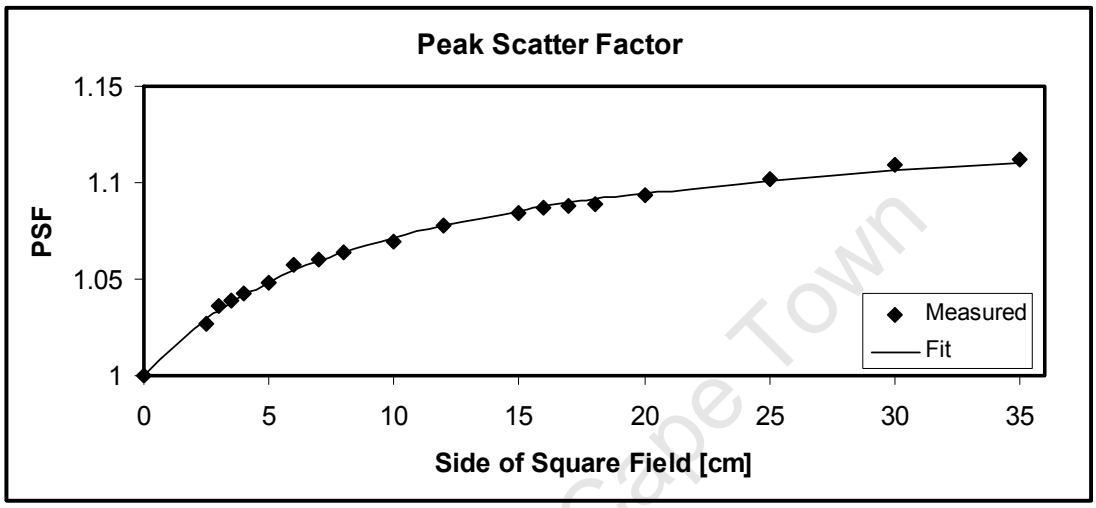

Figure 6.11: Peak Scatter Factors and Fitted Equation

Scatter-Maximum Ratios were calculated using equation 2.12 and are shown in Appendix C. Some of the SMRs are shown in Figure 6.12 and Figure 6.13.

$$SMR(d,S) = TMR(d,S)\cdot\frac{S_p(S)}{S_p(0)} - TMR(d,0) \qquad (2.12)$$

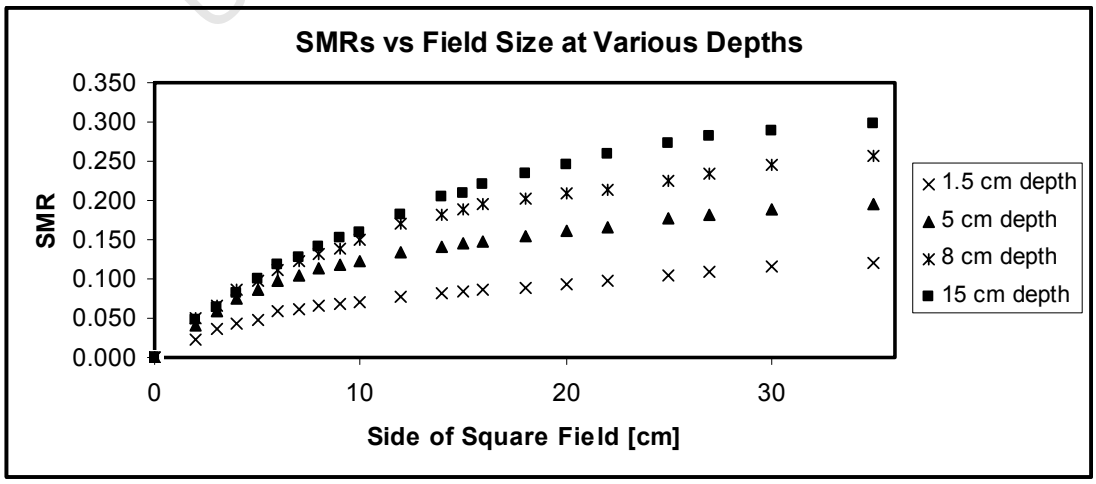

Figure 6.12: SMRs vs. Field Size at Various Depths

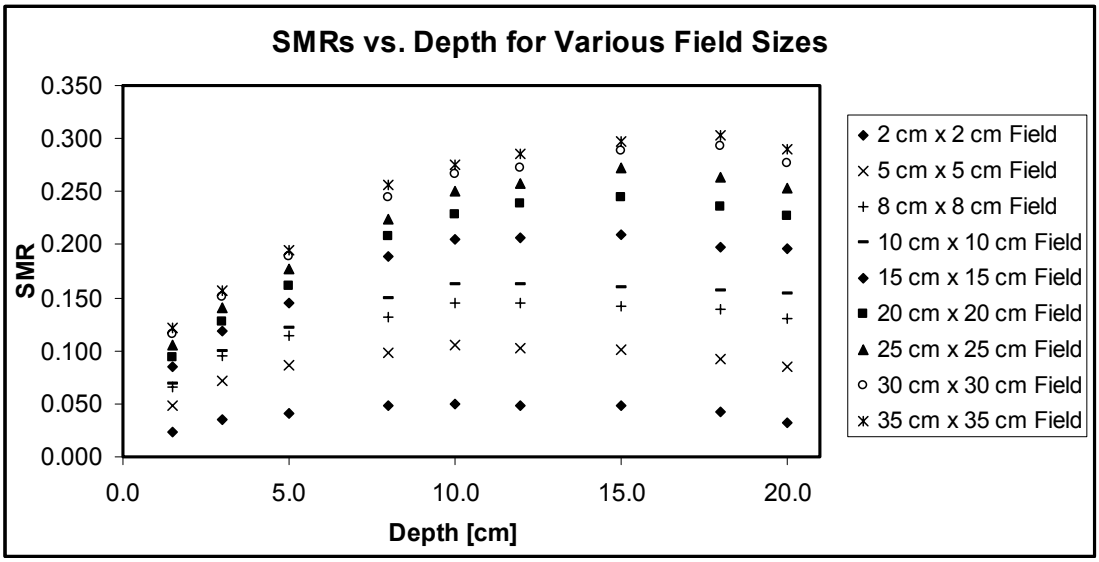

Figure 6.13: SMRs vs. Depth for Various Field Sizes

The SMRs obtained with Equation 2.12 are identical to Scatter-Air Ratios as defined in Chapter 2.8.5. The SARs on the TPP Planning System at Groote Schuur Hospital follow a very similar pattern to the SMRs obtained in this work.

6.5 Total Dose

The separation of the dose in terms of primary and scattered dose components can be done in terms of the tissue-air ratio and the scatter-air ratio, or in terms of the tissue-maximum ratio and the scatter-maximum ratio.

$$\text{Day (1983 \& 1996): } TAR(d,S) = TAR(d,0) + SAR(d,S) \tag{3.1}$$

$$\text{Khan } et\ al. \text{ (1980): } TMR(d,S) = [TMR(d,0) + SMR(d,S)] \cdot \frac{S_p(0)}{S_p(S)} \tag{6.27}$$

where $S_p(S)$ and $S_p(0)$ are the phantom scatter correction factors at field size S and field size 0.

The dose at depth in a phantom consists of two components: the effective primary dose and the phantom scatter. The reference dose in the definition of Khan's revised SMR is the effective primary dose at the depth of maximum dose (Khan *et al*., 1980). The reference dose is given by:

$$D_R(d_{max}, S) = D_0(d_{max}, SSD_0 + d_{max}) \cdot \left(\frac{SSD_0 + d_{max}}{SSD + d} \right)^2 \cdot S_c(S) \cdot S_p(0) \qquad (6.28)$$

where the field size S is defined at the distance where the collimator scatter correction factors are defined and $D_0(d_{max}, SSD_0 + d_{max})$ is the calibration dose measured in a reference field at depth d_{max}.

The scattered dose is given by:

$$D_s = D_R \cdot SMR(d,S) \qquad (6.29)$$

and the effective primary dose at depth d is given by:

$$D_p = D_R \cdot TMR(d,0) \qquad (3.4)$$

The total dose is given by the sum of the primary and scattered components:

$$D_t = D_p + D_s = D_R \cdot [TMR(d,0) + SMR(d,S)] \qquad (6.30)$$

Thus, the total dose is given by:

$$D_t(d,S) = D_0(d_{max}, SSD_0 + d_{max}) \cdot [TMR(d,0) + SMR(d,S)] \cdot \left(\frac{SSD_0 + d_{max}}{SSD + d} \right)^2 \cdot S_c(S) \cdot S_p(0) \qquad (6.31)$$

Worked examples are shown in Appendix D.

6.6 Comparison to Literature

Rice & Chin (1990) did Monte Carlo calculations of scatter to primary ratios for the normalization of primary and scattered dose.

For a 6 MV beam they found $\mu = 0.048\ cm^{-1}$ and $S_p(0) = 0.928 \pm 0.013$. They used a reference field of 10 cm x 10 cm, equivalent to r = 5.64 cm. The value of $S_p(0)$, defined as the magnitude of the primary dose relative to the total dose at d_{max} in a 10 cm x 10 cm field, ranges from 0.92 - 0.94 for the range of photon beam energies from 4 - 24 MV. They recommend that an average value of 0.93 ± 1 % can be used for this energy range.

The quantity $S_p(0)$ is the identical to the $NPSF_0$ (normalized peak scatter factor) as defined by Day (1983). These quantities are normally defined by extrapolation of measured data to zero field size. No suggestions are made of how the extrapolation should be done and Day (1983) only gives a value of $NPSF_0$ for 8 MV X-rays of 0.960.

Rice & Chin (1990) give an $S_p(0; d = d_{max}=2.5cm) = 0.927 \pm 0.013$ for a 10 MV beam with a reference field of 10 cm x 10 cm, very similar to their result for a 6 MV beam.

Iwasaki (1989) gives an $S_p(0; d = d_{max}=2.5cm) = 0.988$ for a 10 MV beam with a reference field of 10 cm x 10 cm.

Haider & El-Khatib (1995) reported an $S_p(0; d = d_{max}=2.5cm) = 0.972$ for a 10 MV beam. Both of these values are much higher than the one's obtained by Rice & Chin (1990).

Iwasaki (1996) later revised his value of $S_p(0)$ in a 10 MV beam to $S_p(0; d = d_{max}=2.5cm) = 0.912$ and he concludes that the previous value of 0.988 "is not accurate".

The value of $S_p(0) = 0.934$ obtained in this work agrees very well with the published data by Rice & Chin (1990).

A number of primary linear attenuation coefficients for nominal 6 MV beams found in literature are listed below:

Van Dyk (1986): $\mu_0 = 0.0455$ cm^{-1}

Bjärngard *et al*. (1989): $\mu_0 = 0.0505$ cm^{-1}

Bjärngard & Vadash (1995): $\mu_0 = 0.0473$ cm^{-1}

Zefkili *et al.* (1994): $\mu_0 = 0.0481$ cm^{-1} and $\mu_0 = 0.0462$ cm^{-1}

Lee *et al*. (1999): $\mu_0(d_{max}) = 0.0474$ cm^{-1} and $\mu_0(20) = 0.0436$ cm^{-1}

The value obtained in this work is $\mu_0 = 0.0455$ cm^{-1} with μ_0 ranging from $\mu_0 = 0.0445$ cm^{-1} to $\mu_0 = 0.0469$ cm^{-1}. These values are also in agreement with quoted values in the literature.

CHAPTER 7 DISCUSSION AND CONCLUSION

Absorbed dose measurements must take place under charged particle equilibrium, i.e. forward and lateral charged particle equilibrium (AAPM TG 21 protocol, 1983, IAEA TRS 398 protocol, 2000). Therefore it is important to know the range of released charged particles in the forward and lateral directions. The average range of the charged particles in the forward direction was found to be 1.5 cm in water, which is the depth of maximum dose for a 6 MV photon beam. This agrees with the value for the depth of maximum dose for a 6 MV beam published in the BJR Supplement 25 (Jordan, 1996), which is also 1.5 cm in water.

The lateral range of charged particles in water was found to be about 0.6 cm. It is important to know this value, because narrow-beam measurements should not be done in beams with a radius of less than this value. The central axis dose is reduced significantly for beams with radii smaller than this value. The obtained value is slightly smaller than the value quoted by Bjärngard *et al*. (1990), who wrote that the central axis dose of a 6 MV beam is progressively reduced due to electron disequilibrium for beam radii < 1.0 cm. Rice *et al*. (1987) estimated an uncertainty for the central axis dose in a 6 MV beam due to a lack of lateral electronic equilibrium of 2.5 % in a 12.5 mm diameter circular field. This value is fairly close to the obtained value of r = 0.6 cm for lateral electronic equilibrium.

Narrow-beam measurements in this work were done in beams of dimensions down to 2 cm x 2 cm. The measurements in such narrow beams had to be done at an extended source-detector distance, so that the build-up cap was fully covered by the beam.

A high-energy photon beam undergoes a number of different interactions in a medium. It is a common technique to separate the dose to a point in a medium in terms of primary and scattered dose components (Meredith and Neary, 1944, Khan *et al.*, 1980, Day, 1983, Kijewski *et al.*, 1986, Bjärngard *et al.*, 1988, Holt *et al.*, 1970). This separation can be done in terms the tissue-air ratio and scatter-air ratio, or in terms of the tissue-maximum ratio and the scatter maximum ratio (see Chapter 6.5). These parameters describe the beam in a simple and understandable manner and can also be entered into a treatment planning system and used for radiotherapy dose calculations.

The primary beam is not field size dependent and under full equilibrium conditions has a radius equal to the lateral range of the released electrons. However, any measured dose will include some scatter from the collimator system. Therefore the effective primary dose is the dose due to the primary beam plus the photons scattered from the collimating system (Bjärngard & Cunningham, 1986). This means that the effective primary dose is field size dependent. The scattered dose component ($S_{c,p}$) is conveniently subdivided into two parts: the collimator scatter (S_c) and phantom scatter (S_p). As the field size is increased, scatter from both the collimating system and from the object being irradiated contribute to the total dose.

The effective primary dose D_p at depth d is given by (Khan *et al.*, 1980):

$D_p = D_R \cdot TMR\ (d,0)$ (Equation 3.4),

where D_R is the effective primary dose at maximum depth in the reference field and TMR(d,0) is the tissue maximum ratio at the measurement depth extrapolated to zero field size.

Two extrapolation techniques were used to extrapolate the measured tissue-maximum ratios to zero field size. In the first technique an exponential function was fitted to the measured TMRs at every field size to obtain a set of linear attenuation coefficients as a function of field size. A cubic, fourth- and fifth order polynomial was fitted to the linear attenuation coefficient as a function of field size to extrapolate these attenuation coefficients to zero field size. The fourth and fifth order polynomials gave the same result for $\mu(0)$ with the same R^2 value of $R^2 = 0.9996$.

The obtained value was $\mu(0) = 0.0472 \pm 0.0002\ cm^{-1}$

The TMRs were also expressed as a function of z, where $z = \frac{r \cdot d}{r + d}$. A linear extrapolation for small field sizes yielded $\mu_0 = 0.0466 \pm 0.0006\ cm^{-1}$. The validity of this extrapolation technique was confirmed in Chapter 6.3 where it was shown that the SPRs can indeed be expressed as $SPR = K \cdot \mu \cdot z$, i.e. the SPRs are a linear function in z. Thus the average primary linear attenuation coefficient for the TMR extrapolation to zero field size was taken to be $\mu_0 = 0.0469 \pm 0.0006\ cm^{-1}$. The TMR(d,0) can be approximated by $TMR(d,0) = e^{-\mu_0 \cdot (d - d_{max})}$ (Paul *et al.*, 1983, Khan, 2003), where μ_0 is the primary beam linear attenuation coefficient. Therefore it is important to know the value of μ_0 as accurately as possible.

Attenuation measurements in the 6 MV photon beam were done for nine field sizes ranging from 2 cm x 2 cm to 20 cm x 20 cm with water depths ranging from 0 cm to 20 cm. A cubic fit of the obtained attenuation coefficients vs. field size (Robinson *et al.*, 1991) resulted in a μ_0 of $\mu_0 = 0.0460 \pm 0.0001\ cm^{-1}$. It is interesting to note that the linear attenuation coefficient in a 3 cm x 3 cm field is less than 0.5% different than

the zero field size attenuation coefficient. This may lead to the conclusion that a beam of dimensions up to 3 cm x 3 cm can be considered a narrow beam.

The effect of beam hardening was also investigated. The same attenuation data was analyzed in terms of an attenuation coefficient μ and a beam hardening coefficient η in Chapter 5.2.1.

The values were found to be $\mu = 0.0469\ cm^{-1}$ and $\eta = 0.0015\ cm^{-1}$. Bjärngard & Shackford (1994) estimate the uncertainty in μ to be about 1 % and the uncertainty in η to be about 20 %. The μ obtained here is not the same as the primary linear attenuation coefficient except at zero depth. It was found that if the beam hardening is disregarded, then the maximum error in transmission through 20 cm of water is about 3 %. However, this is not an issue when empirical central-axis data is used in dose calculations.

The quality index of the beam was calculated using the obtained values of μ and η (equation 5.3) and was found to be QI = 0.679. Varying μ by 1% gives the QI a range from 0.676 to 0.681, while varying η by 20% gives the QI a range from 0.676 to 0.682.

The QI calculated using the $\frac{TPR_{20}}{TPR_{10}}$ gives a QI = 0.685 ± 0.004. The error bars in the determination of the quality index overlap in the two methods.

The quality index of a 6 MV beam is quoted in literature in a range from at least 0.650 (NCS Report 12, 1998) to 0.689 (Sätherberg *et al*., 1996). The values for the QI obtained in this work fall into this range.

It is interesting to note that the quality index of a ^{60}Co beam is quoted in literature in a range from 0.570 - 0.579 (Johns & Cunningham, 1983, Shortt *et al*., 1993, Nutbrown

et al., 2002, Godden, 1983, McKenzie, 1996). This variation in the quality index is larger than the variation of the quality index for this beam using two different methods. Therefore the values obtained for the quality index in this work are in fairly good agreement with each other.

Measured percentage depth doses were smoothed and Pistorius's central axis kerma model was fitted to the data with the Marquard-Levenberg non-linear least squares algorithm. The obtained PDDs are shown in Appendix B. Chauvenet's criterion was applied to the residuals of the fit to check for any outliers. There were only three outliers in 1224 data points. The removal of the three outliers did not influence the results significantly. The mean of the residuals of the fit was 0.0 % with a standard deviation of 0.465 %. The fit resulted in a primary linear attenuation coefficient of $\mu_0 = 0.0445 \pm 0.0001$ cm^{-1}. This value is smaller than the values obtained from the TMR extrapolation to zero field size and from the attenuation measurements; nonetheless did the model fit the data excellently.

The equivalent squares calculated from the value of the obtained exponential scatter growth factor ($\lambda = 0.0696 \pm 0.0008$ cm^{-1}) of the fit agree very well with the values published in the BJR Supplement 17 & 25 (Day & Aird, 1983 and Day & Aird, 1996). The equivalent squares obtained from the use of Equation 3.27 are consistently larger than those from BJR Supplement 17 & 25. The differences become larger for larger field sizes, the largest difference occurs for a 35 cm x 35 cm field, where the difference between the two methods is 1.4%.

One major advantage of the central axis kerma model is that it only uses measured percentage depth dose data as input. No other measurements are necessary, which makes this a very convenient method of determining the primary linear attenuation coefficient.

The central axis attenuator method was applied to three different field sizes with two different central axis attenuators, giving a total of six values for the primary attenuation coefficient. The values of μ_0 obtained with the central axis attenuator method were very consistent and averaged $\mu_0 = 0.0445 \pm 0.0007$ cm^{-1}. No field size dependence of μ_0 was observed using this method. Therefore this method is very useful to determine the primary linear attenuation coefficient. It is, however, rather tedious to perform. No reference to the use of this technique in a beam other than ^{60}Co was found in peer-reviewed literature. However, Schreuder (1992) also applied this technique in the neutron beam at iThemba LABS with success.

The average of the primary linear attenuation coefficient was taken to be the average of the coefficients obtained using the four different methods. This resulted in $\mu_0 = 0.0455 \pm 0.0012$ cm^{-1}. The uncertainty in this value is the standard deviation of the mean.

Primary linear attenuation coefficients for nominal 6 MV beams found in literature range from $\mu_0 = 0.0436$ cm^{-1} (Lee *et al*., 1999) to $\mu_0 = 0.0505$ cm^{-1} (Bjärngard *et al*., 1989). The values obtained in this work fall within this range.

The value of the effective primary dose component using the central axis attenuator method was found to be 0.933 ± 4.5 % for the 10 cm x 10 cm field at d_{max}. Great care must be taken when using this method to determine the effective primary dose component, because the expression of C_D (Equation 3.42) is extremely sensitive to small changes in measured ionization and can thus result in large variations in the primary dose component. Nonetheless, it is a very useful technique to complement the more common extrapolation of the phantom scatter correction factor to zero field size.

Various parametrization methods from literature for the collimator (Chapter 6.1.1.1) and phantom scatter correction factors (Chapter 6.1.3.1) were investigated. It is of particular interest to extrapolate the phantom scatter correction factor to zero field size to obtain $S_p(0)$. The reference dose in $D_p = D_R \cdot TMR\ (d,0)$ (Equation 3.4) is given by

$$D_R = D_0(d_{max}, SSD_0 + d_{max}) \cdot \left(\frac{SSD_0 + d_{max}}{SSD + d} \right)^2 \cdot S_c(r_c) \cdot S_p(0)$$ (Khan *et al.*, 1980).

Under the reference conditions (i.e. D_0 = 1 Gy/100 MU in a 10 cm x 10 cm field at the depth of maximum dose), it turns out that the reference dose D_R is given by $S_p(0)$, because the collimator scatter factor is normalized to 1 for the reference field. Since $TMR(d_{max},0) = 1$ the effective primary dose at d_{max} in a 10 cm x 10 cm field is thus given by $D_p = S_p(0)$.

Unfortunately none of the parametrization methods for the phantom scatter correction factors in Chapter 6.1.3.1 can be extrapolated to zero field size. Therefore a cubic, fourth- and fifth order polynomial extrapolation of the phantom scatter correction factors to zero field was performed. The fourth- and fifth order polynomials gave a better fit than the cubic polynomial. They had an identical R^2 value of $R^2 = 0.9987$

and gave $S_p(0) = 0.935$ and $S_p(0) = 0.934$ respectively. These values are in excellent agreement with the value of 0.933 obtained from the central axis attenuator method. The effective primary dose was taken as the average of the value obtained using the central axis attenuator method and the value obtained by extrapolating the phantom scatter correction factor to zero field size. This resulted in an effective primary dose component of 0.934 Gy/100 MU.

Therefore, if the 10 cm x 10 cm field is calibrated to yield 1 cGy/MU at the depth of maximum dose and the effective primary dose is 0.934 cGy/MU at the same point, then the rest of the dose is made up of scattered radiation, i.e. 6.6 % of the dose at that point is due to scattered radiation.

Rice & Chin (1990) published a value for the magnitude of the primary dose relative to the total dose at d_{max} in a 10 cm x 10 cm field, of $S_p(0) = 0.928 \pm 0.013$ in a 6 MV beam. The obtained value in this work of 0.934 agrees very well with the value from Rice & Chin.

The separation of the total dose into primary and scattered dose components can be written as (Equation 6.30): $D_t = D_p + D_s = D_R \cdot [TMR(d,0) + SMR(d,S)]$.

The reference dose D_R has been established, as have the zero area tissue-maximum ratios. Scatter-maximum ratios were constructed, these are shown together with the tissue-maximum ratios and various scatter factors in Appendix C.

For any field size and depth other than the reference field size and depth, the reference dose D_R needs to be adjusted by the collimator scatter factor for the appropriate field size, as well as an inverse square correction factor. The total dose for any field size

can then be calculated according to Equation 6.31. Two worked examples are shown in Appendix D.

Venselaar *et al*. (1999) stated that it is important that a coherent system is used when doing dose calculations. These systems are generally based on quantities defined and normalized at d_{max}. If measurements are performed at a depth of 10 cm, but the treatment planning system requires scatter correction factors at d_{max} together with PSF and TAR data, then the electron contamination needs to be taken into account. This is why for example the NCS Report 12 (1998) recommends that all data is measured with a reference depth of 10 cm, regardless of the beam quality. However, Frye *et al*. (1995) reports on the dangers of using scatter factors measured at 5 cm or 10 cm depth to determine the TMRs, saying that phantom scatter correction factors could be overestimated for small field sizes and underestimated for large field sizes, when head-scatter factors are determined with a mini-phantom at depth 5 cm or 10 cm. This can lead to inaccuracies in the monitor unit calculation. Therefore d_{max} was chosen as reference depth in this work.

Even though the separation of dose into primary and scattered dose components has been questioned (Mohan & Chui, 1985), mainly because of the finite range of energetic electrons, the "questioning of calculation techniques that separate the primary and scatter components is … unwarranted." (Bjärngard & Cunningham, 1986). In this work it was shown that the 6 MV beam of the SL75-5 LINAC can be expressed in terms of tissue-maximum ratios and scatter-maximum ratios. In this way dose deposited by the beam is described in a simple and concise manner and this can be implemented on a treatment planning system.

APPENDIX A: SIGMAPLOT CODE

Initial Parameters:

```
a = 0.045                    ; Starting estimates of the fitting parameters
b = 1.04
Ninf = 0.27
lambda = 0.09
```

Variables:

```
x = col(1)                   ; Depth in cm
y = col(2)                   ; Percentage Depth Dose at SSD = 100 cm
FS = col(3)                  ; Field size
G = col(4)                   ; Inverse square correction factor
```

Equation:

```
mu = a                                                  ; Primary attenuation coefficient
N2 = Ninf * (1 - exp(-FS*lambda))                       ; Relative scattering fraction N2(S)
C = 1 / N2                                              ;
F = b                                                   ; Empirical factor
eta = mu * F * C / 2                                    ; η(S) = μ0 · F / (2 · N2(S))
gamma = eta - mu * (1 - N2)                             ; Γ = η(S) - μ0·(1 - N2(S) )
A = eta - 1/x * ln( (C * exp (gamma * x) - 1) / (C - 1))   ; Apply at all depths
A1 = eta - 1/1.5 * ln( (C * exp (gamma * 1.5) - 1) / (C - 1))   ; Let PDD(dmax) = 100%
A2 = 100*exp(A1*1.5)                                    ;
f = A2* exp (-A*x)*G                                    ; Fit the model
fit f to y
```

Options:

```
Iterations: 500      ; Maximum number of iterations
Step Size: 0.01      ; Limit of the initial change in parameter values used by the curve fitter
Tolerance: 1E-8      ; When the absolute value of the difference between the norm of the
                     ; residuals (square root of the sum of squares of the residuals), from
                     ; one iteration to the next, is less than the tolerance value, the iteration
                     ; stops
```

APPENDIX B: PERCENTAGE DEPTH DOSE DATA

	Field Size [cm x cm]																
Depth [cm]	**2**	**3**	**4**	**5**	**6**	**8**	**10**	**12**	**14**	**16**	**18**	**20**	**22**	**25**	**27**	**30**	**35**
1.5	100	100	100	100	100	100	100	100	100	100	100	100	100	100	100	100	100
2.0	97.3	97.6	97.7	97.8	97.9	98.0	98.1	98.2	98.2	98.3	98.3	98.4	98.4	98.4	98.4	98.5	98.5
2.5	94.7	95.1	95.4	95.6	95.7	96.0	96.2	96.3	96.4	96.5	96.6	96.7	96.7	96.8	96.9	96.9	97.0
3.0	92.0	92.6	93.0	93.3	93.6	94.0	94.2	94.5	94.6	94.8	94.9	95.0	95.1	95.2	95.3	95.4	95.5
3.5	89.3	90.0	90.6	91.0	91.4	91.9	92.3	92.6	92.8	93.0	93.2	93.3	93.4	93.6	93.7	93.8	93.9
4.0	86.7	87.6	88.2	88.8	89.2	89.8	90.3	90.7	91.0	91.2	91.4	91.6	91.8	92.0	92.1	92.2	92.4
4.5	84.1	85.1	85.9	86.5	87.0	87.8	88.4	88.8	89.2	89.5	89.7	89.9	90.1	90.3	90.5	90.6	90.8
5.0	81.6	82.7	83.6	84.3	84.8	85.7	86.5	86.9	87.3	87.7	88.0	88.2	88.5	88.7	88.9	89.1	89.3
5.5	79.2	80.3	81.3	82.0	82.7	83.7	84.5	85.1	85.5	85.9	86.3	86.5	86.8	87.1	87.3	87.5	87.7
6.0	76.8	78.0	79.0	79.9	80.6	81.7	82.5	83.2	83.7	84.2	84.5	84.9	85.1	85.5	85.7	85.9	86.2
6.5	74.5	75.7	76.8	77.7	78.5	79.7	80.6	81.4	81.9	82.4	82.8	83.2	83.5	83.9	84.1	84.3	84.7
7.0	72.2	73.5	74.6	75.6	76.4	77.7	78.7	79.5	80.2	80.7	81.2	81.5	81.9	82.3	82.5	82.8	83.1
7.5	70.1	71.4	72.5	73.5	74.4	75.8	76.9	77.7	78.4	79.0	79.5	79.9	80.2	80.7	80.9	81.2	81.6
8.0	68.0	69.3	70.5	71.5	72.4	73.9	75.0	75.9	76.7	77.3	77.8	78.3	78.6	79.1	79.4	79.7	80.1
8.5	65.9	67.2	68.5	69.5	70.5	72.0	73.2	74.2	75.0	75.6	76.2	76.6	77.0	77.5	77.8	78.2	78.6
9.0	63.9	65.3	66.5	67.6	68.6	70.2	71.4	72.4	73.3	74.0	74.5	75.0	75.5	76.0	76.3	76.6	77.1
9.5	62.0	63.3	64.6	65.7	66.7	68.4	69.7	70.7	71.6	72.3	72.9	73.5	73.9	74.5	74.8	75.2	75.6
10.0	60.2	61.5	62.7	63.9	64.9	66.6	68.0	69.1	70.0	70.7	71.4	71.9	72.4	72.9	73.3	73.7	74.2
10.5	58.4	59.7	60.9	62.1	63.1	64.9	66.3	67.4	68.3	69.1	69.8	70.4	70.8	71.4	71.8	72.2	72.7
11.0	56.6	57.9	59.2	60.3	61.4	63.2	64.6	65.8	66.7	67.6	68.3	68.8	69.3	70.0	70.3	70.8	71.3
11.5	54.9	56.2	57.5	58.6	59.7	61.5	63.0	64.2	65.2	66.0	66.7	67.3	67.9	68.5	68.9	69.3	69.9
12.0	53.3	54.6	55.8	57.0	58.1	59.9	61.4	62.6	63.7	64.5	65.2	65.9	66.4	67.1	67.5	67.9	68.5
12.5	51.7	53.0	54.2	55.4	56.5	58.3	59.8	61.1	62.1	63.0	63.8	64.4	65.0	65.7	66.1	66.5	67.1
13.0	50.2	51.4	52.6	53.8	54.9	56.8	58.3	59.6	60.7	61.6	62.3	63.0	63.6	64.3	64.7	65.2	65.8
13.5	48.7	49.9	51.1	52.3	53.4	55.3	56.8	58.1	59.2	60.1	60.9	61.6	62.2	62.9	63.3	63.8	64.5
14.0	47.2	48.4	49.7	50.8	51.9	53.8	55.4	56.7	57.8	58.7	59.5	60.2	60.8	61.6	62.0	62.5	63.1
14.5	45.8	47.0	48.2	49.4	50.5	52.4	53.9	55.3	56.4	57.4	58.2	58.9	59.5	60.2	60.7	61.2	61.9
15.0	44.5	45.7	46.8	48.0	49.1	51.0	52.6	53.9	55.0	56.0	56.8	57.5	58.2	58.9	59.4	59.9	60.6
15.5	43.2	44.3	45.5	46.6	47.7	49.6	51.2	52.6	53.7	54.7	55.5	56.2	56.9	57.7	58.1	58.6	59.3
16.0	41.9	43.0	44.2	45.3	46.4	48.3	49.9	51.2	52.4	53.4	54.2	55.0	55.6	56.4	56.8	57.4	58.1
16.5	40.6	41.8	42.9	44.0	45.1	47.0	48.6	50.0	51.1	52.1	53.0	53.7	54.4	55.2	55.6	56.2	56.9
17.0	39.4	40.6	41.7	42.8	43.8	45.7	47.3	48.7	49.9	50.9	51.7	52.5	53.1	53.9	54.4	55.0	55.7
17.5	38.3	39.4	40.5	41.6	42.6	44.5	46.1	47.5	48.6	49.7	50.5	51.3	51.9	52.8	53.2	53.8	54.5
18.0	37.2	38.2	39.3	40.4	41.4	43.3	44.9	46.3	47.5	48.5	49.3	50.1	50.8	51.6	52.0	52.6	53.4
18.5	36.1	37.1	38.2	39.3	40.3	42.1	43.7	45.1	46.3	47.3	48.2	49.0	49.6	50.4	50.9	51.5	52.2
19.0	35.0	36.1	37.1	38.2	39.2	41.0	42.6	44.0	45.1	46.2	47.1	47.8	48.5	49.3	49.8	50.4	51.1
19.5	34.0	35.0	36.1	37.1	38.1	39.9	41.5	42.8	44.0	45.1	45.9	46.7	47.4	48.2	48.7	49.3	50.0
20.0	33.0	34.0	35.0	36.1	37.0	38.8	40.4	41.8	42.9	44.0	44.9	45.6	46.3	47.1	47.6	48.2	49.0
20.5	32.0	33.0	34.0	35.0	36.0	37.8	39.3	40.7	41.9	42.9	43.8	44.6	45.2	46.1	46.6	47.2	47.9
21.0	31.1	32.1	33.1	34.1	35.0	36.8	38.3	39.7	40.8	41.9	42.8	43.5	44.2	45.0	45.5	46.1	46.9
21.5	30.2	31.2	32.1	33.1	34.0	35.8	37.3	38.7	39.8	40.8	41.7	42.5	43.2	44.0	44.5	45.1	45.9
22.0	29.3	30.3	31.2	32.2	33.1	34.8	36.3	37.7	38.8	39.9	40.7	41.5	42.2	43.0	43.5	44.1	44.9
22.5	28.5	29.4	30.3	31.3	32.2	33.9	35.4	36.7	37.9	38.9	39.8	40.5	41.2	42.1	42.5	43.1	43.9
23.0	27.6	28.6	29.5	30.4	31.3	33.0	34.5	35.8	36.9	37.9	38.8	39.6	40.3	41.1	41.6	42.2	43.0
23.5	26.8	27.7	28.6	29.6	30.4	32.1	33.6	34.9	36.0	37.0	37.9	38.7	39.3	40.2	40.7	41.3	42.0
24.0	26.1	26.9	27.8	28.7	29.6	31.2	32.7	34.0	35.1	36.1	37.0	37.8	38.4	39.3	39.7	40.3	41.1
24.5	25.3	26.2	27.1	27.9	28.8	30.4	31.8	33.1	34.2	35.2	36.1	36.9	37.5	38.4	38.8	39.5	40.2
25.0	24.6	25.4	26.3	27.2	28.0	29.6	31.0	32.3	33.4	34.4	35.2	36.0	36.7	37.5	38.0	38.6	39.3
25.5	23.9	24.7	25.6	26.4	27.2	28.8	30.2	31.4	32.6	33.5	34.4	35.1	35.8	36.6	37.1	37.7	38.5
26.0	23.2	24.0	24.8	25.7	26.5	28.0	29.4	30.6	31.7	32.7	33.6	34.3	35.0	35.8	36.3	36.9	37.6
26.5	22.5	23.3	24.1	25.0	25.8	27.3	28.6	29.9	31.0	31.9	32.8	33.5	34.2	35.0	35.5	36.1	36.8
27.0	21.9	22.6	23.5	24.3	25.0	26.5	27.9	29.1	30.2	31.1	32.0	32.7	33.4	34.2	34.7	35.2	36.0
27.5	21.2	22.0	22.8	23.6	24.4	25.8	27.2	28.4	29.4	30.4	31.2	31.9	32.6	33.4	33.9	34.5	35.2
28.0	20.6	21.4	22.2	22.9	23.7	25.1	26.5	27.6	28.7	29.6	30.5	31.2	31.8	32.6	33.1	33.7	34.4
28.5	20.0	20.8	21.5	22.3	23.0	24.5	25.8	26.9	28.0	28.9	29.7	30.4	31.1	31.9	32.4	32.9	33.7
29.0	19.4	20.2	20.9	21.7	22.4	23.8	25.1	26.2	27.3	28.2	29.0	29.7	30.4	31.2	31.6	32.2	32.9
29.5	18.9	19.6	20.4	21.1	21.8	23.2	24.4	25.6	26.6	27.5	28.3	29.0	29.6	30.4	30.9	31.5	32.2
30.0	18.3	19.1	19.8	20.5	21.2	22.6	23.8	24.9	25.9	26.8	27.6	28.3	29.0	29.7	30.2	30.8	31.5
30.5	17.8	18.5	19.2	19.9	20.6	22.0	23.2	24.3	25.3	26.2	27.0	27.7	28.3	29.1	29.5	30.1	30.8
31.0	17.3	18.0	18.7	19.4	20.1	21.4	22.6	23.7	24.7	25.5	26.3	27.0	27.6	28.4	28.8	29.4	30.1
31.5	16.8	17.5	18.2	18.9	19.5	20.8	22.0	23.1	24.0	24.9	25.7	26.4	27.0	27.7	28.2	28.7	29.5
32.0	16.3	17.0	17.7	18.3	19.0	20.3	21.4	22.5	23.4	24.3	25.1	25.7	26.3	27.1	27.5	28.1	28.8
32.5	15.9	16.5	17.2	17.8	18.5	19.7	20.9	21.9	22.9	23.7	24.5	25.1	25.7	26.5	26.9	27.5	28.2
33.0	15.4	16.1	16.7	17.4	18.0	19.2	20.3	21.4	22.3	23.1	23.9	24.5	25.1	25.9	26.3	26.8	27.5
33.5	15.0	15.6	16.3	16.9	17.5	18.7	19.8	20.8	21.7	22.6	23.3	24.0	24.5	25.3	25.7	26.2	26.9
34.0	14.6	15.2	15.8	16.4	17.0	18.2	19.3	20.3	21.2	22.0	22.7	23.4	24.0	24.7	25.1	25.6	26.3
34.5	14.1	14.8	15.4	16.0	16.6	17.7	18.8	19.8	20.7	21.5	22.2	22.8	23.4	24.1	24.5	25.1	25.8
35.0	13.7	14.3	14.9	15.5	16.1	17.3	18.3	19.3	20.2	21.0	21.7	22.3	22.9	23.6	24.0	24.5	25.2

APPENDIX C: TISSUE-MAXIMUM RATIOS, SCATTER-MAXIMUM RATIOS AND SCATTER FACTORS

TMR Data

Field Size [cm x cm]	0	2	3	4	5	6	7	8	9	10	12	14	15	16	18	20	22	25	27	30	35
BJR Radius [cm]	0	1.12	1.68	2.24	2.80	3.36	3.91	4.47	5.03	5.58	6.69	7.80	8.35	8.90	10.00	11.10	12.19	13.83	14.92	16.54	19.24
Equation 3.27	0	1.12	1.68	2.24	2.80	3.36	3.92	4.48	5.04	5.60	6.72	7.83	8.39	8.95	10.07	11.18	12.29	13.96	15.07	16.74	19.51
Depth [cm]																					
1.5	1.000	1.000	1.000	1.000	1.000	1.000	1.000	1.000	1.000	1.000	1.000	1.000	1.000	1.000	1.000	1.000	1.000	1.000	1.000	1.000	1.000
3	0.946	0.959	0.965	0.969	0.971	0.972	0.974	0.976	0.977	0.978	0.979	0.980	0.981	0.981	0.981	0.981	0.981	0.982	0.982	0.982	0.983
5	0.870	0.887	0.897	0.907	0.914	0.917	0.921	0.925	0.928	0.929	0.932	0.936	0.937	0.939	0.942	0.945	0.946	0.948	0.949	0.950	0.951
8	0.748	0.779	0.785	0.800	0.807	0.813	0.821	0.826	0.832	0.840	0.852	0.860	0.864	0.868	0.872	0.875	0.877	0.880	0.884	0.889	0.896
10	0.682	0.712	0.722	0.736	0.751	0.760	0.768	0.776	0.782	0.790	0.801	0.814	0.818	0.824	0.830	0.834	0.841	0.844	0.848	0.850	0.855
12	0.620	0.651	0.660	0.673	0.680	0.698	0.710	0.717	0.723	0.729	0.742	0.756	0.762	0.767	0.777	0.785	0.788	0.791	0.796	0.799	0.801
15	0.535	0.560	0.576	0.590	0.604	0.611	0.622	0.632	0.638	0.647	0.663	0.681	0.686	0.692	0.704	0.711	0.721	0.729	0.734	0.735	0.738
18	0.464	0.495	0.504	0.516	0.530	0.538	0.553	0.566	0.576	0.581	0.591	0.602	0.610	0.611	0.628	0.640	0.647	0.658	0.667	0.678	0.684
20	0.426	0.448	0.461	0.474	0.488	0.497	0.514	0.522	0.533	0.541	0.555	0.566	0.574	0.582	0.594	0.597	0.605	0.615	0.618	0.629	0.639

SMR Data

Field Size [cm x cm]	0	2	3	4	5	6	7	8	9	10	12	14	15	16	18	20	22	25	27	30	35
BJR Radius [cm]	0	1.12	1.68	2.24	2.80	3.36	3.91	4.47	5.03	5.58	6.69	7.80	8.35	8.90	10.00	11.10	12.19	13.83	14.92	16.54	19.24
Equation 3.27	0	1.12	1.68	2.24	2.80	3.36	3.92	4.48	5.04	5.60	6.72	7.83	8.39	8.95	10.07	11.18	12.29	13.96	15.07	16.74	19.51
Depth [cm]																					
1.5	0.000	0.024	0.036	0.043	0.048	0.058	0.060	0.065	0.067	0.070	0.078	0.082	0.085	0.087	0.089	0.093	0.097	0.106	0.110	0.116	0.121
3	0.000	0.035	0.055	0.065	0.072	0.082	0.087	0.095	0.097	0.100	0.109	0.115	0.118	0.120	0.123	0.127	0.131	0.140	0.144	0.151	0.156
5	0.000	0.041	0.058	0.074	0.087	0.098	0.105	0.115	0.119	0.122	0.133	0.142	0.145	0.149	0.155	0.161	0.167	0.177	0.182	0.189	0.195
8	0.000	0.049	0.065	0.086	0.098	0.112	0.122	0.131	0.140	0.150	0.170	0.182	0.189	0.195	0.201	0.208	0.214	0.224	0.233	0.244	0.256
10	0.000	0.050	0.066	0.085	0.105	0.122	0.132	0.145	0.152	0.163	0.181	0.199	0.205	0.209	0.221	0.229	0.241	0.251	0.259	0.266	0.276
12	0.000	0.049	0.065	0.084	0.103	0.119	0.133	0.144	0.152	0.160	0.182	0.199	0.207	0.215	0.227	0.238	0.248	0.258	0.269	0.272	0.285
15	0.000	0.048	0.065	0.083	0.101	0.115	0.127	0.141	0.151	0.160	0.182	0.204	0.210	0.220	0.234	0.245	0.258	0.273	0.283	0.288	0.298
18	0.000	0.043	0.058	0.074	0.092	0.105	0.122	0.139	0.147	0.157	0.173	0.188	0.198	0.208	0.223	0.236	0.246	0.263	0.276	0.293	0.303
20	0.000	0.033	0.052	0.069	0.086	0.100	0.119	0.130	0.143	0.153	0.169	0.187	0.197	0.203	0.216	0.227	0.238	0.254	0.260	0.276	0.290

Scatter Factors

Field Size [cm x cm]	0	2.5	3	3.5	4	5	6	7	8	10	12	15	16	17	18	20	25	30	35
BJR Radius [cm]	0	1.40	1.68	1.96	2.24	2.80	3.36	3.91	4.47	5.58	6.69	8.35	8.90	9.45	10.00	11.10	13.83	16.54	19.24
Equation 3.27 [cm]	0	1.40	1.68	1.96	2.24	2.80	3.36	3.92	4.48	5.60	6.72	8.39	8.95	9.51	10.07	11.18	13.96	16.74	19.51
S_c	0.896	0.934	0.949	0.960	0.966	0.976	0.983	0.989	0.992	1.000	1.005	1.010	1.013	1.014	1.014	1.017	1.021	1.024	1.027
S_{cp}	0.837	0.897	0.919	0.932	0.942	0.957	0.972	0.981	0.987	1.000	1.013	1.024	1.029	1.031	1.032	1.039	1.052	1.065	1.071
S_p	0.934	0.960	0.968	0.971	0.975	0.980	0.989	0.992	0.995	1.000	1.008	1.014	1.016	1.017	1.018	1.022	1.030	1.040	1.043
PSF	1.000	1.027	1.036	1.039	1.043	1.048	1.057	1.060	1.064	1.070	1.078	1.084	1.087	1.088	1.089	1.093	1.102	1.109	1.112

APPENDIX D: WORKED EXAMPLES

Dose in a 10 cm x 10 cm field at 5 cm depth for 100 MU:

$$D_t(d,S) = D_0(d_{max}, SSD_0 + d_{max}) \cdot [TMR(d,0) + SMR(d,S)] \cdot \left(\frac{SSD_0 + d_{max}}{SSD + d}\right)^2 \cdot S_c(S) \cdot S_p(0)$$

TMR(5 cm, 0) = 0.870 (Appendix C)

SMR(5 cm, 10 cm x 10 cm) = 0.122 (Appendix C)

D_0 = 1.00 Gy / 100 MU (measured calibration dose)

S_c(10 cm x 10 cm) = 1.000 (Appendix C)

$S_p(0)$ = 0.934 (Appendix C)

$$D_t(5cm,\ 10cmx10cm) = 1.00 \cdot [0.870 + 0.122] \cdot \left(\frac{101.5}{105}\right)^2 \cdot 1.000 \cdot 0.934 \ \text{Gy/100MU}$$

= 0.866 Gy/100 MU

Measured dose = 0.865 Gy/100MU

Dose in a 8 cm x 14 cm field at 20 cm depth for 100 MU:

$$D_t(d,S) = D_0(d_{max}, SSD_0 + d_{max}) \cdot [TMR(d,0) + SMR(d,S)] \cdot \left(\frac{SSD_0 + d_{max}}{SSD + d}\right)^2 \cdot S_c(S) \cdot S_p(0)$$

Equivalent Square = 4 · Area / Perimeter = 10.2 cm x 10.2 cm

TMR(20 cm, 0) = 0.427 (Appendix C)

SMR(20 cm, 10.2 cm x 10.2 cm) = 0.155 (Interpolated, Appendix C)

D_0 = 1.00 Gy / 100 MU (measured calibration dose)

S_c(10.2 cm x 10.2 cm) = 1.001 (Interpolated, Appendix C)

$S_p(0)$ = 0.934 (Appendix C)

$$D_t(20cm,\ 10.2cmx10.2cm) = 1 \cdot [0.427 + 0.155] \cdot \left(\frac{101.5}{120}\right)^2 \cdot 1.001 \cdot 0.934 \ \text{Gy/100MU}$$

= 0.389 Gy/100 MU

Measured dose = 0.392 Gy/100MU

REFERENCES

AAPM TG 21: *A protocol for the determination of absorbed dose from high-energy photon and electron beams*, Task Group 21, Med. Phys. 10(6), 741-771 (1983)

AAPM TG 51: *Protocol for clinical reference dosimetry of high-energy photon and electron beams*, Task Group 51, Med. Phys. 26, 1847-1870 (1999)

AAPM Report 85: *Tissue Inhomogeneity Corrections for Megavoltage Beams*, 2004

Abdulla, Y.A., Amin, Y.M. and Khoo, H.B.: *Determination of percentage depth dose for 6 and 10 MV x-rays using Ge-doped optical fibre and TLD-100*, J. Radiol. Prot. 22, 417-421 (2002)

Ahnesjö, A. and Aspradakis, M.M.: *Dose calculations for external photon beams in radiotherapy*, Topical Review, Phys. Med. Biol. 44, R99-R155 (1999)

Aird, E.G.A. and Farmer, F.T.: *The Design of a Thimble Chamber for the Farmer Dosemeter*, Phys. Med. Biol. 17(2), 169-174 (1972)

Almond, P., Browne, R., Millcamp, J. and Williams, C.B.: *Variation in the position of the central axis maximum build-up point with field size for high-energy photon beams*, Br. J. Radiol 43, 911 (1970)

Andreo, P. and Brahme, A.: *Stopping power data for high-energy photon beams*, Phys. Med. Biol. 31(8), 839-858 (1986)

Arcovito, G., Piermattei, A., D'Abrama, G. and Bassi, R.A.: *Dose measurements and calculations of small radiation fields for 9-MV X-rays*, Med. Phys. 12, 779-784 (1985)

Attix, F.H.: *Energy imparted, energy transferred and net energy transferred*, Phys. Med. Biol. 28(12), 1385-1390 (1983)

Attix, F.H.: *Introduction to radiological physics and radiation dosimetry*, A Wiley-Interscience Publication, 1986

Attix, F.H., Lopez, F., Owolabi, S. and Paliwal, B.R.: *Electron contamination in ^{60}Co gamma-ray beams*, Med. Phys. 10(3), 301-306 (1983)

Bagne, F.: *Physical aspects of supervoltage x-ray therapy*, Med. Phys. 1(5), 266-274 (1974)

Bagne, F.: *Choice of reference point in megavoltage dosimetry*, Med. Phys. 6(6), 510-514 (1979)

Berger, M.J. and Seltzer, S.M.: *Stopping powers and ranges of electrons and positrons*, NBSIR 82-2550-A, NBS Washington DC (1982)

Berger, M.J., Hubbell, J.H., Seltzer, S.M., Chang, J., Coursey, J.S., Sukumar, R. and Zucker, D.S.: *XCOM: Photon Cross Sections Database* http://physics.nist.gov/PhysRefData/Xcom/Text/XCOM.html

Biggs, P.J. and Ling, C.C.: *Electrons as the cause of the observed d_{max} shift with field size in high energy beams*, Med. Phys. 6(4), 291-295 (1979)

Bjärngard, B.E.: *Comments on "Zero-field dose data in water"*, Med. Phys. 21(7), 1091-1092 (1994)

Bjärngard, B.E. and Cunningham, J.R.: *Comments on "Validity of the concept of separating primary and scatter dose"*, Med. Phys. 13(5), 760-762 (1986)

Bjärngard, B.E. and Petti, P.L.: *Description of the scatter component in photon-beam data*, Phys. Med. Biol. 33(1), 21-32 (1988)

Bjärngard, B.E., Rashid, H. and Obcemea, C.H.: *Separation of primary and scatter components of measured photon beam data*, Phys. Med. Biol. 34(12), 1939-1945 (1989)

Bjärngard, B.E. and Shackford, H.: *Attenuation in high-energy x-ray beams*, Med. Phys. 21(7), 1069-1073 (1994)

Bjärngard, B.E. and Siddon, R.L.: *A note on equivalent circles, squares and rectangles*, Med. Phys. 9(2), 258-260 (1982)

Bjärngard, B.E., Tsai, J.-S. and Rice, R.K.: *Attenuation in very narrow photon beams*, Radiation Research 118, 195-200 (1989)

Bjärngard, B.E., Tsai, J.-S. and Rice, R.K.: *Doses on the central axes of narrow 6-MV x-ray beams*, Med. Phys. 17(5), 794-799 (1990)

Bjärngard, B.E. and Vadash, P.: *Analysis of central-axis doses for high-energy x rays*, Med. Phys. 22(7), 1191-1195 (1995)

Bjärngard, B.E. and Vadash, P.: *Relations between scatter factor, quality index and attenuation for x-ray beams*, Phys. Med. Biol. 43, 1325-1330 (1998)

Bjärngard, B.E., Vadash, P. and Zhu, T.: *Doses near the surface in high-energy x-ray beams*, Med. Phys. 22(4), 465-468 (1995)

Bjärngard, B.E., Zhu, T.C. and Ceberg, C.: *Tissue-phantom ratios from percentage depth doses*, Med. Phys. 23(5), 629-634 (1996)

Bradshaw, A.L.: *The variation of percentage depth dose and scatter factor with beam quality*, Br. J. Radiol. Suppl. 17, 125-130 (1983)

Brahme, A. and Andreo, P.: *Dosimetry and quality specification of high energy photon beams*, Acta Radiologica Oncology 25(3), 213-223 (1986)

Brahme, A. and Svensson, H.: *Radiation beam characteristics of a 22 MeV microtron*, Acta Radiologica Oncology 18(3), 244-272 (1979)

Burcham, W.E.: *Elements of Nuclear Physics*, Longman Text, 1979

Burns, J.E.: *Conversion of percentage depth doses for photon beams from one SSD to another and calculation of TAR, TMR and TPR*, Br. J. Radiol. Suppl. 17, 115-119 (1983)

Burns, J.E.: *Definition of tissue-air ratio*, Br. J. Radiol. Suppl. 17, 137-142 (1983)

Burns, J.E.: *Conversion of PDD for photon beams from one SSD to another and calculation of TAR, TMR and TPR*, Br. J. Radiol. Suppl. 25, 153-157 (1996)

Burns, J.E.: *Definition of tissue-air ratio*, Br. J. Radiol. Suppl. 25, 177-182 (1996)

Burns, J.E., Pritchard, D.H. and Knight, R.T.: *Peak scatter factors for ^{60}Co gamma-radiation*, Phys. Med. Biol. 37(12), 2309-2318 (1992)

Bushberg, J.T., Seibert, J.A., Leidholdt, E.M. and Boone, J.M.: *The Essential Physics of Medical Imaging, Second Edition*, Lippincott Williams & Wilkins, 2002

Bushong, S.C.: *Radiologic Science for Technologists, Eigth Edition*, Elsevier Mosby, 2004

Butson, M.J., Cheung, T., Yu, P.K.N. and Currie, M.: *Surface dose extrapolation measurements with radiographic film*, Phys. Med. Biol. 49, N197-N201 (2004)

Butson, M.J., Yu, P.K.N. and Metcalfe, P.E.: *Extrapolated surface dose measurements with radiochromic film*, Med. Phys. 26(3), 485-488 (1999)

Castellanos, M.E. and Rosenwald, J.C.: *Evaluation of the scatter field for high-energy photon beam attenuators*, Phys. Med. Biol. 43, 277-290 (1998)

Chen, F.S.: *Applying a polynomial formula to photon beam output and equivalent square field*, Med. Phys. 17, 464-469 (1990)

Clarkson, J.R.: *A note on depth doses in fields of irregular shape*, Brit. J. Radiol. 14, 265-268 (1941)

Coffey, C.W., Beach, J.L., Thompson, D.J. and Mendiondo, M.: *x-ray beam characteristics of the Varian Clinac 6-100 linear accelerator*, Med. Phys. 7(6), 716-722 (1980)

Cunningham, J.R.: *Scatter-Air Ratios*, Phys. Med. Biol. 17(1), 42-51 (1972)

Dawson, D.J.: *Percentage Depth Doses for High Energy X-rays*, Phys. Med. Biol. 21(2), 226-235 (1976)

Dawson, D.J.: *Elongation effects on the Therac 6 linear accelerator*, Med. Phys. 5(5), 439-442 (1978)

Day, M.J.: *The normalized peak scatter factor and normalized scatter functions for high energy photon beams*, Br. J. Radiol. Suppl. 17, 131-136 (1983)

Day, M.J. and Aird, E.G.A.: *The equivalent field method for dose determinations in rectangular fields*, Br. J. Radiol. Suppl. 17, 105-114 (1983)

Day, M.J. and Aird, E.G.A.: *The equivalent field method for dose determinations in rectangular fields*, Br. J. Radiol. Suppl. 25, 138-151 (1996)

Day, M.J. and Pitchford, W.G.: *The normalized peak scatter factor and normalized scatter functions for high energy photon beams*, Br. J. Radiol. Suppl. 25, 168-175 (1996)

Du Plessis, F.C.P.: *Personal Communication*, 2009

Farmer, F.T.: *A sub-standard x-ray dose-meter*, Br. J. Radiol. 28, 304-306 (1955)

Followill, D.S., Tailor, R.C., Tello, V.M. and Hanson, W.F.: *An empirical relationship for determining photon beam quality in TG-21 from a ratio of percent depth doses*, Med. Phys. 25(7), 1202-1205 (1998)

Frye, D.M.D., Paliwal, B.R., Thomadsen, B.R. and Jursinic, P.: *Intercomparison of normalized head-scatter factor measurement techniques*, Med. Phys. 22(2), 249-253 (1995)

Georg, D., Olofsson, J., Künzler, T. and Karlsson, M.: *On empirical methods to determine scatter factors for irregular MLC shaped beams*, Med. Phys. 31(8), 2222-2229 (2004)

Gerbi, B.J. and Khan, F.M.: *Measurements of dose in the buildup region using fixed-separation plane-parallel ionization chambers*, Med. Phys. 17(1), 17-26 (1990)

Godden, T.J.: *Gamma Radiation from Cobalt 60 Teletherapy Units*, Br. J. Radiol. Suppl. 17, 45-59 (1983)

Greene, D. and Williams, P.C.: *X Rays: 2-43MV*, Br. J. Radiol. Suppl. 17, 61-69 (1983)

Gupta, S.K. and Cunningham, J.R.: *Measurement of tissue-air ratios and scatter functions for large field sizes, for cobalt 60 gamma radiation*, Br. J. Radiol. 39, 7-11 (1966)

Haider, T.K. and El-Khatib, E.E.: *Differential scatter integration in regions of electronic non-equilibrium*, Phys. Med. Biol. 40, 31-34 (1995)

Haryanto, F., Fippel, M., Laub, W., Dohm, O. and Nüsslin, F.: *Investigation of photon beam output factors for conformal radiation therapy - Monte Carlo simulations and measurements*, Phys. Med. Biol. 47, N133-N143 (2002)

Henry, W.H.: *Tissue-Air Ratio, Peak Scatter Factor and Consistency*, Phys. Med. Biol. 19(1), 43-50 (1974)

Hering, E.R.: *Radiotherapy Physics and Equipment (3rd edition)*, 1996

Higgins, P.D., Sohn, W.H., Sibata, C.H. and McCarthy, W.A.: *Scatter factor corrections for elongated fields*, Med. Phys. 16(5), 800-802 (1989)

Holt, J.G.: AAPM Q. Bull. 6, 127 (1972)

Holt, J.G., Laughlin, J.S. and Moroney, J.P.: *The extension of the concept of tissue-air ratios (TAR) to high-energy x-ray beams*, Radiology 96, 437-446 (1970)

Hossain, M., Xiao, Y. and Saiful Huq, M.: *An Investigation of a Model of Percentage Depth Dose for Irregularly Shaped Fields*, Int. J. Cancer 96, 140-145 (2001)

Huda, W. and Slone, R.: *Review of Radiologic Physics*, Lippincott Williams & Wilkins,

IAEA TRS 398: *Absorbed dose determination in external beam radiotherapy*, (2000)

ICRU Report 33: *Radiation Quantities and Units*, 1980

ICRU Report 51: *Quantities and Units in Radiation Protection Dosimetry*, 1993

ICRU Report 60: *Fundamental Quantities and Units for Ionizing Radiation*, 1998

Isaev, V.I. and Kovalev, V.P.: *Energy and Angular Distributions of Electron Bremsstrahlung from Thick Targets*, Atomnaya Energiya, Vol. 57(3), 195-198 (1984)

Islam, M.K. and Van Dyk, J.: *Effects of scatter generated by beam-modifying absorbers in megavoltage photon beams*, Med. Phys. 22(12), 2075-2081 (1995)

Iwasaki, A.: *A method of making contamination-free scatter-maximum ratios (SMRs) for 10 MV x-rays*, Phys. Med. Biol. 34, 1003-1012 (1989)

Iwasaki, A.: *10 MV x-ray SMRs obtained using zero-area S_p correction factors derived by means of the Bjärngard-Petti method*, Phys. Med. Biol. 41, 625-636 (1996)

Jager, H.N., Heukelom, S., van Kleffens, H.J., van Gasteren, H., van der Laarse, R., Venselaar, J.L.M. and Westermann, C.F.: *Comparison of parametrization methods of the collimator scatter correction factor for open rectangular fields of 6-25 MV photon beams*, Radiotherapy and Oncology 45, 235-243 (1997)

Jayachandran, C.A.: *Calculated Effective Atomic Number and Kerma Values for Tissue-Equivalent and Dosimetry Materials*, Phys. Med. Biol. 16(4), 617-623 (1971)

Johns, H.E. and Cunningham, J.R.: *The Physics of Radiology (4th edition)*, Charles C Thomas, 1983

Johns, H.E., Whitmore, G.F., Watson T.A. and Umberg, F.H.: *A system of dosimetry for rotation therapy with typical rotation distributions*, J. Canad. Ass. Radiol. 4,1 (1953)

Jones, D.E.A.: *4, 6 and 8 MV X-rays produced by linear electron accelerators*, Br. J. Radiol. Suppl. 11, 63-67 (1978)

Jordan, T.J.: *Megavoltage X-ray beams: 2-50 MV*, Br. J. Radiol. Supp. 25, 62-109 (1996)

Jursinic, P.A. and Mackie, T.R.: *Characteristics of secondary electrons produced by 6, 10 and 24 MV x-ray beams*, Phys. Med. Biol. 41, 1499-1509 (1996)

Kappas, K. and Rosenwald, J.C.: *Theoretical and experimental analysis of scatter from inhomogeneous slabs in a ^{60}Co beam: the differential tissue-air ratio method (DTAR)*, Phys. Med. Biol. 31(11), 1211-1228 (1986)

Karzmark, C.J., Deubert, A. and Loevinger, R.: *Tissue-phantom ratios - an aid to treatment planning*, Br. J. Radiol. 38, 158 (1965)

Kase, K.R. and Svensson, G.K.: *Head scatter data for several linear accelerators (4-18 MV)*, Med. Phys. 13(4), 530-532 (1986)

Khan, F.M.: *The Physics of Radiation Therapy (3rd edition)*, Lippincott Williams & Wilkins, 2003

Khan, F.M., Sewchand, W., Lee, J. and Williamson, J.F.: *Revision of tissue-maximum ratio and scatter-maximum ratio concepts for cobalt 60 and higher energy x-ray beams*, Med. Phys. 7(3), 230-237 (1980)

Kijewski, P.K., Bjärngard, B.E. and Petti, P.L.: *Monte Carlo calculations of scatter dose for small field sizes in a ^{60}Co beam*, Med. Phys. 13(1), 74-77 (1986)

Klevenhagen, S.C.: *Physics of Electron Beam Therapy*, Medical Physics Handbooks, 1985

Knoll, G.F.: *Radiation Detection and Measurement (3rd edition)*, John Wiley & Sons, 2000

Koch, H.W. and Motz, J.W., *Bremsstrahlung Cross-Section Formulas and Related Data*, Rev. Mod. Phys. 31(4), 920-955 (1959)

Kosunen, A. and Rogers, D.W.O.: *Beam quality specification for photon beam dosimetry*, Med. Phys. 20(4), 1181-1188 (1993)

Lam, K.L. and Ten Haken, R.K.: *In phantom determination of collimator scatter factor*, Med. Phys. 23(7), 1207-1212, (1996)

LaRiviere, P.D.: *Surface dose from 6 MV photon interactions in air*, Phys. Med. Biol. 28(3), 285-287 (1983)

Lee, N.E., Chen, D., Waggener, R.G. and Blough, M.M.: *Measured water transmission curves and calculated zero field size tumor maximum ratios for 4, 6, and 15 MV x-rays*, Med. Phys. 26(6), 956-961 (1999)

Li, X.A.: *Peak scatter factors for high energy photon beams*, Med. Phys. 26(6), 962-966 (1999)

Li, X.A., Soubra, M., Szanto, J. and Gerig, L.H.: *Lateral electron equilibrium and electron contamination in measurements of head-scatter factors using miniphantoms and brass caps*, Med. Phys. 22(7), 1167-1170 (1995)

Lind, M.: *Characteristics of a flattening filter free photon beam - measurements and Monte Carlo simulations*, M.Sc. Thesis, 2008

Ling, C.C., Schell, M.C. and Rustgi, S.N.: *Magnetic analysis of the radiation components of a 10 MV photon beam*, Med. Phys. 9(1), 20-26 (1982)

Loevinger, R.: *A formalism for calculation of absorbed dose to a medium from photon and electron beams*, Med. Phys. 8(1), 1-12 (1981)

Lovelock, D.M.J., Chui, C.S., Kutcher, G.J. and Mohan, R.: *Analysis of the photon beam treatment planning data for a scanning beam machine*, Med. Phys. 21(12), 1969-1977 (1994)

Luxton, G. and Astrahan, M.A.: *Output factor constituents of a high-energy photon beam*, Med. Phys. 15(1), 88-91 (1988)

Ma, C-M. and Nahum, A.E.: *Bragg-Gray theory and ion chamber dosimetry for photon beams*, Phys. Med. Biol. 36(4), 413-428 (1991)

Marmier, P. and Sheldon, E.: *Physics of nuclei and particles, Volume 1*, Academic Press, 1969

Marquardt, D.W.: *An algorithm for least squares estimation of non-linear parameters*, J Soc Industrial Applied Mathematics 11(2), 431-444 (1963)

McDonough, J., Xiao, Y. and Bjärngard, B.E.: *Comparing two methods for calculating phantom scatter*, Phys. Med. Biol. 44, N9-N14 (1999)

McKenzie, *Cobalt-60 Gamma-Ray Beams*, Br. J. Radiol. Suppl. 25, 46-61 (1996)

Mellenberg, D.E.: *Determination of build-up region over-response corrections for a Markus-type chamber*, Med. Phys. 17(6), 1041-1044 (1990)

Meredith, W.J. and Neary, G.J.: *The production of isodose curves and the calculation of energy absorption from standard depth dose data, Part I*, Br. J. Radiol. 17 (195), 75-82, 1944

Meredith, W.J. and Neary, G.J.: *The production of isodose curves and the calculation of energy absorption from standard depth dose data, Part II*, Br. J. Radiol. 17 (196), 126-130, 1944

Mohan, R. and Chui, C.-S.: *Validity of the concept of separating primary and scatter dose*, Med. Phys. 12(6), 726-730 (1985)

NCS Report 12 (Nederlandse Commissie voor Stralingsdosimetrie): *Determination and use of scatter correction factors of megavoltage photon beams*, 1998

Nilsson, B. and Montelius, A.: *Fluence perturbation in photon beams under nonequilibrium conditions*, Med. Phys. 13(2), 191-195 (1986)

Nizin, P.S.: *Geometrical aspects of scatter-to-primary ratio and primary dose*, Med. Phys. 18(2), 153-160 (1991)

Nizin, P.S.: *Electronic equilibrium and primary dose in collimated photon beams*, Med. Phys. 20(6), 1721-1729 (1993)

Nizin, P.S.: *Phenomenological dose model for therapeutic photon beams: Basic concepts and definitions*, Med. Phys. 26(9), 1893-1900 (1999)

Nizin, P.S., Bellezza, D.M. and Mooij, R.B.: *The elements of tissue-air ratio and systematic error*, Med. Phys. 23(7), 1191-1197 (1996)

Nizin, P.S. and Chang, X.S.: *Primary dose in photon beams with lateral electron disequilibrium*, Med. Phys. 18(4), 744-748 (1991)

Nizin, P. and Kase, K.: *A method of measuring the primary dose component in high-energy photon beams*, Med. Phys. 15(5), 683-685 (1988)

Nizin, P.S. and Kase, K.R.: *Determination of primary dose in ^{60}Co gamma beam using a small attenuator*, Med. Phys. 17(1), 92-94 (1990)

Nizin, P.S. and Mooij, R.B.: *Tissue-air ratios for narrow ^{60}Co gamma-ray beams*, Med. Phys. 25(8), 1458-1463 (1998)

Nizin, P.S., Qian, G.-X and Rashid, H.: *"Zero-field" dose data for ^{60}Co and other high-energy photon beams in water*, Med. Phys. 20(5), 1353-1460 (1993)

Nordell, B. and Brahme, A.: *Angular distribution and yield from bremsstrahlung targets*, Phys. Med. Biol. 29(7), 797-810 (1984)

NPL (1990): Lillicrap, S.C. (chairman) *et al.*: *Code of practice for high-energy therapy dosimetry based on the NPL absorbed dose calibration service*, Phys. Med. Biol. 35(10), 1355-1360 (1990)

Nutbrown, R.F., Duane, S., Shipley, D.R. and Thomas, R.A.S.: *Evaluation of factors to convert absorbed dose calibrations from graphite to water for the NPL high-energy photon calibration service*, Phys. Med. Biol. 47, 441-454 (2002)

O'Connor, J.E.: *The Variation of Scattered X-Rays with Density in an Irradiated Body*, Phys. Med. Biol. 1: 352-369 (1957)

Padikal, T.N. and Deye, J.A.: *Electron Contamination of a High-energy X-ray Beam*, Phys. Med. Biol. 23(6), 1086-1092 (1978)

Palta, J.R., Ayyangar, K., Daftari, I. and Suntharalingam, N.: *Characteristics of photon beams from Philips SL25 linear accelerators*, Med. Phys. 17(1), 106-116 (1990)

Patomäki, L.K.: *The equivalent field principle and its use in beam therapy dose calculations*, Br. J. Radiol. 41, 381-383 (1968)

Paul, J.M., Koch, R.F., Khan, F.R. and Devi, B.S.: *Characteristics of Mevatron 77 15-MV photon beam*, Med. Phys. 10(2), 237-242 (1983)

Petti, P.L. and Goodman, M.S.: *Investigation of buildup dose from electron contamination of clinical photon beams*, Med. Phys. 10(1), 18-24 (1983)

Pfalzner, P.M.: *A revised equation relating tissue-air ratio to per cent depth-dose*, Phys. Med. Biol. 26(3), 510-513 (1981)

Pistorius, S.: *The Analysis and Modelling of Broad Beams of Photons and Electrons*, PhD thesis (1991)

Podgorsak, E.B.: *Radiation Oncology Physics: A Handbook for Teachers and Students*, IAEA, 2005

Purdy, J.A.: *Relationship between tissue-phantom ratio and percentage depth dose*, Med. Phys. 4(1), 66-67 (1977)

Purdy, J.A.: *Buildup/surface dose and exit dose measurements for a 6-MV linear accelerator*, Med. Phys, 13(2), 259-262 (1986)

Rice, R.K. and Chin, L.M.: *Monte Carlo calculations of scatter to primary ratios for normalization of primary and scatter dose*, Phys. Med. Biol. 35(3), 333-338 (1990)

Rice, R.K., Hansen, J.L., Svensson, G.K. and Siddon, R.L.: *Measurements of dose distributions in small beams of 6 MV x-rays*, Phys. Med. Biol. 32(9), 1087-1099 (1987)

Robinson, D.M. and Scrimger, J.W.: *Monoenergetic approximation of a polyenergetic beam: a theoretical approach*, Brit. J. Radiol. 64, 452-454 (1991)

Saw, C.B.: *Foundation of Radiological Physics*, C.B. Saw Publishing, 2002

Sätherberg, A., Karlsson, M. and Karlsson, M.: *Theoretical and experimental determination of phantom scatter correction factors for photon fields with different radial energy variation*, Phys. Med. Biol. 41, 2687-2694 (1996)

Schreuder, A.N.: *Characterisation of the NAC's p(66)/Be(40) Neutron Therapy Beam in Terms of Primary and Scattered Dose Components*, MSc thesis (1992)

Schreuder, A.N., Jones, D.T.L. and Kiefer, A.: *A small ionization chamber for dose distribution measurements in a clinical proton beam*, Advances in Hadrontherapy, Eds. U Amaldi, B Larsson and Y Lemoigne, Elsevier BV, 284-289 (1997)

Shortt, K.R., Ross, C.K., Schneider, M., Hohlfeld, K., Roos, M. and Perroche, A-M.: *A comparison of absorbed dose standards for high-energy x-rays*, Phys. Med. Biol. 38, 1937-1955 (1993)

Sixel, K.E. and Podgorsak, E.B.: *Buildup region and depth of dose maximum for megavoltage x-ray beams*, Med. Phys. 21(3), 411-416 (1994)

Sjögren, R., Karlsson, M.G., Karlsson, M. And Svensson, H.: *Depth for dose calibration in high energy photon beams*, Radiotherapy and Oncology 43, 313-313 (1997)

Solberg, T.D., Holly, F.E., De Salles, A.A.F., Wallace, R.E. and Smathers, J.B.: *Implications of tissue heterogeneity for radiosurgery in head and neck tumors*, Int. J. Radiation Oncology Biol. Phys. 32(1), 235-239 (1995)

Stanton, R. and Stinson, D.: *Applied Physics for Radiation Oncology*, Medical Physics Pub, 1996

Sterling, T.D., Perry, H. and Katz, L.: *Automation of radiation treatment planning*, Br. J. Radiol. 37, 544-550 (1964)

Storchi, P. and van Gasteren, J.J.M.: *A table of phantom scatter factors of photon beams as a function of the quality index and field size*, Phys. Med. Biol. 41, 563-571 (1996)

Szymczyk, W., Goraczko, A. and Lesiak, J.: *Prediction of Saturne II + 10 MV and 23 MV photon beam output factors*, Int. J. Radiat. Oncol. Biol. Phys. 21, 789-793 (1991)

Tannous, N.B.J, Gagnon, W.F. and Almond, P.R.: *Buildup region and skin-dose measurements for the Therac 6 linear accelerator for radiation therapy*, Med. Phys. 8(3), 378-381 (1981)

Tatcher, M. and Bjärngard, B.E.: *Head-scatter factors in rectangular photon fields*, Med. Phys. 20(1), 205-206 (1993)

Tatcher, M. and Bjärngard, B.E.: *Equivalent squares of irregular photon fields*, Med. Phys. 20(4), 1229-1232 (1993)

Taylor, J.R.: *An introduction to error analysis*, Oxford University Press, 1982

Ten Haken, R.K.: *Comment on "Intercomparison on normalized head-scatter factor measurement techniques"*, Med. Phys. 22(9), 1471 (1995)

Thames, H.D.: *First scatter to off-axis points and the Clarkson method*, Phys. Med. Biol. 18(3), 444-451 (1973)

Thomadsen, B.R., Kubsad, S.S., Paliwal, B.R. and Shahabi, S.: *On the cause of the variation in tissue-maximum ratio values with source-to-detector distance*, Med. Phys. 20(3), 723-727 (1993)

Topping, J.: *Errors of Observation and Their Treatment*, Chapman and Hall, 1971

Underhill, L. and Bradfield, D.: *IntroSTAT 5.0*, Juta & Co (1994)

Vadash, P. and Bjärngard, B.E.: *An equivalent-square formula for head-scatter factors*, Med. Phys. 20(3), 733-734 (1993)

Van de Geijn, J. and Fraass, B.A.: *The net fractional depth dose: A basis for a unified analytical description of FDD, TAR, TMR and TPR*, Med. Phys. 11(6), 784-793 (1984)

Van der Zee, W. and Welleweerd, J.: *Calculating photon beam characteristics with Monte Carlo techniques*, Med. Phys. 26(9), 1883-1892 (1999)

Van Dyk, J.: *Practical dosimetric considerations of a 10-MV photon beam*, Med. Phys. 4(2), 145-153 (1977)

Van Dyk, J.: *Broad beam attenuation of cobalt-60 gamma rays and 6-, 18- and 25-MV x-rays by lead*, Med. Phys. 13(1), 105-110 (1986)

Van Gasteren, J.J.M., Heukelom, S., van Kleffens, H.J., van der Laarse, R., Venselaar, J.L.M. and Westermann, C.F.: *The determination of phantom and collimator scatter components of the output of megavoltage photon beams: measurement of the collimator scatter part with a beam-coaxial narrow cylindrical phantom*, Radiotherapy and Oncology 20, 250-257 (1991)

Van Gasteren, J.J.M., van der Laarse, R., Venselaar, J.L.M., Heukelom, S., Jager, H.N., van Kleffens, H.J. and Westermann, C.F.: *A three-Gaussian fit of phantom scatter correction data*, Phys. Med. Biol. 43, 577-585 (1998)

Velkely, D.E., Manson D.J., Purdy, J.A. and Oliver, G.D.: *Build-up region of megavoltage photon radiation sources*, Med. Phys. 2(1), 14-19 (1975)

Venselaar, J., Heukelom, S., Jager, N., Mijnheer, B., van der Laarse, R., van Gasteren, H., van Kleffens, H. and Westermann, C.: *Effect of electron contamination on scatter correction factors for photon beam dosimetry*, Med. Phys. 26(10), 2099-2106 (1999)

Wayne Scott, W.: *Angular Distribution of Thick-Target Bremsstrahlung which Includes Multiple Electron Scatterings*, NASA Technical Note D-4063 (1967)

Weber, L., Nilsson, P. and Ahnesjö, A.: *Build-up cap materials for measurement of photon head-scatter factors*, Phys. Med. Biol. 42, 1875-1886 (1997)

Williams, J.R. and Thwaites, D.I.: *Radiotherapy physics in practice*, Oxford University Press, 1993

Woo, M.K., Cunningham, J.R. and Jezioranski, J.J.: *Extending the concept of primary and scatter separation to the condition of electronic disequilibrium*, Med. Phys. 17(4), 588-595 (1990)

Xiao, Y. and Bjärngard, B.: *An expression for backscatter factors for orthovoltage x-rays*, Phys. Med. Biol. 43, 1331-1334 (1998)

Yu, M.K., Murray, B. and Sloboda, R.: *Parametrization of head-scatter factors for rectangular photon fields using an equivalent square formalism*, Med. Phys. 22, 1329-1332 (1995)

Yu, M.K., Sloboda, R.S. and Murray, B.: *Linear accelerator photon beam quality at off-axis points*, Med. Phys. 24(2), 233-239 (1997)

Zefkili, S., Kappas, C. and Rosenwald, J.-C.: *On-axis and off-axis primary dose component in high energy photon beams*, Med. Phys. 21(6), 799-808 (1994)

Zhengming, L. and Brahme, A.: *High-energy electron transport*, Physical Review B, 46(24), 15739-15752 (1992)

Zhu, T.C. and Bjärngard, B.E.: *The head-scatter factor for small field sizes*, Med. Phys. 21(1), 65-68 (1994)

Zhu, T.C. and Bjärngard, B.E.: *Head scatter off-axis for megavoltage x-rays*, Med. Phys. 30(4), 533-543 (2003)

Zhu, T.C., Bjärngard, B.E., Xiao, Y. and Yang, C.J.: *Modeling the output ratio in air for megavoltage photon beams*, Med. Phys. 28(6), 925-937 (2001)